1-1-2015

Developing A Toolbox To Probe Reaction Dynamics With Strong Field Ionization And Non-Linear Attosecond Spectroscopy

Thushani Nikeshala Herath
Wayne State University,

DEVELOPING A TOOLBOX TO PROBE REACTION DYNAMICS WITH STRONG FIELD IONIZATION AND NON-LINEAR ATTOSECOND SPECTROSCOPY

by

THUSHANI N. HERATH

DISSERTATION

Submitted to the Graduate School

of Wayne State University,

Detroit, Michigan

in partial fulfillment of the requirements

for the degree of

DOCTOR OF PHILOSOPHY

2015

MAJOR: CHEMISTRY (Analytical)

Approved by:

_____

Advisor Date

_____

_____

_____

DEDICATION

To my loving Ammi, Thatthi and Sanju,

For their Unconditional Love.....

ACKNOWLEDGEMENTS

I have spent an amazing and remarkable six years in my life as a graduate student at Wayne State University and in the Li Lab. My heartfelt gratitude goes to many people who helped me in various ways among all those years.

First and foremost, I would like to express my sincere gratitude to my advisor, Prof. Wen Li for his guidance and support throughout this challenging time period. He is always being a leader instead of a boss, who worked together and support through setting examples to be a successful scientist. His patience, enthusiasm and motivation highly influence me to improve my skills as an effective researcher and step up as an independent scientist in the future. I am truly thankful for his enormous support, guidance and time dedicated to make my path as a scientist. I feel very fortunate to graduate under the supervision of amazing advisor as you.

I would also like to be grateful to my thesis committee, Prof. Arthur Suits, Prof. Colin Poole and Prof. Erhard Rothe for their encouragement and insights on my research. I am also thankful to Prof. Tiffany Mathews who was a former member in my thesis committee for her valuable suggestions.

I am thankful to Dr. Suk Kyoung Lee for sharing her knowledge and experiences to help me with my efforts in all the aspects. Thank you Dr. Cunshun Huang for working with me and provide the courage and enthusiasm to make these experiments successful.

My heartiest thank goes to all of my lab mates, Yunfei, Alex, Pradip and Lin, who supported me in anyways they can. I really enjoyed the simulating discussions and the team work we have done to make our experiments happen. Especially to the support they have given to me to manage the time with my family emergencies. Thanks for taking all the night shifts to make it convenient for me. You all are the best colleagues and best friends I could ask for.

It is also important to mention the former and current Suits group members and thank them for letting me borrow things from their lab when we needed to.

I am also thankful for the supportive administrative departmental staff including Melissa, Debbie, Diane, Bernadette, Nestor and numerous other people who has helped me from the beginning to the end. I also want to include the Sri Lankan Student Association (SLSA) and Great Lakes Buddhist Vihara for helping me and other Sri Lankan students to get used to the life away from home.

Last but not least, I am thankful to my loving family from bottom of my heart for making this achievement possible. My parents, thank you so much for all the support and sacrifice you have done to make my dreams come true. Without them none of this would have been possible. The love, kindness and care I have received from you is incomparable and that made me the person who I am today. My loving brother deserves thanks for taking care of my parents while I am away from home. Thank you for taking all the responsibilities and letting me have a clear mind to focus on my studies. I am also grateful to the support I received from my in-laws. Finally, I would like to convey my gratitude to my beloved husband, Dananjaya, for his encouragement, support,

motivation, patience and most of all, his love. It would have not been possible without you being walking with me throughout those good and bad moments. And also to my loving son, Thevindu, for being a good boy, through all those years and bear with me for missing out most of the exciting moments in his childhood. Thank you.

TABLE OF CONTENTS

LIST OF TABLES

LIST OF FIGURES

CHAPTER 1

Introduction

1.1 Motivation

Developing tools to follow fast motions has been a fairly demanding field for many years. In 1878, the invention of camera flashes with high speed shutters, opened up a whole new world at that time as it could capture the events on the milisecond time scale. As the field progressed, new inventions such as stroboscopy in the time scale of microseconds, which make an object moving in the dark visible to a detector gave hope of the improvements of this concept towards the field of science. The advent of laser technology then took this process elevated to an even faster time scale, achieving femtosecond resolutions. With the aid of lasers, not only probing the microscale properties but also manipulating and ultimately controlling those processes became possible. These inventions have created a novel field of science known as ultrafast science. During the past few decades, the evolution of ultrafast measurements happened through three main time scale regimes; picosecond, femtosecond and attosecond[1]. Revolution of the technology has opened doors for the transition of picoseconds to attoseconds. The invention of microwave electronics led to fast switching of electric current introducing picosecond time resolved measurements, while the ultrafast optics such as laser provided ultra short light pulse generation and measurements in the femtosecond time domain. Recently the interest of ultrafast science was directed towards light wave electronics, which facilitate the attosecond level waveforms. These waveforms can be used in studies of atomic scale electronic dynamics which has not been studied before (Figure 1).

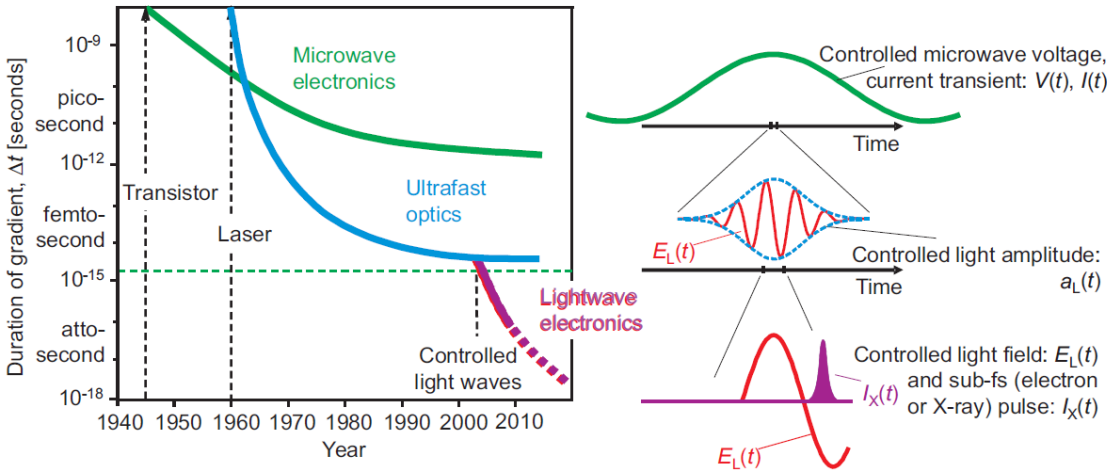

Figure 1: Evolution of ultrafast measurements. The resolution of the time-resolved microscopic measurements has evolved from picoseconds to attoseconds with the progress in technology from microwave electronics, ultrafast optics to light wave electronics. (Adopted from Krausz *et al.*)

Laser technology is advantageous for studying atomic/molecular systems because the interaction between light with matter is one of the best approaches to extract details of atomic/molecular systems. Current laser technology is capable of producing light with the frequency of 1 part in 10^{15} or even more precise 1 part in 10^{18}. High intensity laser field consist of light waves with sufficient electric strength to be able to break the forces that bind the atom. Before ultrafast lasers are introduced, there was no other tool which capable of controlling forces in macroscopic matter. Thus, the implications of ultrafast science and related findings are applicable for the entire science community: physics, chemistry, biology and engineering. Validating the importance of ultrafast science, in 1999 Prof. A. Zeiwail, was awarded with the Nobel Prize in chemistry for femto-chemistry. Prof. Zeiwali used laser science for time resolved key photochemical reaction, which demonstrated the possibilities to monitor atomic motion

during a chemical reaction[2]. With the aid of femto-chemistry, a deeper understanding of chemical reactions has been achieved. Over the past decade, many technical improvements have been achieved in the field of ultrafast science. Scientists were able to generate coherent pulses on attosecond time scale at which electronic dynamics are taking place. The use of an intense light pulse with attosecond pulse duration will provide a direct probe on the dynamics of the building blocks of life processes. Ability to reach such a detailed level will lead to several important scientific breakthroughs including:

- Direct monitoring of the motion of electrons in the natural processes such as photosynthesis, dynamics of proteins and dynamic responses in solid state matter.
- Compact sources of high intensity particle beams for research in physics and medicine.
- Study the motion of atoms in semiconductors.
- Optical telecommunication studies.

With such versatility in extracting detailed dynamics, developing a tool to probe and eventually manipulate the electronic dynamics in attosecond time domain will become an important task for the entire scientific community.

Developing tools to pin down reaction dynamics is a demanding task. The ultimate building block of many chemical, biological or physical processes is governed by bond breaking and bond formation. More strictly, the motion of electrons, which is in the attosecond time domain, is the most fundamental level related to chemistry.

Changes of the molecular structure, photosynthesis in green plants, emission of light, transport of signals in nerves are a few of those among many other examples. Consequently, probing and controlling the motion of electrons at the most fundamental level will provide new insight into the fields of medicine, information technology, life science and basic energy science. The challenge on this microscopic level is that the boundaries between different fields of science have blurred and the processes are bridged through the motion of electrons on the microscopic scale. To understand these elementary processes and uncover the new details of the system, one has to take a close look at the same timescale of this fundamental level. To accomplish such a demanding goal, it is necessary to dig deeper in to the atomic level and closely follow the electronic dynamics. As a result, the necessities of experimental tools to observe electron and nuclear motions in real time become essential and yet challenging. In order to make these ultrafast movements visible, we need a series of freeze-frame snap shots of the movement similar to the mechanism in high speed photography. Such probe will be able to extract information of the events taking place within measured brief time intervals, thus called time-resolved measurements.

Towards developing a probe with natural time resolution, we have chosen the photo-induced reaction systems based upon the light-matter interaction. Studies of photo-induced processes have been an interesting topic over decades as it is an information-rich process. Studying the dynamics of such processes makes it possible to reveal important fundamental information, such as quantum mechanical behavior of molecular systems[3]. One way to understand reaction dynamics is to explore the potential energy surface of a photodissociation event where the dissociation evolves. A

promising approach would be to use an ultrafast probe to look at the detailed dynamics of different potential energy surfaces from reactants to products in natural time scale. A probe with such a capability will be utilized as a benchmark in order to obtain the illuminating time-resolved details of the reaction pathways.

This thesis work has focused on developing real-time probes to achieve the ultrafast measurements which will ultimately be useful in controlling chemical reactions in the natural time domain. The effort was based on two interesting topics related to the ultrafast optics and light wave electronics; (1) strong field Ionization (SFI) and (2) attosecond spectroscopy.

1.2 Strong Field Physics and Strong field Ionization Probe

Generally, strong field phenomena take place in the presence of a laser field with the intensity higher than 10^{11} W/cm^2. In the presence of such an intense laser, the potential barrier of an atom or a molecule is distorted. The strong interactions of electrons of the atom/molecule with the laser field lead to instantaneous ionization and released from the suppressed coulomb barrier producing tunnel ionization (Figure 2)[4].

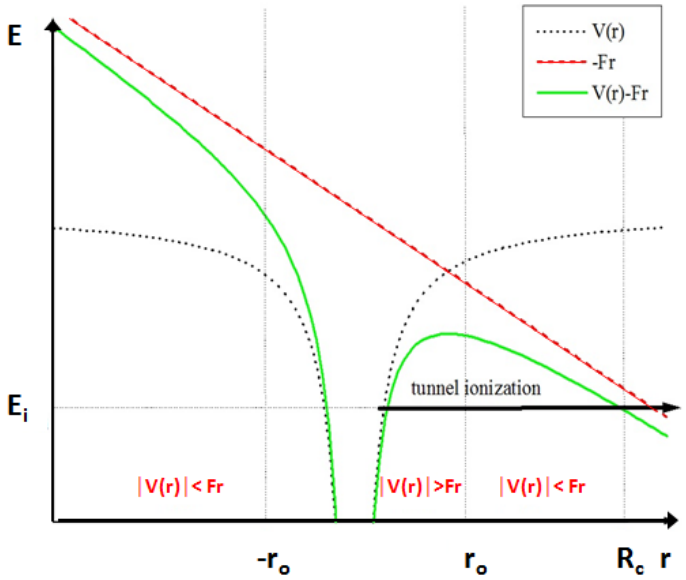

Figure 2: Tunnel Ionization: In the presence of an intense laser filed (potential Fr) the combined potential between the atom (potential V(r)) and the laser is distorted (V(r)-Fr). If E_i is the ionization potential of the atom, the ionized electron can release from the suppressed coulomb barrier at r=R_c producing tunnel ionization.

In laser matter interaction there are two fundamental regimes, the perturbative regime (Pondermotive potential (U_p) <<< Ionization potential (I_p)) and non-perturbative regime (U_p > I_p). The ponderomotive potential can be defined as the average kinetic energy of an electron in an electric field which is given by eq 1.1.

$$U_p = \frac{e^2 E_0^2}{4m\omega^2} = 9.33 \text{ X } 10^{-14} I_0 \lambda^2 (eV) \qquad (1.1)$$

Where, E_0 is the electric field strength, $I_0\,(W/cm^2)$ is the laser intensity and λ is the laser wavelength. The ionization potential is the minimum amount of energy required to remove an electron from an atom or a molecule. Unlike the perturbative regime, in the non-perturbative regime the nonresonance response becomes more important and thereby leads to the phenomena as tunneling ionization, rescattering and non-sequential double ionization. These processes can be explained by the three step model[4, 5]; at the peak of the laser electric field the tunnel ionization takes place and those electrons will be then accelerated with the laser electric field, and as the laser electric field reverses its phase those electrons can be driven back to the parent ion and recollide (Figure 3). This re-encounter between electrons and ionic core results in many interesting and important phenomena, such as non-sequential double ionization, higher order above threshold ionization (ATI), and high order harmonic generation (HHG) facilitating attosecond temporal resolution[6-8].

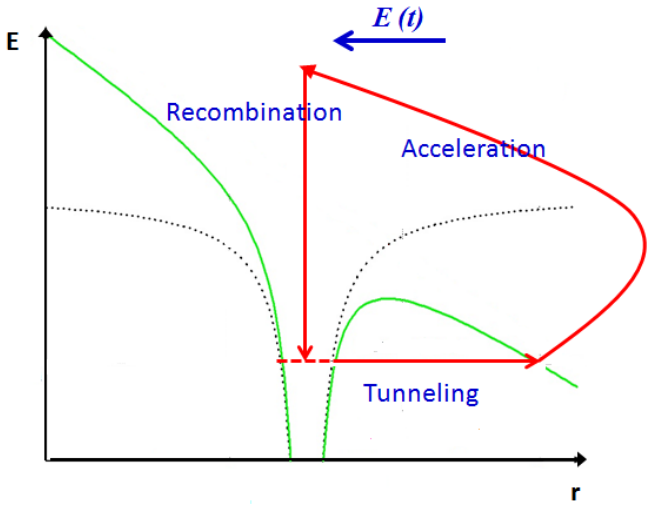

Figure 3: Three step model. Tunneling, accelerating and driving back to the parent ion by the oscillating electric field (*E(t)*), and recombination/recollision with the ground state.

In the strong field regime the perturbative treatment becomes invalid. Instead, for the ionization rate of atoms in strong field, rather simple ionization mechanism comes in to play as predicted by the theory of tunneling ionization[7-9]. In these studies a simple analytical form of ionization rate as a function of the instantaneous laser phase was found with a single active electron approximation and moderate field intensity. However the relationship fails at ultra-strong field intensity where the laser intensity is about (10^{16}-10^{21} W/cm^2), because the atomic quantum state is being scrambled by the high intensity [10].

Theoretically, the multiphoton/strong field ionization rate of an atom can be expressed as the equation (1.1) given below[7-9].

$$w \propto \left(\frac{(2l+1)(l+|m|)!}{2^{|m|}|m|!(l-|m|)!}\right)\left(\frac{3F_0}{\pi F}\right)^{1/2}\left(\frac{2F_0}{F}\right)^{2n-|m|-1} e^{-\frac{2F_0}{3F}} \qquad \text{.....(1.2)}$$

Where;

$F_0 = (2\,E_0)^{3/2}$

E_0 = the ionization potential

F = the laser electric filed strength

w = the ionization rate

According to the equation 1.2, the ionization rate (w) is highly dependent on the magnetic quantum number (m_l). For example, if the laser intensity is 8 X 10^{13} W/cm^2 and the ionization potential is 10 eV, for l=2, ionization rate of m_l=0 is 9 times higher than that of m_l=1 and 230 times higher than that of m_l=2. Due to this nonlinearity and

higher sensitivity combined with its inherited short pulse duration, SFI is capable of probing some weakly aligned or polarized atoms providing the ability to extract useful information about photodissociation dynamics through the direct measurements of the spatial distribution of the electron cloud in atoms allowing direct probing of molecular dynamics. Consequently, SFI provides the advantage over the conventional methods of studying photodissociation dynamics, such as ion imaging techniques[11-21], core-sample time-of-flight (TOF)[22, 23], Doppler spectroscopy[24, 25], fluorescence detection [26], absorption spectroscopy[27, 28] etc, which are based on linear spectroscopy or low-order non-linear spectroscopy. All of these methods are limited to measurements in the asymptotic region. Therefore these methods have less capability for extracting in-detailed dynamics in the natural time scale of a reaction pathway.

Over the years, the utility of SFI as a probe in studying nuclear structure/dynamics has been a competitive topic in ultrafast science. With the closer look on the strong field ionization such as ionization rate, electronic angular distribution or angular dependent ionization rate will provide the information, such as electron density distributions and features of the wave functions. These studies have shown that mapping out the molecular orbital shapes by measuring the alignment dependence of ionization rates[29]. Here in this study they have shown clear evidence of a real picture of the molecular orbital using the measurements of alignment dependence of tunneling ionization rates. These measurements were used to visualize the breakup of molecular ions in to two ion fragments. These studies verify the fact that molecular Ammosov-Delone-Krainov (ADK) theory predicts the molecular frame ionization rate is closely related to HOMO orbital electron density. Then there was another study which took a

further step of SFI as a probe by measuring the angular dependent strong field ionization of dissociating models, and produced a movie about how electrons rearrange during a chemical reaction[30]. In this particular study they have shown that the utility of capturing the rearrangement of entire valance shell electron density as a bond breaks, using a reaction microscope technique. This was done by monitoring the dissociation of a bromine molecule at different times in the event of dissociation using an intense ultra-short laser pulse. Measurements of the total ionization signal and angular distribution of the ionization yield were taken during this process. With the evidence of how long it takes for an electron to localize onto the individual bromine atom, it was concluded that the electron transfer does not take place until the fragments are far enough apart to degenerate the potential energy surfaces in this dissociation event. Such studies reflect the fact that strong field ionization is not only sensitive to the highest occupied molecular orbital (HOMO) but also to the signature of the entire valance shell orbital. Besides the ability of SFI as a probe, recent studies validate its capability in controlling chemical reactions. There have been studies showing a coherent control using tailored strong laser pulses[31-33]. The field-induced Stark shifting and charge polarization in molecules will reshape the potential energy surfaces and thus steer the chemical reaction. Furthermore, due to the large oscillations in a strong laser field, kinetic energy can be effectively pumped into a specific mode to enhance the reaction facilitating the mode selective chemistry which has been a dream of the chemist.

Due to the progress obtained in the field of SFI as a probe in monitoring nuclear/ structural dynamics in our lab we have extended our studies to investigate the sensitivity of the SFI probe to atomic polarization studies. In our effort of developing

strong field ionization as an atomic probe, we have demonstrated its sensitivity to both atomic alignment and atomic orientation. This verifies the additional capabilities of SFI probe in probing reaction dynamics in the natural time domain.

1.3 Attosecond Spectroscopy as a Probe of Electron Dynamics

Attosecond science, the science of generation, control, detection and application of sub-femtosecond laser pulses, became an interesting and yet useful topic in many fields such as physics, chemistry, medicine, engineering, etc[34]. The amazing concept about the attosecond (10^{18}) time domain is that, it is the natural time domain where all the atoms and electrons are teaming up with the activities related to all the elementary processes. Therefore, the monitoring and manipulation of electron degrees of freedom in molecular systems in the attosecond time domain lights-up a hope towards controlling chemical reactions. To date, the shortest electromagnetic pulse known to man, an isolated attosecond pulse of 67 attoseconds, has been produced by Chang and co-workers [35]. These findings opened up a new dimension in science. In this particular time frame the only motion possible is the evolution of an electronic wave function and everything else is considered frozen.

The traditional approaches are rather simple in nature. It was considered that, due to the negligible mass of an electron compared to the mass of a nucleus, electrons are instantaneously adjusting to the motion of the nuclei. Under that assumption the nature of the potential energy surfaces are dominated by the forces wielded on the nuclei. This approximation is known as the Born-Oppenheimer approximation[36]. This adiabatic approximation remains true for the larger energy gaps

between the electronic states. On the other hand, if the energy gap of the electronic states is comparable to the nuclear coordinates, then the Born-Oppenheimer approximation will fail and the relative dynamics are considered as non Born-Oppenheimer. In this scenario, the motion of electrons and nuclei is highly collaborative and small changes in nuclear degrees of freedom influence the electronic properties a great deal[37]. The independent electron approximation, where two or many electron interactions are considered to be negligible[38], also become invalid when the electron dynamics are probed at ultra-short time scales, such as attosecond. At such extreme conditions the dynamics induced by the electron correlation cannot be ignored anymore.

Consequently, the innovation of attosecond pulses together with the non Born-Oppenheimer dynamics influence many electron interactions opened up a new possibility of controlling chemical reactivity via coherent preparation of a number of electronic sates[39]. The proposed studies of monitoring charge migration and charge-directed reactivity using attosecond pulses has become a dream of many researchers in the field of ultrafast science. Among many suggested experimental protocols, attosecond time-resolved pump-probe spectroscopy stands out and much research effort is focused on succeeding with this process. These attosecond tools are also rich with many technological advantages as control of the number of photons which facilitates the control of intensity, wavelength and phase. These technical advances will eventually create a coherent quantum process in a domain where the fundamental dynamics can be followed directly.

The main interest of the attosecond field has been focused on two different areas; (1) generation of shortest attosecond pulses, (2) development of the

experimental tools to extract ultrafast information. The fundamental phenomenon related to attosecond pulse generation is the high harmonic generation (HHG) process. HHG is itself a strong field process. As described by the three-step model, when an intense laser field interacts with matter, it results in tunneling ionization through the combined coulomb barrier of ion and laser potential. Within a half cycle of the laser pulse these electrons are driven back to the parent ion by the laser electric field. Simply, it describes the process of ionization, acceleration and recombination of electrons twice within a laser pulse. This process will cause either elastic or inelastic re-scattering of electrons which leads for some interesting phenomenon, such as high-energy above threshold ionization (ATI), HHG, and non-sequential double ionization (NSDI)[40]. In the elastic collision, the electron will gain up to 10Up energy causing high-energy ATI. When the collision is inelastic, re-scattered electrons can eject another electron from the parent ion where the momentum of the second electron is correlated with the original electron, which results in NSDI. Furthermore, the recolliding electron can also be absorbed by the parent ion, rebounding to its ground state resulting in ejection of high energy photons. In other words, the interaction of an atom with a strong field will lead to an interference of a particle with itself. In the phenomena of ATI, interference between the electron wave packets created from the same valance electronic state near subsequent wave crest, which are travelling towards the same direction will result in a birth of equally spaced electrons separated by the energy of photon of the driving laser field[41]. Likewise HHG is a periodic photon spectrum resulted through the interference of the photon wave packets released twice per laser cycle due to the each recollision process (Figure 4)[42, 43].

The HHG process is the most efficient way of producing attosecond pulses. During HHG process using a high intense few-cycle NIR laser, XUV pulses in attosecond time duration can be generated.

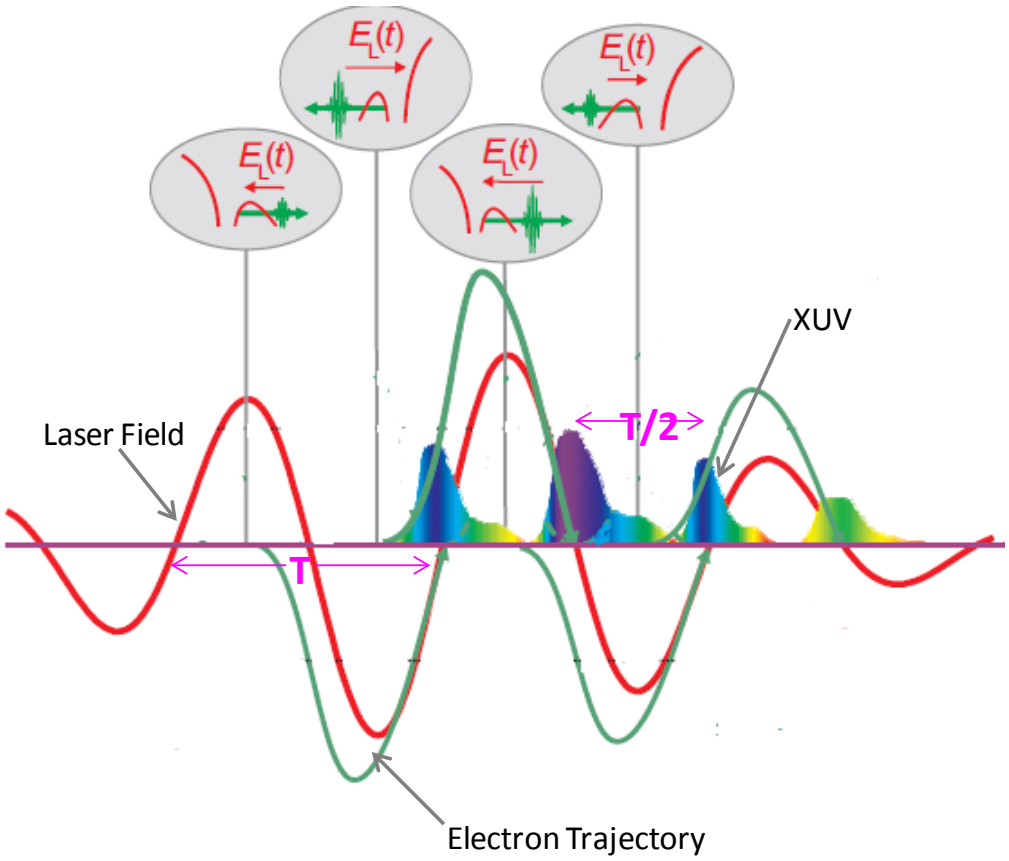

Figure 4: The production of high order harmonics; The periodic photon spectrum resulted through the interference of the photon wave packets released twice per laser cycle due to each recollision process[1].

1.3.1 High harmonic generation (HHG)

According to the classical consideration the recombination of the electron to the ground state in a laser field should emit a photon with maximum energy of I_p + 3.17 U_p. The highest possible energy from rebounding of an electron to a ground sate in a laser field is 3.17U_p (I_p is the ionization potential and U_p is the ponderomotive potential). This energy criterion is in agreement with the cutoff of the HHG spectrum. Therefore, HHG can be regarded as a process of tunneling ionization plus recombination within one laser period and repeated over many periods as a periodic process[42].

HHG process has been implemented with the use of both noble gas atom targets or molecular gases[44, 45]. The process is repeating every half optical cycle producing harmonics separated by twice the optical frequency. During this process usually the odd order harmonics are observed due to the inversion symmetry of the gas targets. Any induced polarization of a media consists of an inversion symmetry as an odd function of the electric field. This process can be simplified as the production of a series of higher frequency radiation of nf_i (n= odd integers) from a high intense laser field of frequency f interacts with a medium of noble gas atoms (Figure 5).

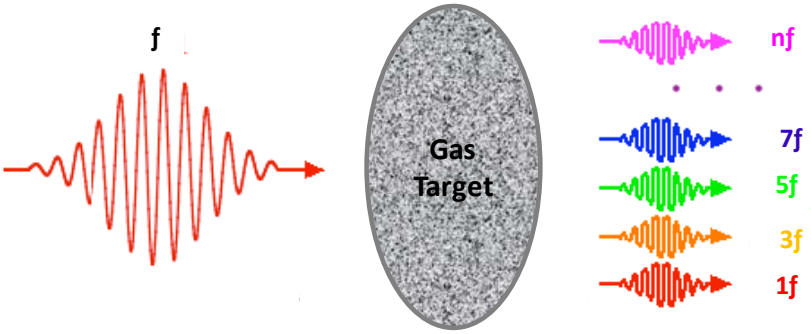

Figure 5**:** The schematic representation of harmonic generation process.

In the high harmonic spectrum, the produced harmonics are showing fairly uniform intensity with the increasing harmonics of equal brightness (plateau region) and a sharp cut off at the end of the spectrum (Figure 6). This feature of the HHG process is explained by the three-step model and it shows that the cut-off = $I_p + 3.17U_p$. The spacing of harmonics in the spectrum is equal to twice of the frequency of the driving laser.

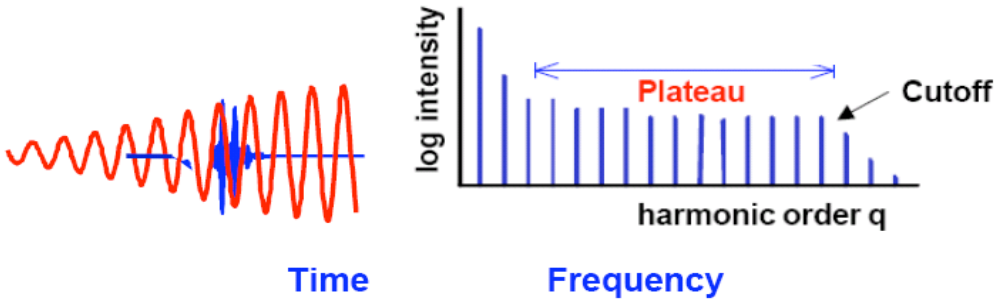

Figure 6: Characteristic feature of the high harmonic spectrum.

The main obstacle in the HHG process as a coherent light source is to achieve the higher conversion efficiency. The phase mismatch of the generated high harmonic pulses is one reason for a lower conversion efficiency[46]. In addition, the usual high intensity lasers used as the driving lasers in HHG has a lower repetition rate to achieve a high pulse energy because this limits the overall flux of the produced high order harmonics. The Different phase matching schemes[47-50] and fundamental laser-matter interaction process [51] were considered to be the main optimization criteria for understanding and increasing the conversion efficiency of the HHG.

1.3.2 Attosecond Pulse Generation

There are two technical approaches in generating attosecond pulses. The attosecond pulse trains (APT) are generated through the process of a combination of the number of harmonics in the plateau region, which results in a broad spectrum of a sequence of attosecond pulses. The resulting attosecond pulses are separated by half of the driving laser period (T) and the duration of each pulse is inversely proportional to the range of the frequencies (Δf) of the added harmonics ((Figure 7(a)). The other approach is the production of isolated attosecond pulses (Figure 7(b)) with the use of a few cycle lasers as the driving laser. Both approaches have their own pros and cons and will be discussed in detail in chapter 4.

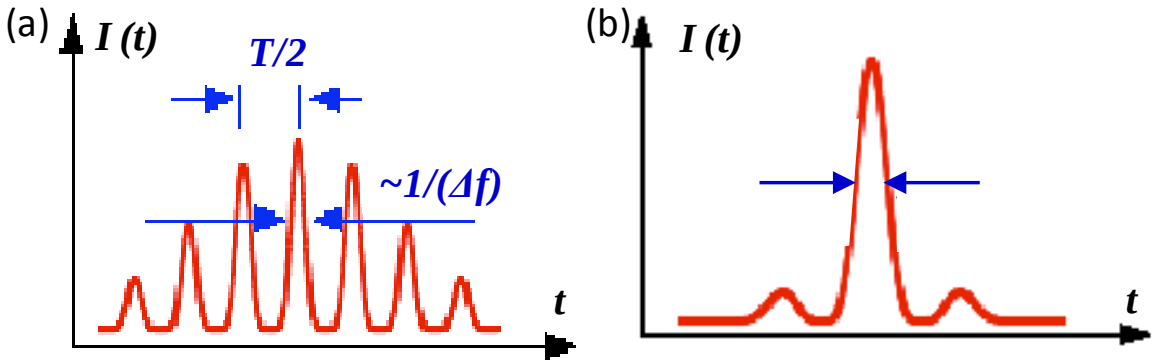

Figure 7: The two frontiers of attosecond pulse generation. (a) attosecond pulse trains (b) Isolated attosecond pulses.

In the studies toward developing a real-time probe for reaction dynamics, many experiments have focused on the production of soft X-ray radiation using HHG

processes. If the driving laser is an infrared (IR) laser, it will produce harmonic radiation with the frequency ranges from optical to the extreme ultraviolet (XUV) range. Consequently, HHG is used as a XUV source and has been utilized in the conventional applications of XUV spectroscopy[52] and XUV interferometry[53]. The interesting feature of this coherent, directional and sub-femtosecond pulses of XUV radiation is that they can be either used as a train of short-pulses separated by the half of the driving laser cycle[54] or a single pulse of coherent XUV radiation[55]. Regardless of a train or an isolated pulse, XUV radiation in the sub-femtosecond duration range is capable of reaching the level of electron dynamics in atoms and molecules thus became a valuable tool in field of attosecond science.

Similar to femtosecond spectroscopy the best and most effective way of implementing attosecond spectroscopy would be using XUV-pump-XUV-probe type experimental approach. Where a sub-femtosecond X-ray pulse is used to excite the ultrafast dynamics and take snapshots of those microscopic events. The few common applications of this type of experiments are non-sequential two-photon double ionization and charge migration driven by electron correlation and relaxation[56]. However, the XUV probe metrology always become crucial due to the limitations bound to the production of XUV-photons with sufficient flux and an appropriate detection system capable of extracting electron-electron correlation dynamics. On the other hand, the conventional attosecond pump-probe experiments are done as two-color XUV plus near-infrared (NIR) setup and was implemented in considerable amount of applications [1, 57, 58]. In this case a NIR pulse (few-cycle laser pulse used to generate the attosecond pulse) is used as the pump or probe beam while, the optical cycle of the NIR

provide the attosecond time resolution. However, the moderately strong NIR pulse tends to affect the dynamics instead of observing them. Those types of obstacles are assumed to be avoided by the XUV-pump-XUV-probe experiments. The other approach is to use one IAP as pump followed by another IAP as probe[59, 60]. Still the fairly lower intensity inherited by IAPs seems problematic.

The above discussed importance of attosecond spectroscopy and the limitations of the conventional experimental approaches have motivated the novel implementations for attosecond spectroscopy experiments. The sophisticated detection systems as coincidence measurements are also considered. Therefore, this thesis was focused on implementing an experimental setup which is capable of performing XUV-pump-XUV-probe experiment with a suitable detection method. We believe this approach would be beneficial as a probe in studying electron dynamics in its natural timescale. Under these research goals, an effort was made to produce a focused attosecond pulse trains with sufficient flux for two photon double ionization using loose focusing geometry with a Ti:Sapphier laser system at 1 kHz repetition rate. This high pulse energy and high repetition rate would allow state-of-the-art ion-electron coincidence measurements on two-photon-double-ionization experiments. A detection system of ion-electron coincidence measurements will be built to carry out coincidence measurement of resulted two electrons; or even more strictly, a coincidence among two electrons and one dication, which has never been reported so far.

To encapsulate, this thesis work has been focused on developing probes to study nuclear and electronic dynamics in real time. Considerable attention was given to investigate the utility of SFI in probing atomic orientation effect which will indeed be

useful in the wide application areas of circularly polarized light as angular streaking technique and isolated attosecond pulse generation from polarization gating experiments. Through these studies, it has successfully revealed the dependence of SFI rate to the sign of magnetic quantum number using double ionization of argon. Also the extended studies have provided the information of the helicity dependence of SFI in krypton and xenon and the role of laser intensity on this manner. In the process of developing tools to pin down the electron dynamics by studying electron-electron correlations non-linear attosecond spectroscopy become an interesting field which still has not been implemented successfully enough. Therefore, the second focus of this thesis work lies in developing an experimental setup capable of producing high flux attosecond pulse trains to enable two photon double ionization together with ion-electron coincidence measurement capabilities. Last part of this thesis work provides a detailed demonstration of the experimental apparatus of the HHG setup and the background optimization to achieve the ion-electron coincidence measurements. Finally, the very first ion-electron coincidence measurements of two-photon double ionization of xenon obtained from the intense attosecond pulse trains are presented.

CHAPTER 2

Strong Field Ionization Probe[1]

2.1 Introduction

In the process of developing an ultrafast probe, effort has been taken to explore the ability of strong field ionization (SFI) to probe photodissociation dynamics. SFI becomes good choice due to its high sensitivity to the detailed atomic properties combined with an inherited short pulse width. It has been used previously as a probe to study the photodissociation of Br_2 by monitoring the electron rearrangement[29, 30]. Taking another step to extend the utilities of SFI probe, in this particular study we have demonstrated SFI as a successful probe in probing orbital alignment[61] and atomic orientation[62].

The orbital polarization (alignment or orientation) of atomic fragments arising from dissociation is a unique property, which reflects the information regarding the potential energy surface where the photodissociation event has taken place. This type of information is fairly useful since it describes the detailed dynamical parameters such as state symmetry, coherent effects, and non-adiabatic transitions, which will help reveal the underlying dynamics of the photodissociation process. Therefore, a considerable effort has been taken over past decades to study and understand the atomic orbital polarization using ion imaging techniques[11-16, 18-21, 63], core-sample time-of-flight (TOF)[22, 23], Doppler spectroscopy[24, 25], fluorescence detection[26],

[1] Portions of the text in this chapter were reprinted or adapted with permission from 61. Lin, Y.F., et al., *Orbital alignment in photodissociation probed using strong field ionization.* Journal of Chemical Physics, 2011. **135**(23): p. 234311. and 62. Herath, T., et al., *Strong-Field Ionization Rate Depends on the Sign of the Magnetic Quantum Number.* Physical Review Letters, 2012. **109**(4): p. 043004. .

absorption spectroscopy[27, 28], and etc. However these methods have drawbacks such as time consuming measurements, complicated analysis and the difficulty of performing time-domain atomic polarization studies. For example, ion imaging accompanied with resonance enhanced multi-photon ionization (REMPI)[64], the general tool of current polarization measurements is also limited only to extract the dynamics in asymptotic region due to the nanosecond time scale. Therefore, in theory by conducting REMPI studies using a tunable femtosecond pulse, one can extend their studies to much more detailed level by extracting dynamics in Frank-Condon region and the long-range region. However, the broad bandwidth of short pulses can over shadow the state selectivity of the measurements which makes the ultrafast REMPI studies extra difficult. On the other hand SFI, an extreme extension of REMPI shows higher sensitivity to detailed atomic properties, thus useable in probing even weak atomic polarization. This will open doors to reveal the detailed reaction dynamics which has never been observed.

The atomic polarization can be referred to atomic alignment and orientation, which can be directly illustrated by the population distributions among the magnetic sublevels (m_l). The equal populations over magnetic sublevels are evidence of an isotropic electron density distribution (Figurer 8(A)). An unequal m_l distribution reflects a polarization of the electron orbital angular momentum, thus causes in an anisotropic electron density distribution. As shown in figure 8(B), alignment can be represented by the unequal population distribution proportional to the different non-statistical m_l levels. Sensitivity of SFI facilitates the probing of such anisotropic distributions using linearly or circularly polarized light. On the other hand, the orientation

is reflected by the unequal population distribution proportional to each m_l (Figure8(C)) which can only be probed by the circularly polarized light. The sensitivity of SFI rate to the sign of m_l provoked the SFI as a probe of atomic orientation.

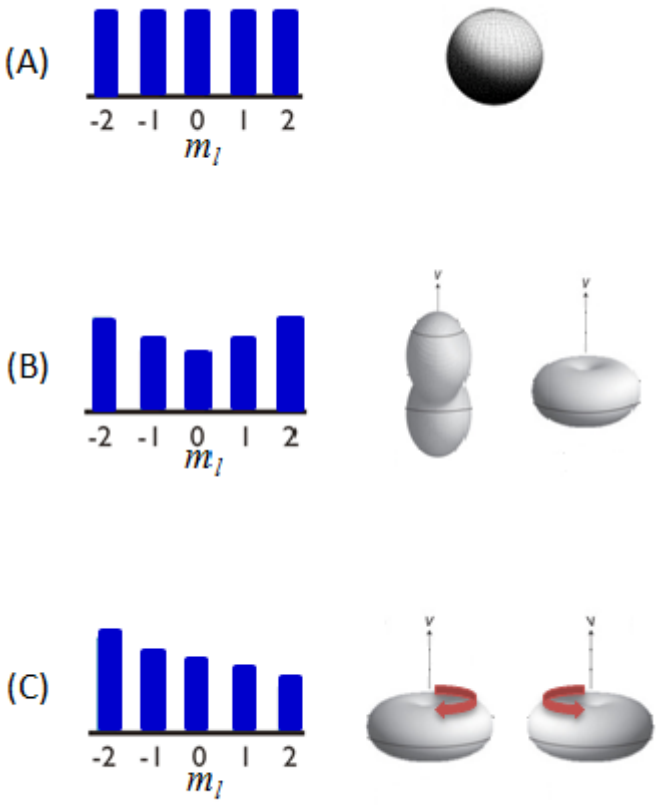

Figure 8: Schematic illustration of atomic polarization effects and electron density distributions. (A) Isotropic, (B) alignment, (C) orientation, effects represented by the populations among the magnetic sublevels and corresponding electron density distribution.

Next two sections of this thesis describe the experimental characterization of SFI as a tool in probing atomic orbital alignment and the atomic orbital orientation.

2.2 Strong Field Ionization Probe of Orbital Alignment

The ion imaging methods employing the REMPI probe used to probe orbital alignment is sensitive to the angular momentum polarization as a function of photo-fragment recoil direction described by a series of multiple moments related to the density matrix of the excitation function[19]. Recall the equation 1.1 in Chapter 1;

$$w \propto \left(\frac{(2l+1)(l+|m|)!}{2^{|m|}|m|!(l-|m|)!} \right) \left(\frac{3F_0}{\pi F} \right)^{1/2} \left(\frac{2F_0}{F} \right)^{2n-|m|-1} e^{-\frac{2F_0}{3F}}$$

SFI rate shows a higher sensitivity to the nonstatistical m_l numbers. In this particular study the sensitivity of SFI in atomic polarization/alignment was studied by looking at the anisotropy of the electron charge cloud. This was done by mapping out the shape of electron density of sulfur atoms in ethylene sulfide (C_2H_4S) and carbonyl sulfide (OCS). This angular dependent ionization rate is an evidence of the charge cloud anisotropy and the degree of anisotropy indicates the m_l distributions. Therefore, the shape of the electron density of sulfur atoms in the photodissociation of C_2H_4S and OCS were mapped with respect to the rotation of the polarization of the probe laser electric field.

2.2.1 Experimental Approach

The experiment was carried out in a similar setup to the "raster imaging" methods, introduced by Suits and co-workers[65] (Figure 9) developed to slice the photo-fragments with a particular recoil velocity and an angle. A pulsed supersonic molecular beam of C_2H_4S produced by bubbling the carrier gas through a liquid sample

of C_2H_4S (Sigma-Aldrich, 98%) was introduced to the differentially pumped apparatus through the pulsed valve. In the analysis of OCS, a neat OCS sample was expanded into the source chamber and collimated by the skimmer. Once the molecular beam enters into the velocity mapping electrode assembly, it was intersected at right angles by two counter-propagating laser beams (Figure 9). The photolysis laser light (193 nm) was generated by an argon fluoride excimer system with a power of 2 mJ/pulse, loosely focused onto the molecular beam using a 50 cm focal length lens. The probe laser light was provided by a femtosecond Ti:sapphire amplified laser system (45 fs, 1 kHz, 800 nm, KMLabs, Wyvern 1000) with the power of 1 mJ. The estimated laser intensity at the focal point is 2×10^{13} W/cm^2.The probe laser was placed downstream, a few millimeters from the photolysis laser, and it was also placed off-axis from the molecular beam. This arrangement will prevent the strong background related to the ionization of the parent ion and minimize the space charge effect. The linear polarization of the photolysis laser was achieved using eight fused silica windows set at their Brewster's angles. Once unpolarized, the 193 nm laser passed through this assembly producing horizontally polarized light, which is also parallel to the plane of detection. However to enhance the signal level of OCS, an unpolarized UV beam was used directly due to its very small absorption cross section at 193 nm. Consequently, we have observed a reduced anisotropy of angular dependent ionization rate. Therefore the modulation we observed for OCS is generally lower. Then the total ion yield was measured by changing the probe laser polarization angle from 0° to 180°, using a half wave plate. The resulted ions were detected using the position sensitive dual MCP/phosphor screen detector plus charge coupled device (CCD) camera combined with the IMACQ acquisition

program[66]. In order to minimize the effects of experimental fluctuations, data was replicated a few times and the average ion yield plotted against the probe polarization angle. Furthermore the data were calibrated for the background signals using water (H_2O) background present in the chamber. With this calibration it was expected to suppress interference of the systematic anisotropy, introduced by the optics, with the measurements itself. In these measurements the furthest sulfur atom was chosen. This condition was achieved by the displacement of the probe laser from both the photolysis laser and the molecular beam.

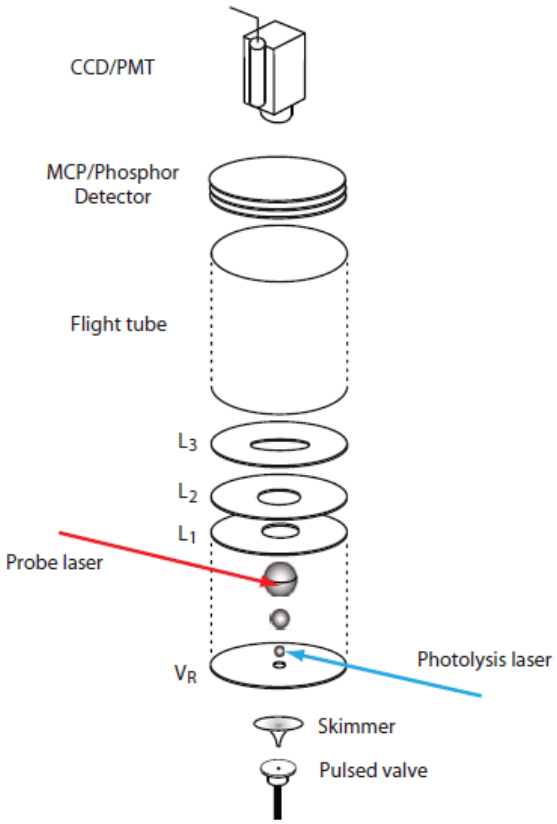

Figure 9: Schematic representation of the experimental setup (adapted from Lin *et al.*).

2.2.2 Results and Discussion

In this experiment, the plotted data of ion yield verses probe polarization angle shows the angular dependent ionization rate of sulfur atoms for the photodissociation of C_2H_4S and OCS at 193 nm (Figure 10). Further, the modulations were verified using carbon disulfide (CS_2) molecules with the measured modulation of CS^+ which indicates that in our setup, there were no clear alignment effects in the parent molecules. With the observed higher noise level for CS^+ verifies the lack of smoothness of the curves observed for the C_2H_4S and OCS were due to the common small fluctuations in experimental conditions. However the same trend of the angular dependent ionization rate of sulfur atoms in both samples was clearly observed.

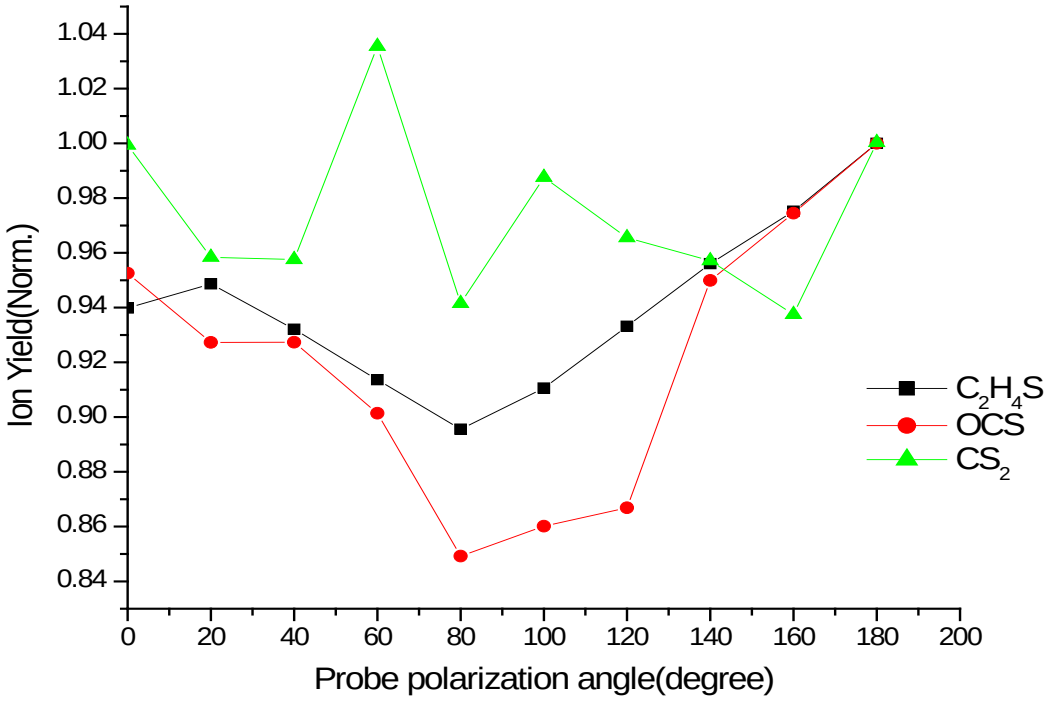

Figure 10: Angular dependent ionization rate of sulfur atom with the recoil velocity along the photolysis laser polarization of C_2H_4S, OCS and CS_2.

These raw data were further analyzed and fitted using the method described below. The resulted angular dependent strong field ionization yields of sulfur atom were plotted against the polarization angle between pump and probe beams (Figure 12(a)) and the fitted results are given in red curves. The angular distribution of ion yields were fitted using the "basis" functions in order to extract the population of each magnetic sublevel. These basis functions were derived using the angular dependent ionization probabilities corresponding to each extreme population. Particularly, for sulfur (S ($^1D_2$)) case, the angular quantum number (l) is 2 (l=2) and the m_l has (2l+1) number of values (-2, -1, 0, 1, 2). Therefore, three possible extreme cases can be found. If P is the population of a magnetic sublevel corresponding to the recoil direction which is parallel to the polarization axis of the photolysis laser, the three extreme cases can be given as $P(|m_l|=0)=1$, $\sum P(|m_l|=1)=1$ and $\sum P(|m_l|=2)=1$. The angular dependent ionization probabilities of these extreme cases were calculated over the laser intensity envelop in time-domain and the density matrix was then transformed with the rotational matrix as given by the equation below.

$$I(\theta)=\sum_{|m_l|} a_{|m_l|}\, D_{|m_l|}(\theta).\int \omega(F,l,|m_l|)F(t)dt \qquad (2.1)$$

Where $I(\theta)$ - Measured angular dependent ion yield

$a_{|m_l|}$ - Population Coefficient of each extreme case

$F(t)$ - Time dependent laser electric field

$D_{|m_l|}(\theta)$- Density matrix at the angle θ

Then equation 2.1 is used to construct the fitting for angular basis functions as shown in figure 11.

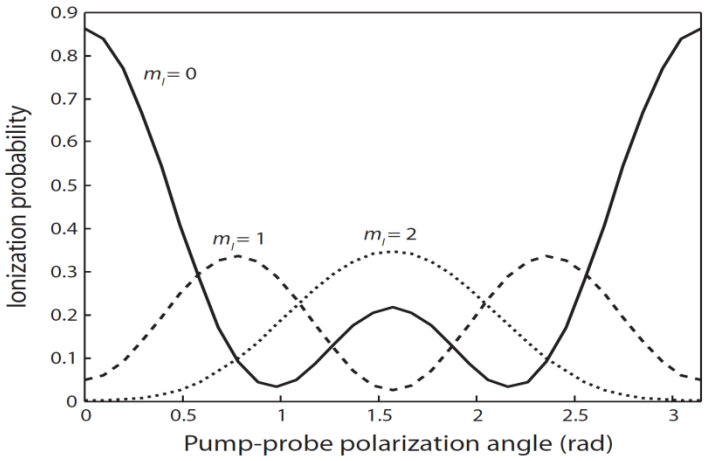

Figure 11: Angular basis functions.

The constructed m_l populations for and OCS are given by figure 12(b). As it indicates a dominant population can be observed at m_l = 0 magnetic sublevel for both molecules. This reflects the fact that recoil velocity is perpendicular to the total angular momentum. Since the non-equilibrium m_l population distributions can be used to construct the electron charge cloud distributions corresponding to the alignment of the total orbital angular momentum[67], the obtained m_l population distributions of sulfur atom for both C_2H_4S and OCS were used to plot the corresponding charge cloud distributions (Figure 12(c)). In this study since we have ignored the off-diagonal elements (these elements are reflecting the coherence effect) of the density matrix, the resulted charge clouds are always showing a cylindrical symmetry.

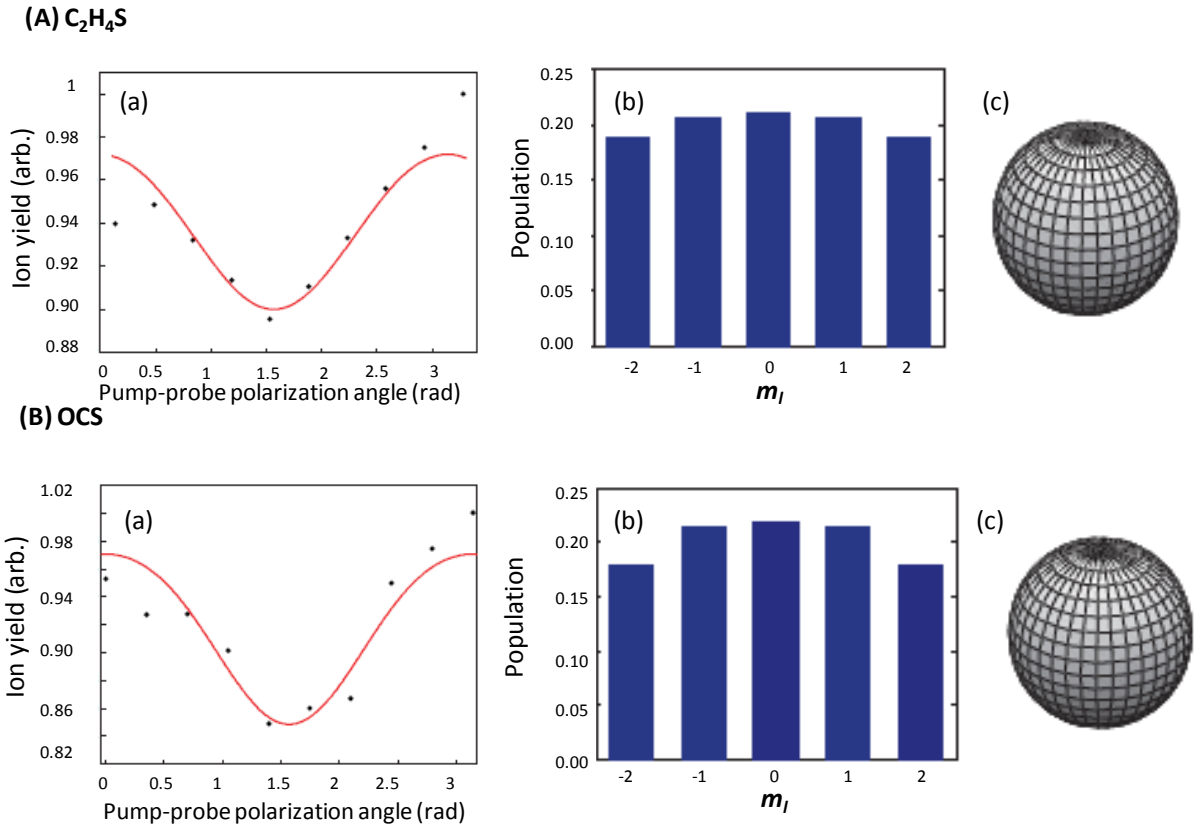

Figure 12: Angular dependent strong field ionization yield of sulfur atoms and the constructed $|m_l|$ distributions of (A) C_2H_4S (B) OCS; (a) SFI yield verses pump probe polarization angle. Red curve represented the fitted curve for the experimental data with the derived basis functions. (b) Extracted $|m_l|$ distributions of sulfur atoms. (c) Constructed electron charge cloud.

According to the results we have obtained for C_2H_4S it can be seen that the alignment in lower magnetic sublevel is favorable. This is due to the perpendicular transition to the vibrationally excited $4p_z$ Rydberg state. This is in agreement with the previous studies carried out using DC slice imaging with a REMPI probe[21]. They also verified that the sulfur atoms dissociate from multiple potential surfaces to $4p_x$ Rydberg

state via parallel transitions. However, in comparison to the ion imaging methods we have obtained higher magnitude in the alignment signal which implies the higher sensitivity of the SFI probe in atomic polarizations.

The results of the OCS show a discrepancy to the previous studies performed by Lee et al.[19] The comparison indicates that they have obtained the highest population at $|m_l|$=1 state. It is worth pointing out a few of the possible reasons for such a discrepancy. First of all, as mentioned in their paper higher order moments can cause overestimation. When only up to quadruple moment was included the results agreed with our results, which shows a peak at $|m_l|$=0. In our data analysis we have neglected the possible yield from the S(^{3}P) channel. If there was a considerable contribution from the yield from S(^{3}P), that could cause a difference in the modulations. This could be because we have used an unpolarized photolysis laser instead of the linear polarized laser in order to achieve a reasonable signal level.

In general we have shown the SFI is capable of probing atomic alignment effect in photodissociation events. SFI probe has its advantages such as simplicity and higher sensitivity than the previously used conventional methods. It also has a drawback in terms of the laser intensity estimations in the interaction region. This could lead for an uncertainty in constructing the basis functions. However, it is possible to use more accurate methods[68] in laser intensity calculation to overcome this obstacle.

As a conclusion, due to its extreme non linearity SFI can be used as a successful tool in probing orbital alignment in photodissociation events as demonstrated by this presented studies. This understanding is valuable in providing extra information

of the dynamical pathway of any photodissociation event and thus, eventually useful in studies of reaction dynamics.

2.3 Strong Field Ionization Probe of Atomic Orbital Orientation

So far the SFI rate dependence was discussed only with the non-statistical m numbers. However it would be even more useful to investigate whether there is a dependence of SFI with the sign of the magnetic quantum number, because it will facilitate the SFI to probe the information, such as time-resolved m distributions. Therefore, further studies were carried out in order to investigate the sensitivity of SFI to the atomic orientation. However, it is well known that in a one-photon ionization and field ionization of Rydberg states, there is a preferable ionization in circularly polarized light to the sign of *m*[69, 70].

In the field of tunnel ionization almost all equations show no dependence of the ionization rate to the sign of magnetic quantum number. A theoretical paper published by Tulenko *et al.* gives an explicit formula for SFI in a circularly polarized laser field, which also contained only the absolute value of the magnetic quantum number[71]. However, parallel to our experimental studies, Barth and co-workers published a theoretical study showing that there is a sensitivity of SFI rate to the sign of magnetic quantum number[72]. They have developed the following equations (2.3) which show an explicit dependence of the ionization rate on the sign of the *m.*

$$w_{p_m}(\varepsilon,\omega) = I_p \left|C_{kl}\right|^2 \frac{\varepsilon}{2\varepsilon_0} h_{p_m}(\gamma) e^{-\frac{2\varepsilon_0}{3\varepsilon} g(\gamma)}, m = \pm 1 \qquad (2.3)$$

Where,

w = Ionization rate

I_p = Ionization potential

$$h_{p_m}(\gamma) = h_s(\gamma)\frac{3(1+\gamma^2)}{2(1-\varsigma_o^2)}\left(\sqrt{\frac{\varsigma_o^2/\gamma^2+1}{1+\gamma^2}} \mp \frac{\varsigma_o}{\gamma}\mathrm{sgn}(m)\right)^2 \quad (2.4)$$

$\varepsilon_0 = (2I_p)^{3/2}$,

k - $\sqrt{2I_p}$

l - orbital quantum number

m - magnetic quantum number

$$g(\gamma) = \frac{3\varsigma_0}{\gamma^2\left(1-\varsigma_0^2\right)}\sqrt{\left(1+\gamma^2\right)\left(\varsigma_0^2/\gamma^2+1\right)}$$

The ζ_o is a parameter, for $0 \leq \zeta_o \leq 1$, ζ_o satisfies the equation of $\sqrt{\frac{1-\delta o}{1+\delta o}} = tanh\frac{1}{1-\delta o}\sqrt{\frac{\delta o^2+\gamma^2}{1+\gamma^2}}$. In their studies they found out that the ionization rate for m=-1 is three times higher than that of the m=+1 in circular fields.

Additionally, these studies become more interested since the circular polarized light has been used widely in the production of isolated attosecond pulses using polarization grating experiments[73, 74] and in the measurement of correlated electron dynamics by the angular streaking technique[75, 76]. Therefore, these studies are very important to the field of attosecond science.

2.3.1 Experimental Approach

In our lab we have conducted a simple pump-probe experiment in order to verify the dependence of the SFI rate on the sign of the magnetic quantum number in a circularly polarized laser field. The concept is to compare the sequential double ionization (SDI) yields of argon by two nearly-circularly polarized laser pulses with the same helicity and that with the opposite helicity. If SFI prefers one sign of the magnetic quantum number to the other, the first pump pulse would produce single ions with the oriented orbital angular momentum. The probe pulse will see this non-statistical *m* distribution and thus the total ion yield will be different depending whether the pump and probe have the same or opposite helicities (Figure 13).

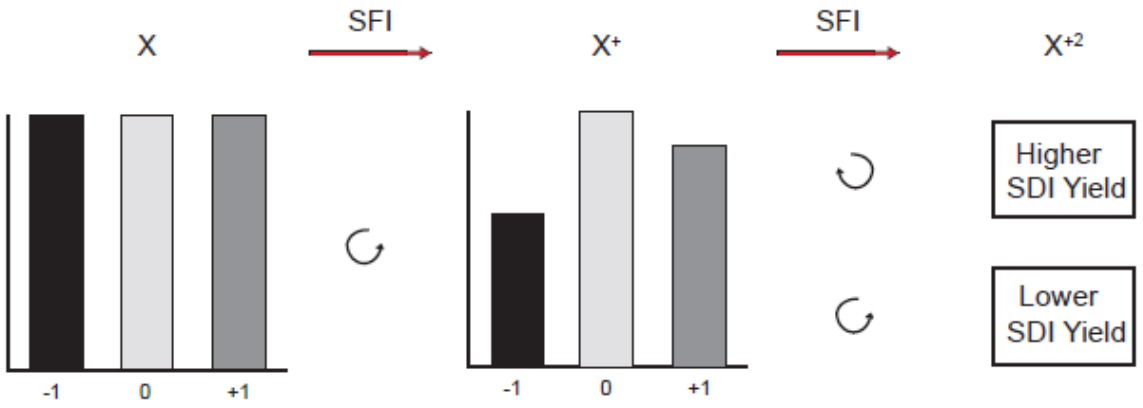

Figure 13: Schematic representation of the experimental approach of verifying dependence of SFI rate to the sign of *m.*

This experiment was performed with a newly built velocity mapping coincidence apparatus used as a time-of-flight spectrometer. As shown in figure 14, the laser beam was split into pump and probe beams with the power of 300 µJ, 600 µJ, and the corresponding laser intensities of ~$9x10^{13}$ W/cm^2 and ~$1.4x10^{14}$ W/cm^2, respectively. The quarter wave plates (QWP) were used in each beam to produce the circularly polarized light and the ellipticity of each beam is 0.8. The helicity of the pump beam was changed by rotating the QWP by 90 degrees and each case has ellipticity of 0.88 and 0.8. Argon gas was introduced to the chamber through a 20-micron diameter aperture. The produced dications, traveled through 20 cm flight tube, were then detected using MCP/Phosphor detector and recorded using a CCD camera conjunction with IMACQ acquisition program.

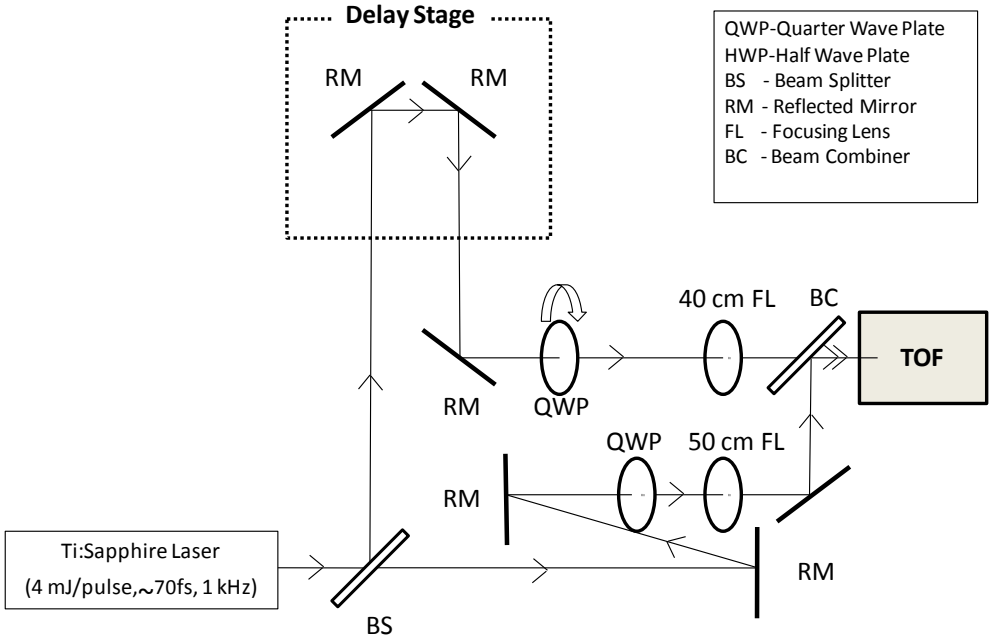

Figure 14: Experimental setup. A sketch diagram of the designed pump-probe experiment using circularly polarized laser field.

2.3.2 Results and Discussion

In this experiment first, the time-dependent ion yield of argon dications were extracted (Figure 15). Then the double ionization yield measurements were extracted when the two beams were delayed by about 500 femtoseconds in order to avoid the implications from the non-sequential double ionization (NSDI).

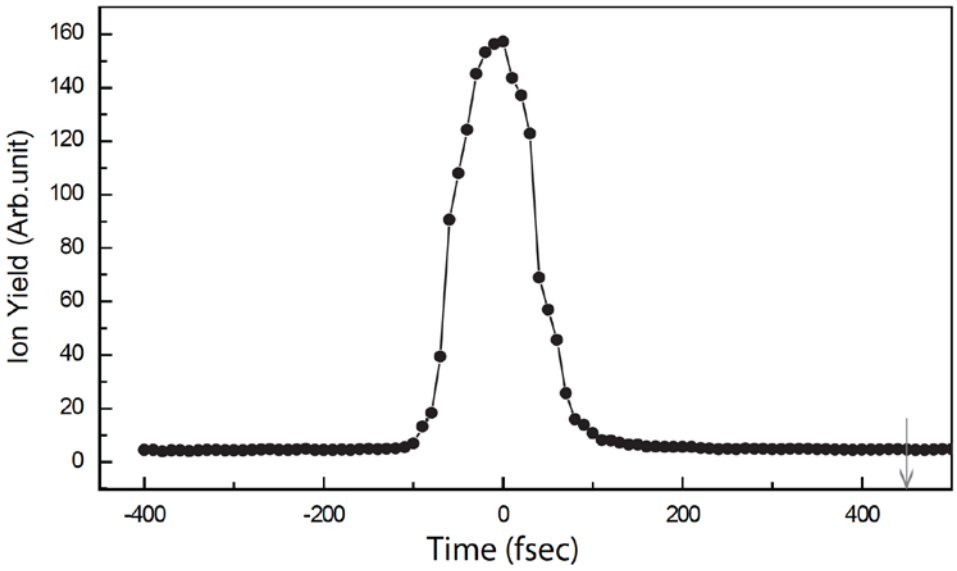

Figure 15: The time dependent Ar^{2+} yield. The grey arrow marks the time delay used for the data extraction.

Then, the SDI yield of argon was measured under four different laser conditions, as both lasers on (ion yield labeled as I_{pp}), pump beam off (I_{pr}), probe beam off (I_{pu}) and both beam off ($I_{d,}$ dark counts). The argon dications produced sequentially by the pump and the probe were calculated using the equation 2.5 given below.

$$I_{SDI}=I_{pp}-I_{pr}-I_{pu}+I_{d} \quad (2.5)$$

We recorded 10 sets of data with alternating pump polarization helicity and then all the data sets were averaged. The averaged data is shown in figure 16. The calculated I_{SDI-LR} (LR stands for the opposite helicity between the pump and the probe) and I_{SDI-RR} are 4.21±0.98 and 1.16±0.92, respectively.

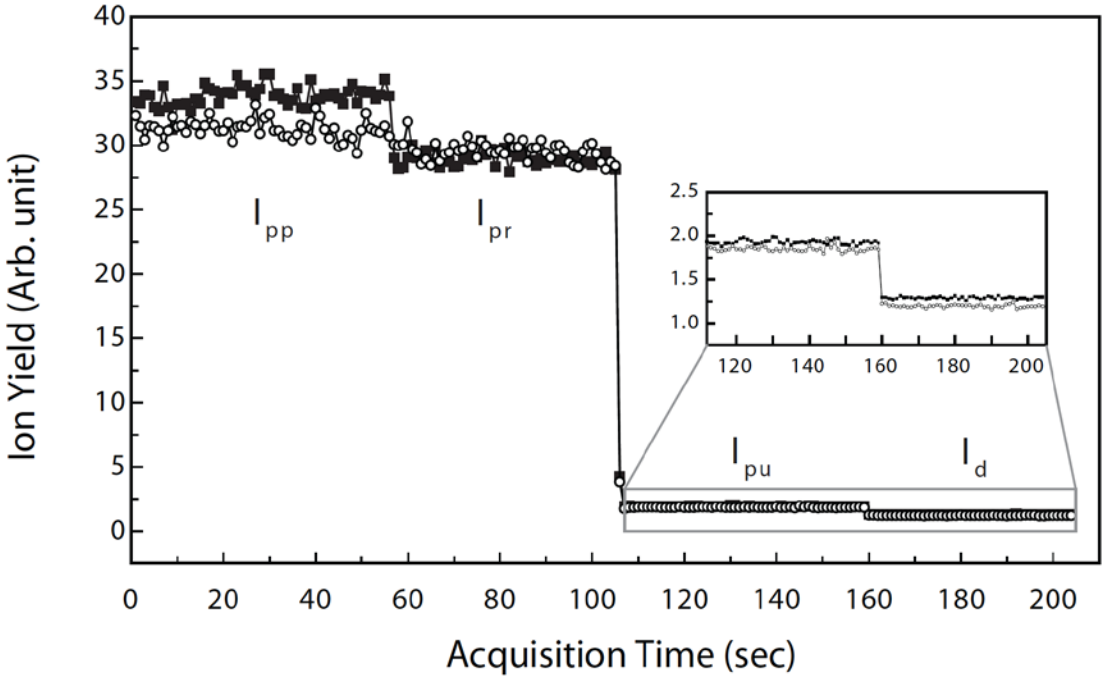

Figure 16: The ion yield of Ar^{2+} under different laser conditions: I_{pp} with both laser on; I_{pr}, the pump laser off; I_{pu}, the probe laser off; I_d, both laser off. Solid squares: opposite pump-probe helicity; hollow circles: same pump-probe helicity. The inset is a zoom-in of the ion yields with the probe laser blocked and both lasers blocked, showing the very small variation in ion yield for the pump alone case.

However, we still need to rule out the slight ellipticity difference between the right and left circular polarization of the pump beam. For this, we measured the single ion yield produced by the pump beam alone, they showed only <3% of difference between right and left circularly polarized light. This number is also consistent with the

dication produced by pump alone I_{pu}, which are varied by ~4% between two helicities. Therefore, the observed difference (>300%) in sequential double ionization of argon has to arise from the difference in relative helicity between the pump and the probe beams.

Data analysis was done by deriving an expression for the ionization rate ratio of m=+1 to m=-1. In argon, 3p sub shell has three magnetic quantum numbers of -1, 0, +1. If their ionization rates in right circularly polarized light are w_{-1R}, w_{0R} and w_{+1R}, respectively, the following expressions are true, $w_{-1R} = w_{+1R}$; $w_{0R} = w_{0R}$; $w_{+1R} = w_{-1R}$ by symmetry. Under the assumption of a flat laser envelope, we have related the expression for the ionization rate ratios at the two different helicity configurations to the measured ion yield ratio as shown by the equation 2.6.

$$\frac{I_{SDI-LR}}{I_{SDI-RR}} = \frac{(\alpha+\beta)\alpha'+(1+\alpha)\beta+(1+\beta)}{(1+\beta)\alpha'+(1+\alpha)\beta+(\alpha+\beta)} \tag{2.6}$$

Where, $$\alpha = \frac{w_{-1R}}{w_{+1R}}; \alpha' = \frac{w'_{-1R}}{w'_{+1R}}; \beta = \frac{w_{0R}}{w_{+1R}}; \beta' = \frac{w'_{0R}}{w'_{+1R}}$$

(Prime denotes the ionizations corresponding to the probe beam.)

Since the ionization rate of m=0 sublevels are comparatively smaller than that if m=±1 the equation 2.5 can be further simplified to the following expression.

$$\frac{I_{SDI-LR}}{I_{SDI-RR}} = \frac{\alpha\alpha'+1}{\alpha+\alpha'} \tag{2.7}$$

It can be seen that if either ratio is 1, which shows no preference between the signs of the magnetic quantum number, the right hand side of equation 2.7 becomes unity no matter what the value of the other ratio is and thus no enhancement or suppression will be observed in the measured ion yields. A non-unity ratio between ion yields requires that strong field ionization in circularly polarized light prefers one sign of *m* to the other in both neutral and single ions.

According to the experimental data we obtained a non-unity value for this ratio which is 3.63. We used this value in equation 4 and plotted α vs. α' (Figure 17). This plot shows that both ratios are higher than 3.63 while the exact values depend on their positions at the hyperbola. These larger than unity ratios indicate the fact that in the processes of ionizing neutral atoms and single ions by circularly polarized light, the same sign of *m* is preferred.

The theoretical ionization rate ratios were calculated as a comparison between the experimental results and the prediction of theory. The Keldysh parameters were calculated according to the intensities of our pump and probe beams and the values turn out to be 1.2 and 1.3. Then by using the equations (2.2) given in the studies of Barth et al, the values of α, α'were calculated to be 4.0, and 4.2, respectively. In experimentally under the assumption of $\alpha=\alpha'$, due to very similar Keldysh parameters, the values of α, α' are 7.1. These are almost twice of the theoretical values. Considering the large uncertainty in the experiment measurement, they appear in fair agreement. However, a more realistic comparison between the experiment and the theory has to include the laser intensity and focal volume averaging. Here we show the

laser intensity averaging tends to reduce the observed ion yield ratio. The laser pulse used is a Gaussian-shaped 70 fs FWHM pulse with a temporal intensity profile of *F(t)*. The peak intensity is adjusted so that the integration of the total pulse envelope matches the average intensity measured in the experiment. The form of equation 2.7 still applies while the ionization rate ratios α and α' are replaced by the ionization probability ratios, which are computed as $\chi = \frac{\int w_{-1R}(F(t))dt}{\int w_{+1R}(F(t))dt}$ and $\chi' = \frac{\int w'_{-1R}(F(t))dt}{\int w'_{+1R}(F(t))dt}$, where $w_{-1R}(F(t))(w'_{-1R}(F(t)))$ and $w_{+1R}(F(t))(w'_{+1R}(F(t)))$ are the ionization rates of *m=-1* and *m=1* for the pump (probe) at a laser intensity of *F(t)*. All ionization rates are taken from reference[72]. The calculated ionization yield ratio between the two helicity configurations is 1.56, which is much smaller than the measured 3.63 and also smaller than that calculated with the average laser intensities. A focal volume averaging is likely to further reduce this ratio. It is possible to achieve a better agreement by varying the laser intensity. However this requires the laser intensity to be at least one order of magnitude lower than the experimental values and this is beyond the uncertainty in estimating the laser intensity. We conclude there is a quantitative discrepancy between experimental measurements and the theoretical predictions. However, recent theoretical work of Bath and co-workers[77] verifies that the origin of this discrepancy can be overcome by focal volume averaging. Further, they have reported the calculated values of ionization rate ratios to be 6.6 which are in close agreement with the experimental values of 7.1. Accordingly, we can now conclude that the results are in a good quantitative and qualitative agreement with the theoretical predictions.

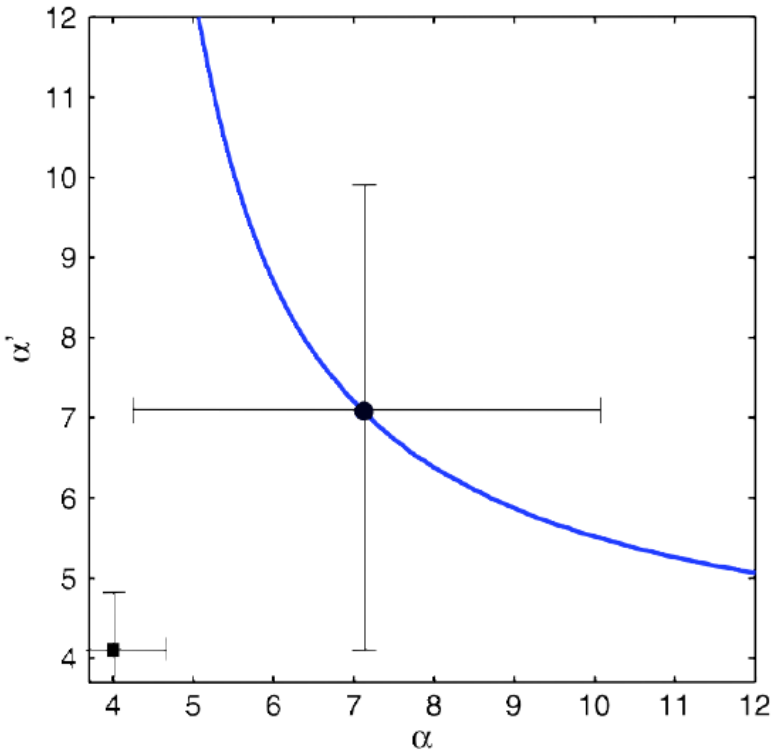

Figure 17: The experimentally constrained ratios of strong field ionization rates between *m=1* and *m=-1* sublevels of neutral argon atom (α) and single argon ion (α') by right circularly polarized light. The black square shows the ionization rate ratios calculated from the theory by Barth et al. (the uncertainty arises from the laser intensity estimate, which is ~20%). The cross marks the values extracted from the experiment if α and α' are assumed to be equal due to similar Keldysh parameters.

In order to understand the observed results in an intuitive way, we proposed the coulomb suppressed barrier as a "doorway" for electron to tunnel out (Figure 18) However, this doorway is not fully open and it is only with a certain probability (*P*) that electrons can tunnel out even though they are spatially close this doorway. For circularly polarized light, this doorway is rotating at the frequency of the laser. For rotating electrons with a nonzero magnetic quantum number, the helicity is determined by the sign of *m*. The relative helicity between electrons and photons affects

the encounter frequency between the electrons and the suppressed barrier (γ). The encounter frequency can be estimated with $\gamma=v_e\pm v_L$ where v_e, v_L are the frequency of the electron rotation and the laser frequency, respectively and the plus sign is used for the opposite helicity. The final ionization probability can be written as γP.

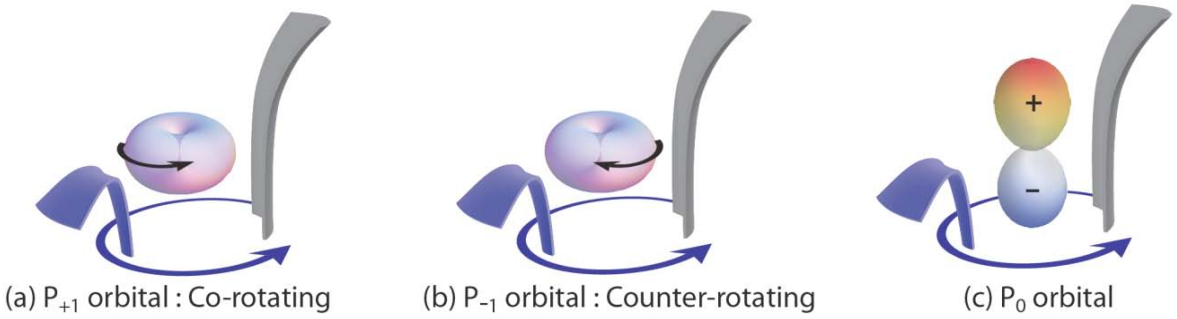

Figure 18: A schematic representation of the effect of the relative rotation of the electron and the photon on the ionization rate when picturing the SCB as a doorway for tunneling. When they are (a) with the same helicities (b) with the opposite helicities (c) at P_z orbital, the ionization rates were considered.

According to this simple picture we can conclude the followings:

(1) Electrons counter-rotating with the laser helicity will be preferably ionized.

(2) The ionization rate increases with the laser frequency for counter rotating but decrease for co-rotating electrons while the ratio between them increases.

(3) The ionization rate for $m=0$ sublevel is greatly reduced due to a destructive interference.

These results are in general agreement with the previous theory[72] except that in their calculation the ionization rate of co-rotating electron also increases slowly with the laser

frequency. It will be interesting to compare these with experimental data at different laser frequencies or numerical methods.

With the observed measurements of the dication yield with two spatially overlapped but temporally delayed near circularly polarized laser we can summarized the strong field ionization rate by circularly polarized light depend on the relative helicities of the photons and electrons. Our measurements indicate that for the argon ionization the dication yield for the opposite photon helicity is three times higher than that with the same helicity. It can be also concluded that the single ionization of both neutral and ion preferred the same sign of magnetic quantum number. Even though these conclusions were made with argon we believe it is common for any atom with non-zero orbital angular momentum.

As a conclusion, the first experimental observational of the dependence of strong field ionization rate on the sign of the magnetic quantum number was seen providing an insight to the studies related to the SFI as an ultrafast probe of photodissociation dynamics that involves orbital orientation.

2.4. Summary

To summarize, the utility of SFI as a probe in nuclear/structural dynamics has taken another step forward with the studies of its sensitivity to atomic alignment and atomic orbital orientation discussed in this chapter. These studies reflect the fact that the developed SFI is an ultrafast probe with the sensitivity of atomic polarization and can be implemented in time-resolved atomic polarization studies. Further investigations on SFI rate dependence of atomic orbital orientation in different systems were performed in order to study the effect of spin orbital coupling and will be described in the next chapter.

CHAPTER 3

Helicity Dependence of SFI in Krypton and Xenon

3.1 Introduction

To date, circularly polarized laser fields have been used in many important studies related to ultrafast science. In production of isolated attosecond pulses using polarization gating experiments[74,78] is one of the known examples. Also in attosecond streaking experiments a strong circularly polarized laser field is used as a probe to study electron dynamics in atoms and molecules[75,79]. With the application of circularly polarized light in the field of ultrafast science, it is important to pay more attention to how the tunneling picture is affected by the ellipticity of the desired laser field. So far, even in the circularly polarized laser field, the tunneling process is treated as an adiabatic process, which implies that the motion of the tunneling barrier does not affect the electron dynamics and those electrons that escape along the direction of the electric field regardless of the rotation in each tunneling event.

It is well known that in one-photon ionization circularly polarized light preferentially ionizes the co-rotating electrons with the circular field than the electron rotated in the opposite direction[80]. Also in the field ionization of Rydberg states, the ionization is dominant for the Rydberg electrons co-rotating with the circularly polarized microwave field[69, 70]. However, as described in chapter 2, recent theoretical studies have placed attention on exploring the selectivity of strong field ionization to the sign of magnetic quantum number in circularly polarized laser fields[72]. In these studies, they have shown that in contrast to one-photon ionization and Rydberg state ionization, in

tunneling, electron counter-rotating with circular laser field preferably escape through the tunneling barrier. This theoretical prediction supported our experimental hypothesis of investigating the dependence of SFI rate to the atomic orbital orientation. In our lab we have designed a fairly simple experiment to empirically verify the dependence of SFI rate on the sign of the magnetic quantum number (m).

As described in chapter 2, we have successfully demonstrated that probing atomic orientation shows a dependence between the SFI rate ionization and the sign of m. The experiment was carried out by measuring the sequential double ionization (SDI) yields of argon, using two nearly-circularly polarized laser fields with the same helicity and opposite helicity [62]. If SFI prefers one sign of the magnetic quantum number over the other, the first pump pulse would produce single ions with a non-statistical m distribution (the ion's orbital angular momentum is orientated). The probe pulse will see this m distribution and thus the total ion yield will be different depending on whether the pump and probe have the same or opposite helicities. With this experiment we discovered the strong field ionization rate depends on the relative helicity of the photon and electron. Particularly, for argon the measured yield of counter-rotating helicities are three times higher than that of the co-rotating case. However, a discrepancy was seen between the theoretical values and the experimental values observed in these studies.

It has occurred that it is worth to extend these studies to further investigate how the helicity dependence of the SFI probe is affected by factors such as laser intensities. Moreover, since argon is the only system which shows such dependence so

far, we have taken a further step to see if the other noble gases are sensitive to the helicity dependence of SFI. Especially, the more complicated atoms with spin orbital effect, such as krypton and xenon. It will be also interesting to see how the helicity dependence would change as it goes from argon to xenon. That might provide additional information regarding the process based on the properties changing over a period in the periodic table. In a circularly polarized laser field with its sensitivity to the electron rotation having the spin orbit interactions will complicate the picture. Therefore, the helicity dependence of krypton and xenon were also studied by comparing the sequential double ionization yield for similar and opposite helicities between the pump and probe beams.

Laser intensity is a key feature which could directly influence the modulations of double ionization yields. As given in the theoretical studies of Bath and co-workers[72] the ionization rate of co-rotating electrons with the laser helicity increases with the laser frequency. This however is not in agreement with our previous understanding as described in chapter 2. To recall, we have concluded that the ionization rate increases with laser frequency for counter-rotating electrons with the laser helicity but decrease for co-rotating electrons while the ratio between them increases. This controversy directed our experimental studies to measure these ratios in order to have a comparison between the experimental verses theoretical understandings. Therefore, the variation of the modulation depth of the helicity dependence with varying laser intensities, were studied as well. There are considerable studies of understanding double ionization probabilities as a function of laser intensities[81-83]. It is been well understood that, in the presence of an intense laser

field there are two possible mechanisms for double ionization. SDI related to a single active electron approximation and the non-sequential double ionization (NSDI), the emission of two electrons due to the e-e recollision between a core electron and the ionized electron which brought back by reverse phase of the laser field. Many experimental and theoretical studies confirmed that in different intensity regimes, different double ionization mechanisms become dominant. Specifically it is known to be that the electron correlated double ionization mechanism, the NSDI is showing several times higher probability of ionization than the SDI for certain intensity regimes. This even resulted a "knee" feature in the plot of double ionization probability as the function of laser intensities[84,85]. These kind of interesting features motivate us to study the intensity dependence on helicity base modulations of double ionization in krypton and xenon.

3.2 Experimental Approach

The experimental setup is similar to the setup used in our previous studies [62]. The velocity mapping coincidence apparatus was used as a time-of-flight spectrometer to measure the ion yield in these studies. The laser was a ~70 fs, 1 kHz Ti:Sapphire amplification system (KMLabs, Red Dragon). The laser beam was split into one pump beam and one probe beam with a Mach-Zenhnder type interferometer (Figure 19(a)). The probe beam was bounced off two turning mirrors, which were both mounted on a motorized translation stage and thus the time delay between the pump and probe beam could be varied continuously. Both beams were focused onto the atomic beam by two plano-convex lenses (FL) (f/40 for pump and f/50 for probe). Before

the lenses, we inserted a quarter wave plate (QWP) in each beam to produce circularly polarized light. The measured ellipticity of the pump beam is 0.9. The helicity of the pump beam was changed by rotating the QWP which was mounted in an automated rotational stage. The measured ellipticities of the probe beam with right and left circularly polarization are 0.92 and -0.94, respectively. A half wave plate (HWP) followed by a grid polarizer (GP) was installed in each beam in order to change the power of each beam independently. The krypton and xenon gases were seeded with helium and introduced into the chamber through a 20-micron diameter aperture in the source chamber. The produced dications were extracted by the multi-lens velocity mapping electrode assembly and impacted upon a micro-channel plate (MCP)/phosphor detector after flying through a 20-cm-long time-of-flight tube. The resulting signal was recorded by a charge coupled device (CCD) camera in conjunction with the IMACQ acquisition program.

For the studies of krypton and xenon the total laser power of 1.8 mJ/pulse was used. In order to minimize the implications from the non-sequential double ionization (NSDI) the measurements were taken with 500 fs delay between the pump and probe beams. The power of the pump beam was changed while that of the probe beam was kept constant in such a way that the SDI regime is achieved[86]. The corresponding laser intensity range of the pump beam was calculated to be (~1.93×10^{14} W/cm^2) to (~2.88×10^{14} W/cm^2) and the laser intensity of the probe beam was (~2.02×10^{14} W/cm^2) for krypton. For the xenon the pump intensity range was varied from (~6.75×10^{13} W/cm^2) to (~3.01×10^{14} W/cm^2) while the probe beam was at (~2.02×10^{14} W/cm^2). The SDI yield was measured by varying the probe beam helicity by rotating the QWP from 300° to (-

300°), with the step size of 5°. The measurements were taken when both beams are present and when only the probe beam is present. Then the double ionization coming only from the pump beam was measured. Next, similar measurements were carried out for both krypton and xenon under different power conditions of the pump beam. Then the single ionization of the pump beam at different laser powers was measured as well.

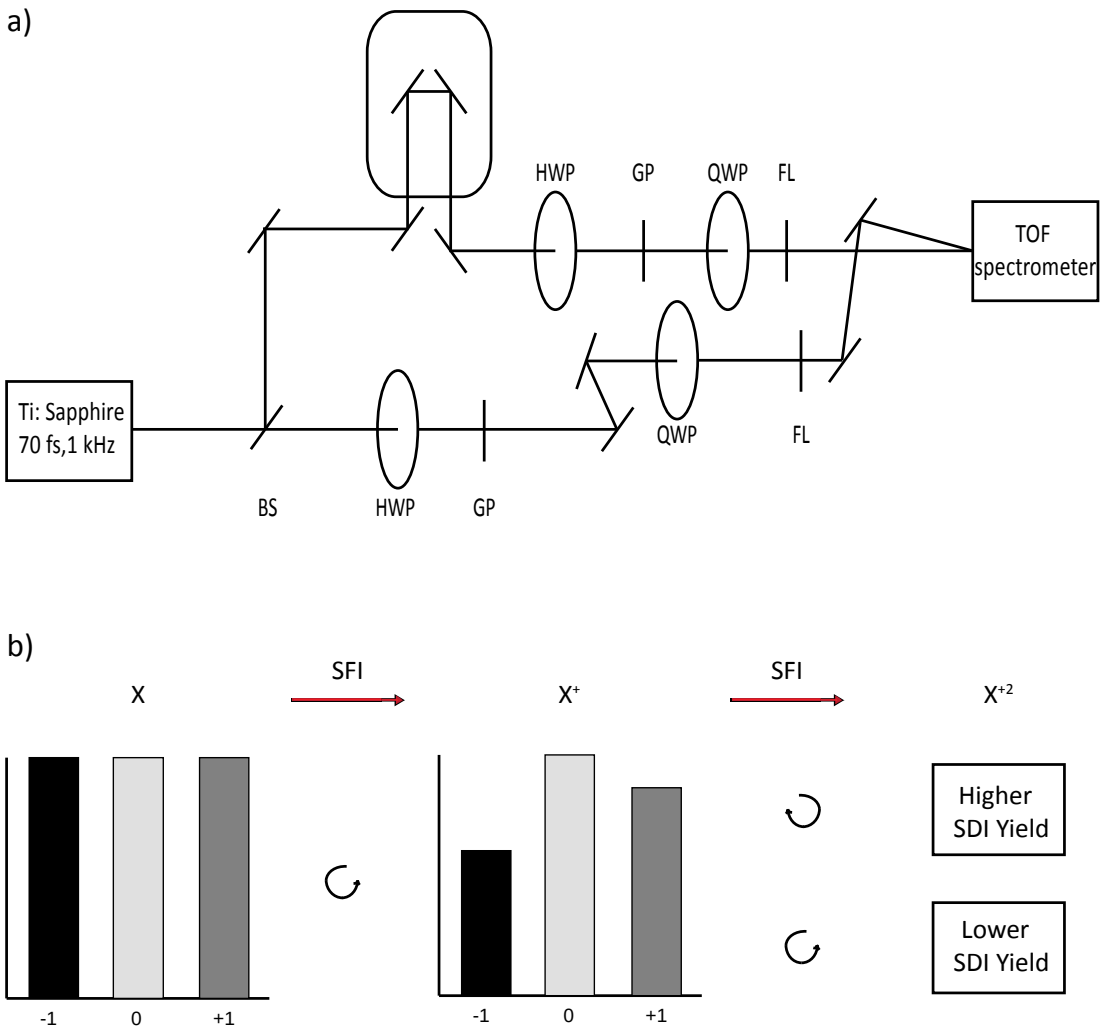

Figure 19: Experimental setup: a) the schematic representation of the optics for the helicity dependent studies (BS-beam splitter, HWP- half wave plate, GP- grid polarizer, QWP- quarter wave plate, FL- focusing lens), b) the schematic illustration of the experimental approach (see the text).

3.3 Results and Data Interpretation

3.3.1 Helicity Dependence of Krypton and Xenon

The SDI yield of krypton and xenon was measured with the varying probe helicity by scanning the angle of the probe-QWP. The ion yields of each species were collected under four laser conditions. The dications of each species produced sequentially by the pump and the probe beams at the highest elipticity, were calculated using 3.1.

$$I_{SDI}=I_{pp}-I_{pr}-I_{pu}+I_{d} \quad (3.1)$$

Ion yields when, both lasers on (I_{pp}), pump beam off (I_{pr}), probe beam off (I_{pu}) and both beam off ($I_{d,}$ dark counts). The raw data of (I_{pp}- I_{pr}) was shown in figure 20 for krypton and xenon. The calculated $I_{SDI\text{-}RL}$ and $I_{SDI\text{-}RR}$ values of each atom is given in table 1 (RL stands for the opposite helicity between the pump and the probe, while RR is the same helicity between pump and probe).

As demonstrated in chapter 2, it is concluded that the SFI rate depends on the sign of magnetic quantum number. In these extended studies with the different atoms, the previous conclusions are still held true. The underlying physical processes of these measurements are as follows: the pump laser first preferably depletes the sublevel of one sign of the magnetic quantum number in the single ions; then, the probe laser with an opposite helicity can further ionize the sublevel with the opposite sign of m, while the probe laser with the same helicity sees a depleted population of the sublevel

with the same sign of *m* and thus the ionization yield of the dication is lower (Figure19 (b)).

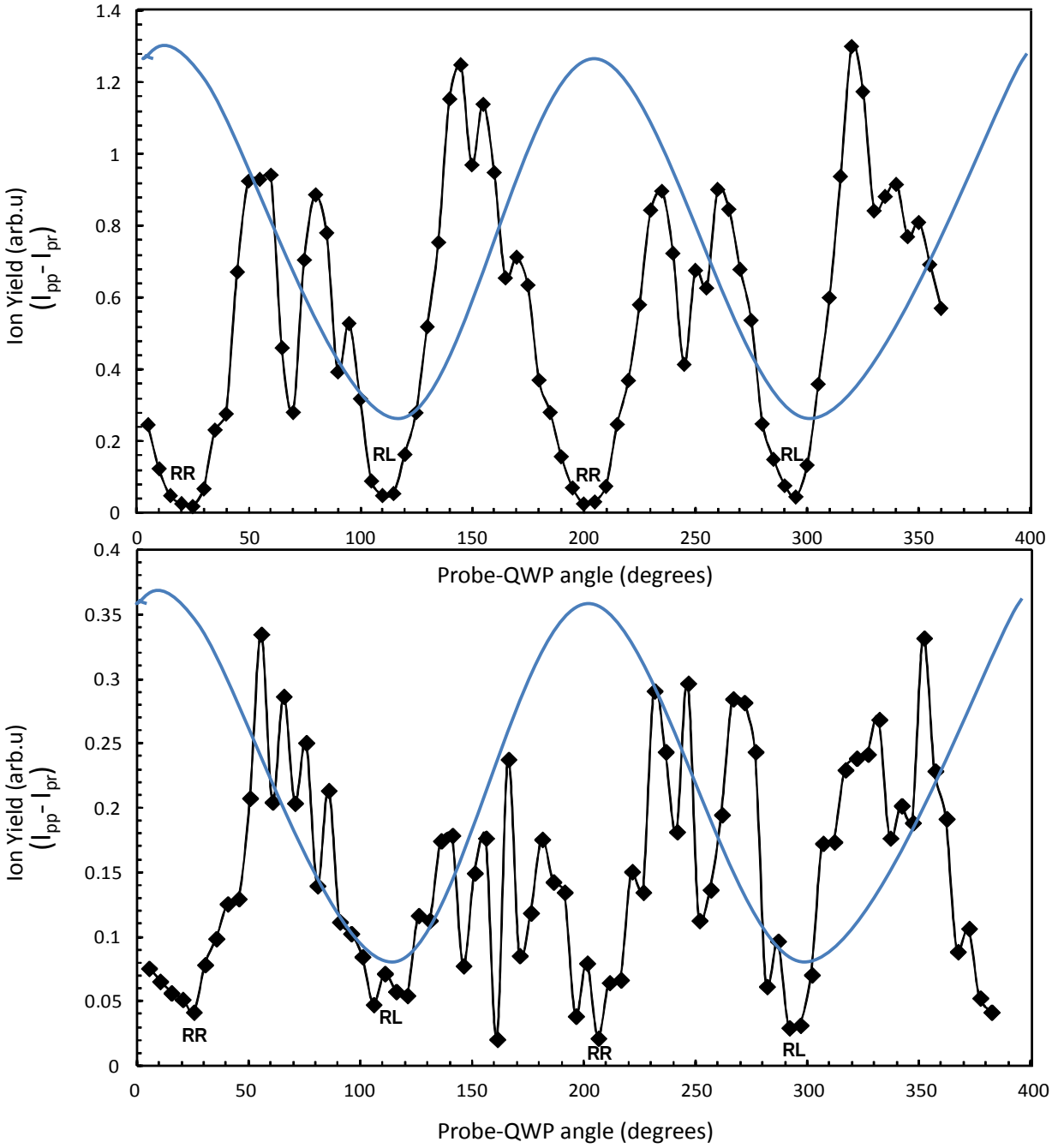

Figure 20: Helicity dependence of (a) krypton (b) xenon. Double ionization yield was plotted against the variation of the elipticity (blue line, minimum and the maximum represent the highest elipticity) of the probe beam.

Species	I_{SDI-RL}	I_{SDI-RR}	$(I_{SDI-RL} - I_{SDI-RR})$
Krypton	0.0325	0.0075	0.025 ± 0.004
Xenon	0.04	0.024	0.016 ± 0.008

Table 3.1: The calculated SDI yields of krypton and xenon at RL and RR of pump and probe.

However, xenon shows less modulation depths compared to both krypton and argon. This could be due to strong spin orbital interactions of xenon[87]. This spin orbital interaction effect can scramble the angular momentum quantum number and it will no more be a good quantum number. Therefore, as it goes from argon to xenon the modulations reflecting the sensitivity of the SFI rate to the helicity observed to be lower.

3.3.2 Laser Power Dependence of the Helicity Effect in Krypton and Xenon

The SDI yield measurements of krypton and xenon were taken under varying laser power. The sequentially produced dication yields by the pump and the probe under each laser intensity, were calculated using 3.1 and also the ratios of single ionization yield of the pump beam between each laser intensities (I_{single}) were calculated. Then the calculated $\{(I_{SDI-LR}-I_{SDI-RR})/I_{single}\}$ plotted with each laser intensity is given in figure 21 (red dots) for both krypton and xenon. The modulations were shown to be decreasing with the increased intensity. In order to compare the observed trend in experimental data, we have preformed the theoretical calculation of ionization rate difference at each laser intensity using the derived equation in ref [72](3.2).

$$w_{p_m}(\varepsilon,\omega) = I_p \left|C_{kl}\right|^2 \frac{\varepsilon}{2\varepsilon_0} h_{p_m}(\gamma) e^{-\frac{2\varepsilon_0}{3\varepsilon} g(\gamma)}, m = \pm 1 \quad (3.2)$$

The relevant Keldysh parameters (γ) ($\gamma = \sqrt{\frac{I_p}{2U_p}}$; where I_p is the ionization potential and the U_p is the ponderomotive potential) were calculated for each laser intensity. Then the corresponding $h_{p_m}(\gamma)$ values were calculated. Since $w_{p_m}(\varepsilon,\omega)\,\alpha\, h_{p_m}(\gamma)$ for *m*=±1, the difference of the ionization rate between *m*=+1 and *m*=-1 can be given as $\left(h_{p_{(+1)}}(\gamma) - h_{p_{(-1)}}(\gamma)\right)$. Finally, these calculated values of ionization yield difference between same and opposite helicities were plotted as a function of laser intensity for comparison with the experimental results. This theory verses the experimental comparison is shown in figure 17.

. According to the laser intensity dependant studies of the sensitivity of SFI rate to the helicicity, as the circularly laser field intensity increases the modulations decreased. The similar trend was observed for the calculated values based on the theoretical representation provided by Barth an co-workers[72]. However, the comparatively the magnitude of the modulations are one order magnitude lower for the experimental case than that of the calculated values.

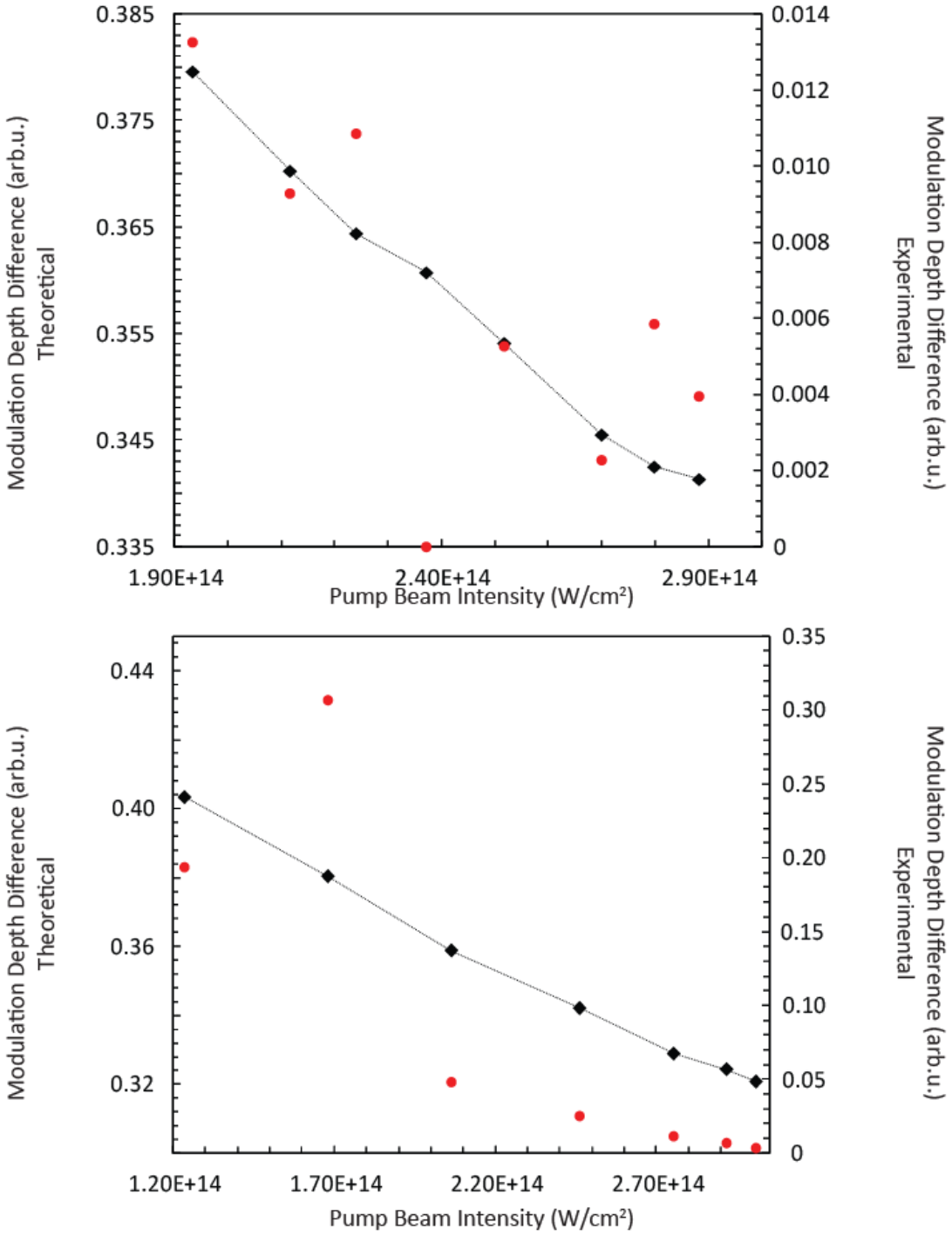

Figure 21: Comparison of experimental verses theoretical. The experimental (black squares) and theoretical (red dots) values of helicity dependent ionization yield with respect to the laser intensities for (a) krypton and (b) xenon.

3.4 Discussion

As mentioned in section 3.1 in the presence of a strong laser field interaction with matter, under the possible phenomena there will be two possibilities for double ionization. Those mechanisms are known to be sequential double ionization (SDI) and non sequential double ionization (NSDI). SDI is when the double ionization process happens step wise where the atom loses two electrons one after the other. On the other hand in NSDI two electrons are emitted together and the emission of the second electron is influenced by the collision of the first electron, which has been driven back towards the core by the reverse phase of the ionized laser field[88]. Based on these understandings, in our experiment we can derive general expression for the total double ionization yield as follows.

$$Total\,X^{+2} = NP_{pump}^{2+} + (N - NP_{pump}^{+} - NP_{pump}^{2+})P_{probe}^{2+} + NP_{pump}^{+}P_{probe}^{1+\to 2+} \quad (3.3)$$

Where, *N* is the initial population and *P* is the ionization probability for each beam. According to equation 3.3, the modulation depth related to the difference between double ionization yields of pump and probe beam having same helicities or the opposite helicities (I_{RL}-I_{RR}), can be written as follows.

$$Total\,X^{+2}\,difference of\,R and\,L = NP_{pump}^{+}(P_{probe}^{1+\to 2+} - P_{probe}^{2+}) \quad (3.4)$$

This relationship simply represents that the total difference in double ionization for same and opposite helicties is proportional to the difference between SDI yield ($P_{probe}^{1+\to 2+}$) and NSDI yield (P_{probe}^{2+}) of this experiment.

However, it is considered that in a presence of a circularly or elliptically polarized laser field the yield of NSDI is highly unlikely or almost impossible. This is due to the fact that the ellipticity prevents the chances of recollision mechanism by steering away the first-ionized electron in a transversal direction. There are early experimental evidence on this manner[89-91].Recently, the NSDI behavior with the elliptically polarized light was also predicted theoretically to be minimized under classical approaches[92]. Under those understandings, in our experiment we have neglect the contribution coming from NSDI from the probe beam assuming that the yield of NSDI is completely suppressed in circularly polarized laser field. However, in our experimental studies with argon, we have shown a discrepancy between the theoretical and experimental values where the experimental values are larger than the calculated values.

On the other hand, recent experimental studies have shown a breakdown of the independent electron assumption in strong field double ionization and suggested that the NSDI is not driven by recollision[93]. There are experiments showing a significant NSDI events in NO and O_2 in a circular polarized laser field[94]. These evidences have complicated the picture of double ionization in a laser field with a considerable ellipticity. Based on these facts, in our experimental approach if we do not assume NSDI yield to be zero, we would have obtained a lower value for ionization ratio of argon which could have been in better agreement with theoretical values. Therefore, in the future more experimental effort will be needed in order to verify the real effect of NSDI in a circular polarized laser field in the tunneling regime.

3.5 Summary

In conclusion, similarly as argon, with krypton and xenon, the strong field ionization rate depends on the sign of quantum number. In general, the modulations of the double ionization yield decreases as going down the periodic table for noble gases. The helicity dependence ion yield modulations of krypton and xenon are decreased with the increased intensities of the laser filed. The data may have represented evidence on the influence of NSDI in double ionization yield in circularly polarized laser field. Closer investigations in verifying and understanding these observations would be useful in the applications of elliptically polarized light.

CHAPTER 4

Experimental Set up for Non-linear Atttosecond Spectroscopy

4.1 Introduction

Even though, the attosecond science and related experiments have great importance to access the fundamental level of natural processes, it comes with many challenges. That makes achieving attosecond spectroscopy a demanding task for many reasons. First of all, as the central wave lengths of produced attosecond pulses are in XUV region very specific optics has to be used. Next, due to its short wavelength, X-rays can be absorbed by most materials, and thereby, the experiment has to be carried out in vacuum to avoid absorption by air. This makes it extra difficult for beam manipulation procedures, such as laser alignment and separation of X-rays from the residual of fundamental laser frequencies. It is also noteworthy that the optical stability of the system is highly required for attosecond experiments. Especially if the beam travels through several meters, the optical path stability becomes one of the key features in maintaining the attosecond time resolution in pump-probe type experiments. On top of these limitations, recent interest in the field of attosecond science has focused on the development of pump-probe type experimental setups to perform XUV-pump-XUV-probe type of studies. Many proposed studies stress the importance of such experiments due to their vast and yet interesting applications, such as real-time probing of the electron dynamics related to charge migration, relaxation and charge-directed reactivity. However, this becomes quite a challenging task due to the major technical issues related to the process of attosecond pulse generation and detection systems.

The main obstacle is the flux of the attosecond source, which has been too low to achieve pump-probe type studies. The conversion efficiency (the energy ratio between the fundamental beam and the resulting harmonics) is low (10^{-5}) in the HHG process, hence limiting the intensities of the output harmonic beam. To date, many studies are aimed at enhancing the intensities of attosecond pulses[95, 96].

The next limitation arises from the lack of an advanced detection system to capture the electron dynamics. Developing a detection system for attosecond experiments is a crucial step. In usual pump-probe experiments there are two kinds of detectors used based on measuring time of flight or measuring the momentum distribution of the photo-fragments; photomultiplier tubes (PMT) and micro channel plates (MCP). However, the best detection approach for attosecond systems is measuring capabilities of both position and the arrival time. These three-dimensional (3D) detectors can measure the 3D momentum vector of each fragment. Such advances will facilitate the assignment of an electron to its parent ion based on the conservation of momentum. These types of electron-ion coincidence measurements will help to understand the ultrafast dynamics occurred in attosecond time domain. For instance, considering a two-photon double ionization process, it has been calculated that electron correlation manifests itself in photoelectron angular distribution when both electrons' momenta can be measured simultaneously. Such a scheme requires coincidence measurements among two electrons and one dication. In this way, the system can extract the two electrons corresponding to the double ionization event by removing the background arising from the dominant single ionization event. Therefore,

coincidence imaging is a good candidate as a detection system for attosecond spectroscopy.

In this thesis, a considerable effort was taken to overcome these common technical difficulties and to develop a unique, novel experimental setup facilitating XUV-pump-XUV-probe capabilities. This chapter will describe the implementation of the instrumentation set up for intense attosecond pulse train (APT) production using high order harmonic generation (HHG) together with the instrument fabrication and optimization for the ion-electron coincidence measurements. In these studies we achieved high flux APTs using a high power, high repetition rate femtosecond laser combined with loose focusing geometry in HHG. The system was verified to provide enough flux by observing two-photon double ionization of xenon with 1 kHz repetition rate. Moreover, in our investigations, an efficient detection system was developed to achieve ion-electron coincidence measurements of the xenon double ionization using APTs, for the first time.

4.2 Experimental Setup

.

Simple schematic representation of the experimental setup was shown in figure 22. A description of each component will be discussed separately.

A femtosecond, Ti:Sapphire 15 mJ (~ 800 nm, 1 kHz) laser was focused through a long focal length lens (f=~4m) inside the HHG gas cell. The gas cell was separated by two fabricated aluminum filters mounted in two manually controlled gate valves. The focused laser beam will burn through the aluminum filters while it passed

though the gas cell. The gas cell was filled with xenon gas and plasma was produced by the ionization of xenon atoms producing high order harmonics. The resulting XUV beam together with the residual IR beam was directed towards the reaction chamber and separated by a harmonic separator. This was done with a super polished silicon substrate placed at its Brewster angle for the red light thus, dominantly reflect the XUV light towards the main chamber while absorbing more than 99.999% of the IR laser. The XUV beam is then collimated using three apertures of 4 mm, 3 mm and 4 mm diameter respectively, before it enters the reaction chamber. Inside the reaction chamber, the laser beam was aligned in such a way that it does not intersect the molecular beam as it travels through the reaction chamber but will hit the reflection

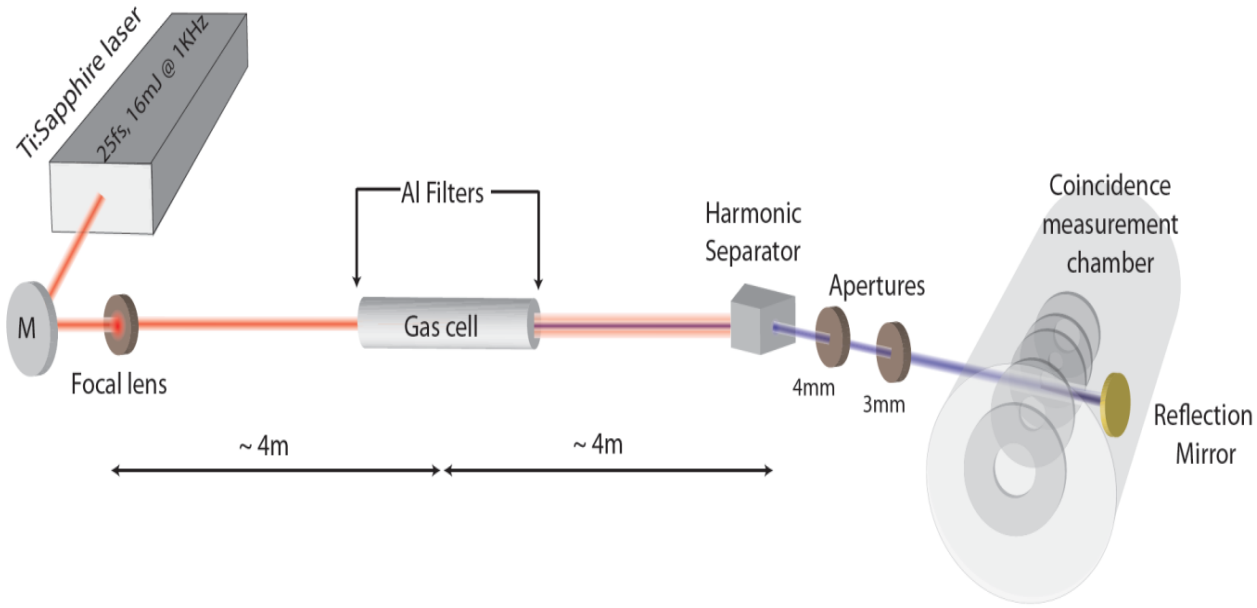

Figure 22: The experimental setup; HHG beam line together with the coincidence measurement chamber.

mirror (a plano-concave boron carbide mirror with the focal length of 12 cm) and is focused back in to the continuous molecular beam providing higher intensity needed for double ionization. The produced ions and electrons were then directed by electric fields towards the micro-channel plate (MCP)/phosphor detector and Delay Line Detector (DLD), respectively. Then the signal was processed through time to digital convertor (TDC) and recorded using CoboldPC software (RoentDek GmbH). A magnetic coil was built around the main chamber to cancel out the effect coming from the earth magnetic field.

4.2.1 Laser System

The femtosecond lasers technology become possible when a fascinating process called laser mode-locking was implemented[97]. Mode-lock is a phenomenon of combining a series of longitudinal laser modes while the phase relationship among them remains fixed. In the presence of synchronized oscillations of highly-coherent, phase-locked will result a short-lived constructive interference between those oscillating waves. This will lead the total energy of the radiation to concentrate in to very short periods. This short-lived field enhancement can be repeated periodically with the period which is similar to the inverse of the frequency between two successive phase-locked modes. Consequently, a train of ultra-short pulses with a duration as short as a few femtoseconds can be produced at the output of a mode-locked laser. Among many techniques in which several modes can be locked, the most efficient implementation is, mirror-dispersion-controlled (MDC), Kerr-lens mode-locked (KLM), titanium sapphire(Ti:Sapphire) oscillators. In Ti:Sapphire systems the lasing medium (sapphire crystal) is doped with titanium ions. This laser system is capable of producing high

power pulses with ultra-short pulse durations typically around 20-100 fs through seeding a chirped pulsed amplification system (CPA) with a mode-locked oscillator beam[98]. Figure 22 demonstrates the basic components of Ti:Sapphire laser systems.

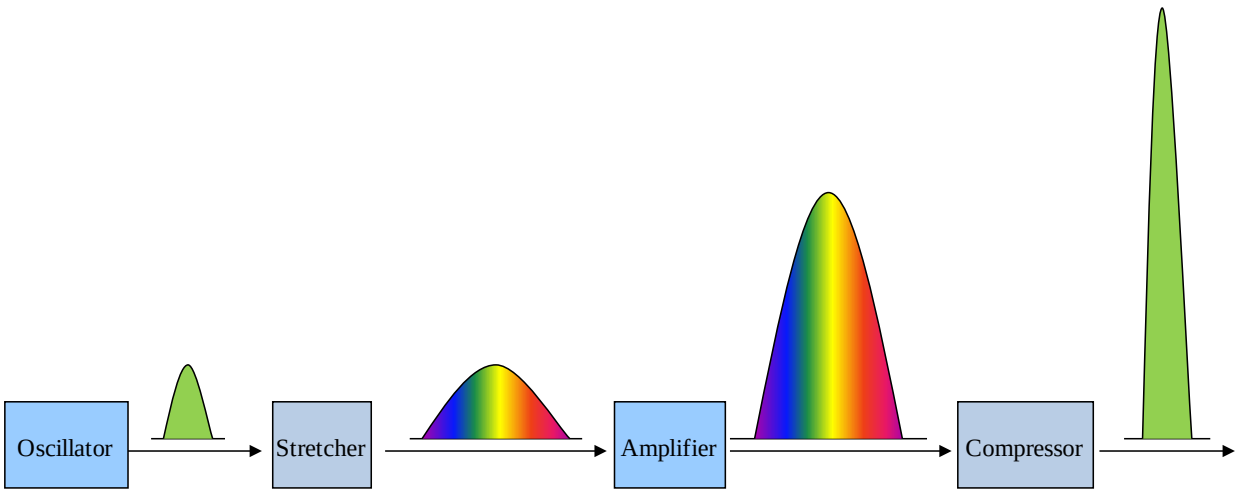

Figure 23: Simple schematic representation of the mechanism of an ultrafast laser (recreated from [99]).

.

In a CPA system the ultra-short pulses are first stretched by the stretcher by introducing a group velocity dispersion (GVD) or chirp. This is to make the pulse longer and thus reduce the intensity to prevent damage to the optics during and after amplification. Then these pulses are amplified to a high energy pulse and sent to a compressor to recompress the long pulse to high power short pulse. These short pulses can then be used to produce XUV attosecond pulses through HHG. In this particular study, a femtosecond 800 nm IR (Red dragon KM labs), Ti:Sapphire laser system of 15 mJ laser energy operating at 1 kHz repetition rate with a 25 fs pulse duration was used

in the production of HHG. The pulse duration was verified using the frequency-resolved optical gating (FROG) (MesaPhotonics) measurements.

4.3 High Harmonic Generation process

High harmonic generation is a process which can convert laser light in a certain wavelength to a coherent light field in several orders lower wavelength range. High order harmonic generation is so far the most successful method of generating attosecond pulses (XUV pulses) among other potential alternatives, such as synchrotrons and free electron lasers. When an intense ultrashort laser focused into a gas cell the tunnel ionization is taking place through the suppressed coulomb barrier. Then these electrons are accelerated and can also be driven back to the atom as the phase of the laser field is changed. The recombination of these electrons with the atoms can produce higher harmonics with the frequency of the driven laser. As this process is repeating at each laser half cycle, a train of coherent, equally spaced pulses are generated with a duration of a few hundred attoseconds. The first experimental evidence of HHG was shown by Ferray *et al.* illustrating infrared light (1047 nm) to XUV (50nm to 180nm)[43]. In general there are two kinds of attosecond pulse generating approaches; attosecond pulse trains and isolated attosecond pulses. Each approach depends on the application and both have related pros and cons. Considerable effort has been taken to implement both of these techniques in performing pump-probe experiments.

Attosecond Pulse Trains (APT): In the process of high order harmonic generation the resulted harmonics are odd integer multiples of the frequency of the fundamental laser providing a broad plateau spectrum. By combining the harmonics over this plateau region a train of attosecond pulses can be created. If the phase is controlled over the summation it will produce a train of sub-femtosecond pulses separated by half of the period of the fundamental laser cycle. The first successful experimental evidences of such sub-femtosecond pulse train production was a train of 250 attosecond pulses measured by Paul and co-workers in 2001[100]. The main disadvantage of APT using pump-probe experiments is the uncertainty in the time-delay between the pump and probe due to the difficulty of differentiating which pulse is the pump or probe. Moreover the multiple pulse structure might complicate the data interpretation process, which would be another complexity in APTs.

Isolated Attosecond Pulses (IAP): When high harmonics are spectrally filtered into one attosecond pulse, it is known as isolated attosecond pulses (IAP). IAP has an advantage in time-resolved experimental approaches. There are a few different techniques of producing IAP. The first scheme uses a phase stabilized few-cycle driving pulse (~5 fs); a spectral filter was then set at the cut-off frequency to produce single attosecond pulses[101]. Polarization gating is another scheme, where allowing the fundamental laser to be linear only during a small time window along the pulse duration. This will let electron to recombined only within that small time window when the laser polarization is linear providing single pulse emission[78]. Most recent scheme is known as attosecond light house, where IAP are extracted from APTs[102]. In this technique a temporal rotation of the wave front will leads to a production of APT where the

successive pulses will be separated in space at the far-field from the source. The main limitation related to the IAP is the lower intensity thus become problematic in achieving pump-probe conditions.

In our studies we have implemented an experimental setup for APT production. To overcome the conventional limitation of lower intensity we used the loose focusing geometry for the HHG process. We have successfully produced high order harmonics from 9^{th} up to 17^{th}. The focused intensities of produced ATPs have provided enough intensity to produced double ionization of various systems as argon, xenon and krypton. This will provide the 14-27 eV energy range. The resulted APTs are estimated to have a few hundred attosecond time duration.

4.3.1 Loose Focusing Geometry and the Gas Cell

Conventionally, simplest method of intense attosecond production is a gas jet of noble gas expanding into a vacuum chamber and the intense driving laser is tightly focused into the gas jet. The pressure of the interaction region is relatively high at several hundred millibars. As the intensity of the driving laser is concentrated into this tight focal spot, this scheme can be used even a laser with a millijoule power range. However, this method is limited by the lower conversion efficiency due to the shorter interaction length with the gas targets. Therefore, the intensity of the produced harmonics is relatively lower. In order to increase the conversion efficiency and related intensities of the output harmonic beam, a different geometry was developed by increasing the interaction length. In that way, the number of gas atoms ionized by the intense laser field can be enhanced. To accomplish this condition laser beam was

loosely focused to a gas cell, thus the length of interaction region can be increased to several centimeters. To focus the laser beam loosely, focusing lens with a long focal length was implemented upstream of the interaction region. According to the general understandings of optics (Appendix A), with a long focal length lens, the focal spot is larger, thus provide larger focal volume and the number of gas atoms contacting with the focal volume become higher. However due to the large focal spot, much higher laser energies are needed for HHG than the conventional gas-jet scheme. The relatively lower pressure in the interaction region will facilitate the phase matching conditions for this geometry. Loose focusing is not the only approach using extended interaction length. The interaction length can further be extended according to some other interesting developments as laser beam guiding. The concept is to extend the focusing of the laser beam further than its Rayleigh length. This can be achieved with plasma waveguides[103]. Gaussian pulses can propagate through these waveguides maintaining same spot size and thus having the same intensity over the entire time of propagation. This will enhance the ionization efficiency in the interaction region. However, the limitation being the plasma generation which can be done using an extra laser pulse or a synchronized discharge. This makes the setup more complicated. This is contradictory to the case in loose focusing geometry. It has comparatively simpler experimental scheme which is relatively easier to setup in practice. However, due to the long focal length of the lens the beam divergence after the cell will take several meters. Therefore, in order to prevent the damages to the optics the experimental setup has to be long enough. This needed a large lab space and more effort on maintaining vacuum

tubes about 10 m long. The stability in optical path will be essential as the beam is traveling through a long distance.

HHG mechanism: HHG is done by ionizing gas density targets using an intense laser field. Intense laser pulse with few femtosecond pulse duration is focused in to an open end cell which is filled with a noble gas. Most commonly used gases are argon, helium, and xenon. Inside the gas cell the interactions between intense fundamental laser and the gas targets are taken place. This non-linear process results an instantaneous production of number of odd integer multiples of the fundamental laser light which is known as high order harmonics. According to the famous 3-step model[40] recombination of the electrons driven back to its parent ion within a half laser cycle after tunnel ionization of the gas targets will lead an emission of a photon with an energy of the ionization potential (I_P) of the gas target plus the kinetic energy gained by the electron at the laser interaction (Figure 24). The number of integer multiples of photons of the fundamental energy ($h\nu$) adding up to produced different order harmonics with the energy of $nh\nu$. Here n represents only odd integers due to the fact that even number of harmonics are removed under interference effect and only the odd once are remaining in the system. The maximum energy of the produced photon is so-called cutoff energy (E_{cutoff}) can be given as; $E_{cutoff} = I_P + 3.17U_p$, where U_p is the ponderomotive potential of the fundamental laser field.

In our studies we have accomplished the loose focusing geometry using a calcium fluoride (CaF_2) convex lens with 4 m focal length. The best condition for the focal spot was optimized by using the measurements from a M^2 machine (Thorlabs

Beam profiler 5.1). The lens was optimized for the minimum astigmatism according to the M^2 measurements. The high intense IR laser at ~15 mJ energy was focused loosely into the gas cell using the 4 m lens. The gas cell was isolated by two aluminum filters

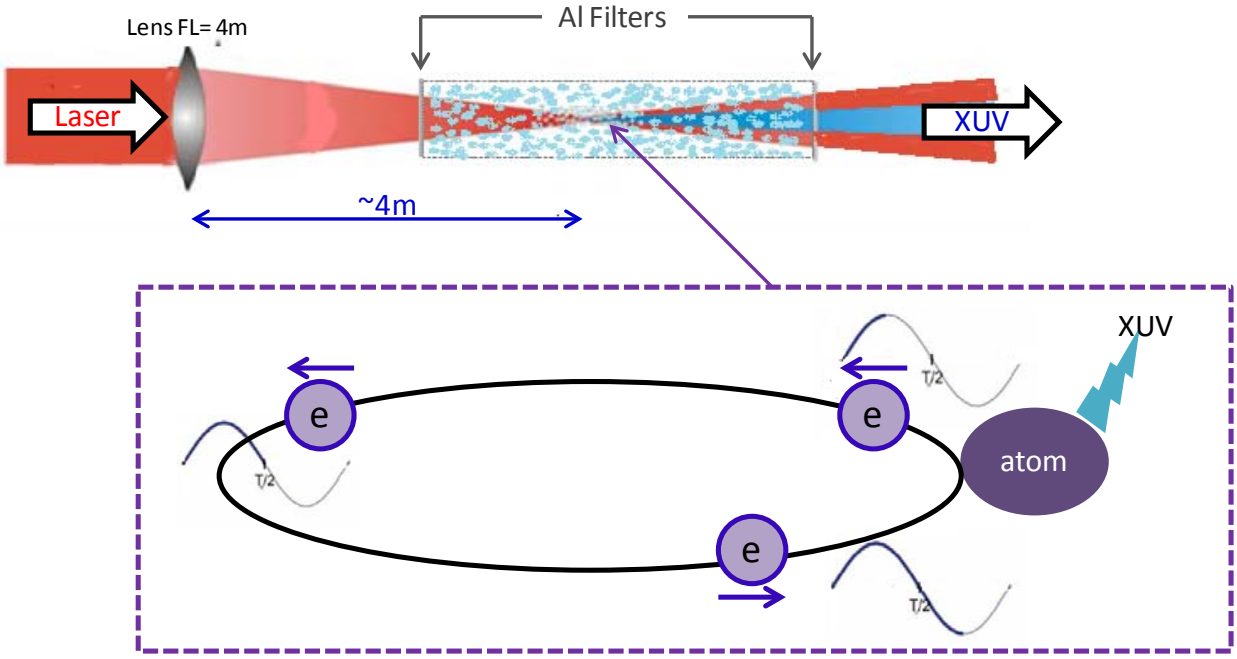

Figure 24: A schematic illustration of the gas cell of HHG. The inset represents the recollision process in production of XUV.

(figure 25(a)). The cell length was optimized to be about 13 cm. This cell was filled with xenon gas. The pressure of the interaction region was optimized and the best harmonic yield was obtained at about 2 Torr pressure. This pressure was maintained using a pressure controller at the gas entrance. The laser field focused in upstream itself burned holes through the two aluminum filters (figure 25(b)) at the entrance and exit of the cell to achieve the open end conditions. The aluminum filters were changed every day prior

to the experiment in order to avoid the enlargement of the burnt hole due to the small variation of laser pointing each day. A recycling system was implemented for xenon gas due to reduce the cost. In this system, a hermetically sealed dry scroll vacuum pump (Agilent technologies) is used to backing the turbo pumps in the beam line and the exhaust of that scroll pump is again connected to the gas cell entrance through another pressure controller followed by a needle valve. Once the pressure inside the cell was built up with the fresh xenon coming from the xenon bottle, the pressure controller for the bottle was closed and the needle valve was open to let the recycling xenon into the cell.

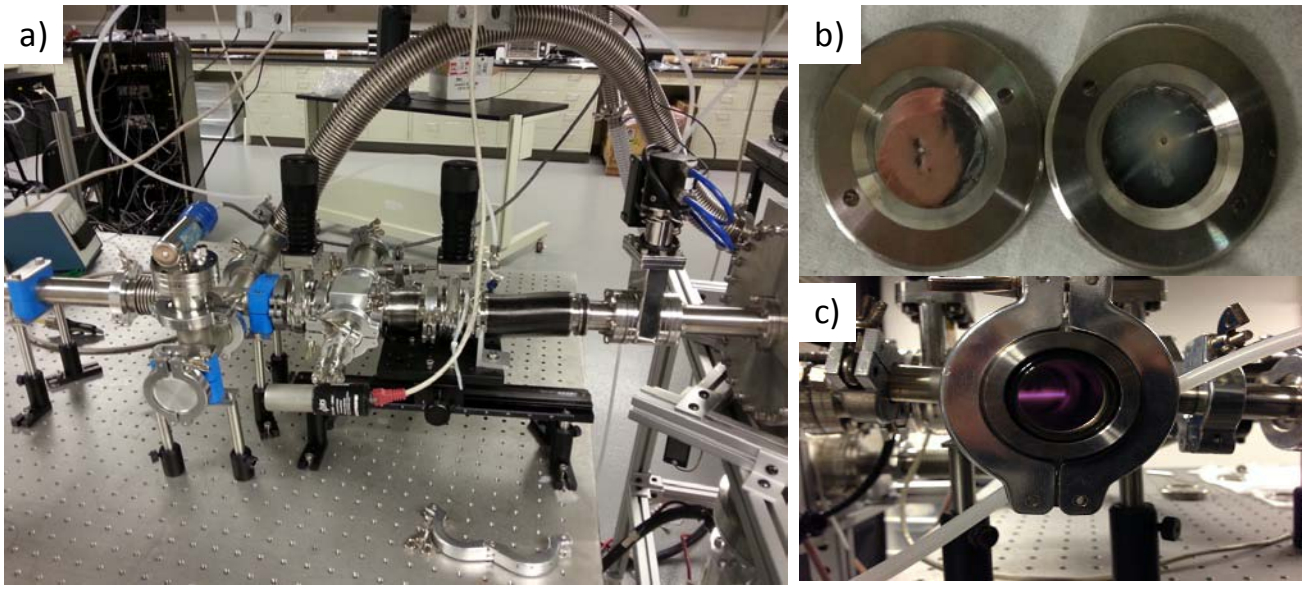

Figure 25: Snap shots of a) the HHG gas cell and its components; b) The aluminum filers with burnt holes c) The plasma produced during the HHG using xenon gas.

4.3.2 Harmonic Separator

As the high harmonics are generated collinearly with the driving laser light, a procedure is needed to separate the produced high order harmonics from the residue of the fundamental laser. In other words, the XUV beam should be separated from the IR beam. There are different experimental approaches were used to achieve this separation. In second harmonic generation, the second harmonics are filtered out from the fundamental using dichoric mirrors[104]. Conventionally, the fundamental laser and also the low order harmonics can be removed using aluminum filters. Based on the constant negative group delay dispersion of aluminum, by choosing the appropriate thickness, it can be used as a bandpass filter for the harmonics of certain orders[105, 106]. In our studies we have separated the XUV beam from the fundamental laser through the use of a super-polished silicon mirror (Coastline Optics) set at near Brewster's angle for the 800 nm (Figure 26(a)). The material silicon becomes a good candidate for this purpose due to its higher absorbance of IR at the Brewster's angle which is closer to its grazing incidence of the beam (75^0). This mirror absorbs 99.999 % of the fundamental beam and reflects ~80% of XUV beam. Ideally a combination of two silicon mirrors were used to suppress the IR throughput but that will reduce the power of the output x-ray beam. Therefore in our setup only one silicon mirror was used. This silicon mirror was mounted on an adjustable mirror mounts and precisely controlled piezo actuators. In this way it is easier to reproduce the best alignment condition of the XUV beam. Even though the silicon mirror is placed more than 8 meters away from the focusing lens, over a few hours of exposure to the laser beam, mirror mount was heated up and that causes changes of the laser beam over the time. Since the data acquisition

has to be carried out continuously over a long period of time (days), changes of the beam position has to be prevented. For this purpose a water-cooling system was implemented on the silicon mirror mounts (Figure 26 (b)). A copper mirror mount is made with a copper tube around it and water is flowing through the tubes. As shown in figure 26 b, water is cooled using an ice bath and recycled with a water pump.

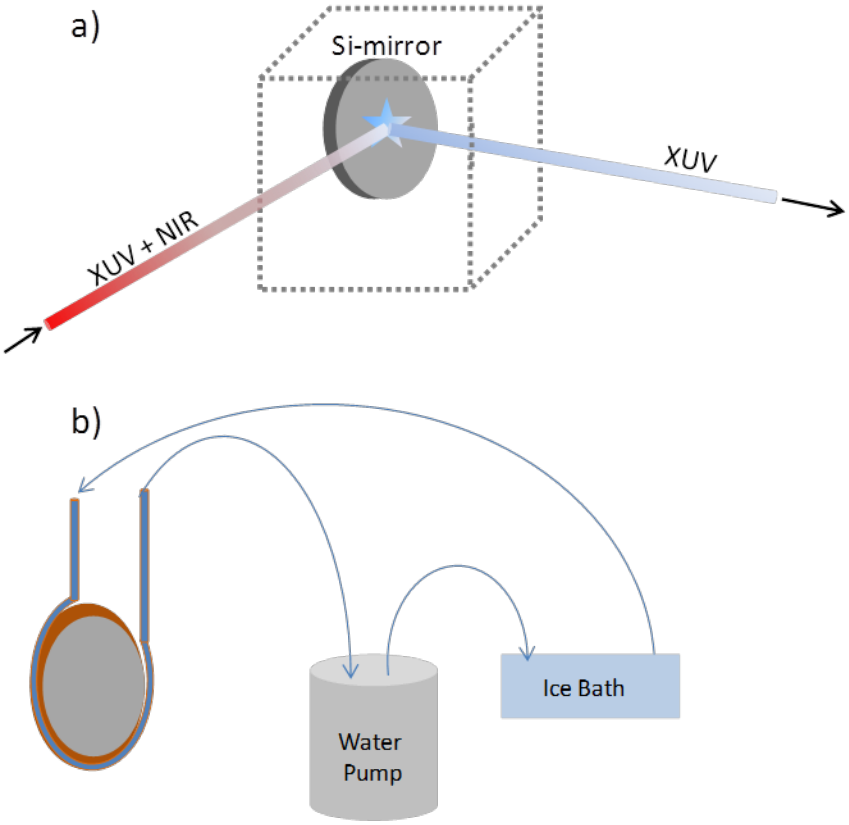

Figure 26: Harmonic separator. a) Schematic illustration of supper polished silicon mirror separate XUV from NIR. b) The water cooling system to prevent the mirror from heating up.

With the aid of this cooling process we were able to have a stable laser beam condition for over 24 hr continuously achieving the long time data acquisition abilities of the system.

4.4 Coincidence Measurements and Detection

Coincidence measurements are rich in information related to the ionization or fragmentation event. It will provide most of the kinematical details about all fragments produced in the event by considering the correlated information between co-fragments, or ions and electrons. In addition these type of measurements are extremely useful for studying the events which are less pronounced compared to a dominant channel (eg. less probable channel with lower ionization yield)[107, 108]. Consequently, coincidence measurements are highly differential and accurate. The ideal setup for coincidence measurements is a three-dimensional (3D) detector which is sensitive to both time and position information. Such a detector should be capable of registering two-dimensional position information as well as the arriving time at the detector. Few good examples for the 3D detectors are delay line detectors[109], cross wire detectors[110], dual CCD detectors[111], and wedge-strip detectors[112,113]. There are different varieties of coincidence measurement apparatus were developed. Two examples are cold target recoil momentum spectroscopy (COLTRIMS)[114] and photoelectron-photoion velocity mapping coincidence imaging (VMI)[115]. Our set up is a combination of these two methodologies (COLTRIMS-VMI). In conventional COLTRIMS a homogeneous extraction field was used and thus the momentum resolution is limited. Therefore in our setup we have used an inhomogeneous electric field as similar to the velocity imaging techniques[116]. This feature will help to focus ions/electrons with the same velocity to a small spot on the detector regardless of the location of birth (the origin of the photo fragments can be different due to the spatial separation of the laser spot to the molecular beam). This COLTRIMS-VMI setup will help to improve the resolution of the

coincidence imaging in a great deal. Furthermore, to avoid the false coincidence conditions it is advantageous to have ionization event for each laser shot less than one. Therefore a higher laser repetition rate is preferred. Specially, considering the coincidence measurements of low yield photo electron experiments, the data acquisition time has to be very large to achieve statistical significance of the data. In order to minimize those long acquisition hours, the laser pulses with higher repetition rates would be ideal. Therefore, our system with 1 kHz repetition rate has an extra advantage for more efficient coincidence measurements.

4.4.1 Coincident Measurement Chamber

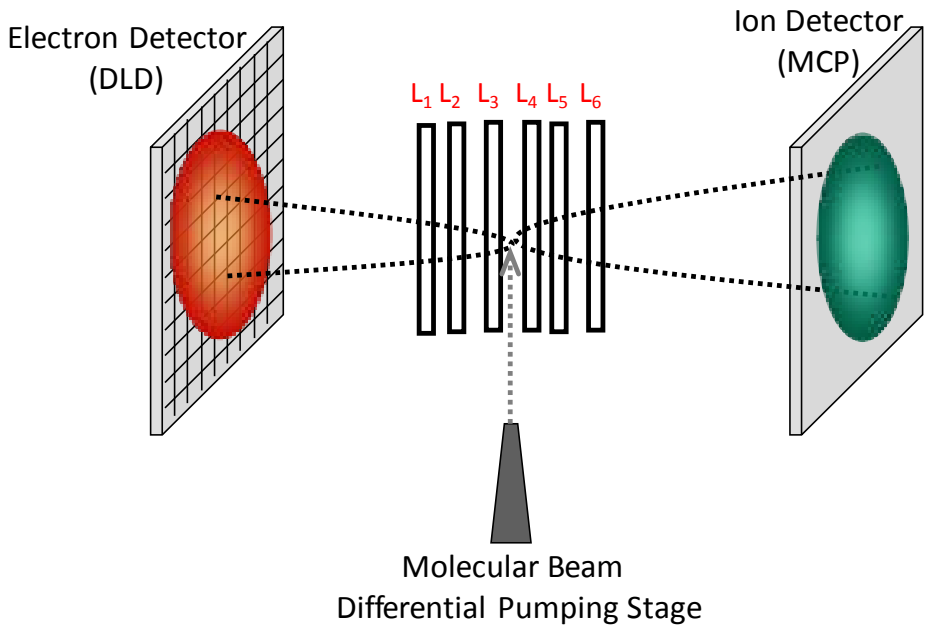

Figure 27: Coincidence measurement chamber for attosecond spectroscopy.

We have built a coincidence velocity map imaging apparatus to accommodate the detection of electron on one side and ions on the opposite side (Figure 27). The electrons and ions are directed toward each side with the aid of five-

electrode electron-ion optics assembly. The molecular beam with a supersonic expansion was introduced perpendicular to the time of flight (TOF) axis. The molecular beam enters to the reaction chamber via a differential pumping stage through an orifice of 500 µm. The molecular beam diameter at the interaction region is around 1 mm. A laser beam with a horizontal polarization propagates perpendicular to the molecular beam direction. The incident beam was aligned in such a way to avoid the molecular beam and hit on a plano-concave reflection mirror installed on the back flange of the chamber. This mirror will reflected the focused XUV beam on to the molecular beam. Two detectors, MCP/Phosphor and delay line detector, for the detection of ion and electron, were mounted at the two ends of the flight tube. A detailed description of each component in the coincident measurement chamber will be described below.

A. Micro Channel Plate (MCP) Detector

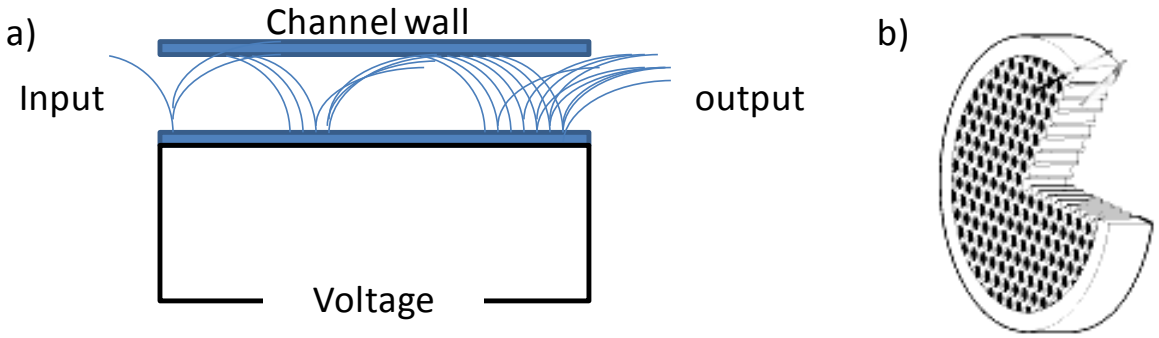

Figure 28: The mechanism of MCP detector a) One MCP channel b) The top view of the detector with a sack of MCP channels.

The MCP detector is made out of a combination of millions of individual small capillaries called micro channel tubes. The size of these tubes is about tens of micrometers in diameter and less than one millimeter in length. The inside of these capillaries is coated

with a semi-conducting material. Thus, when a particle enters these channels they bombard the channel wall and emit secondary electrons. These secondary electrons can be accelerated and influenced to generate more secondary electrons due to the electric field applied to the two ends of the channel. This process continues until a cascade of electrons exit from the exit pore of the channel (Figure 28). As each pulse is limited to an individual channel, a spatial pattern will be generated corresponding to the incident pattern of the particles, which enables spatial resolution. These output electrons can be read out using different methods such as a phosphor screen, delay line readout, or other type of metal anodes.

.

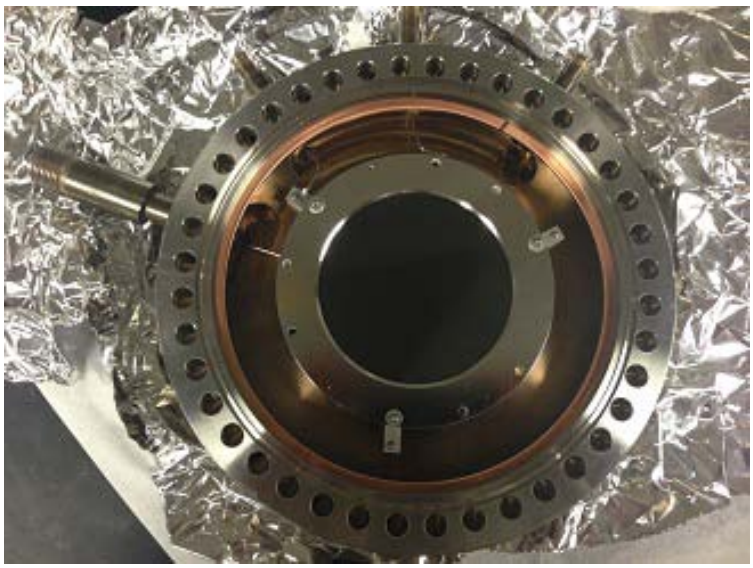

Figure 29: An Image of the MCP detector used in our coincidence measurement setup.

MCP detectors are widely used in the fields as mass spectrometry, imaging spectroscopy, astronomy and atomic physics due to its high spatial and temporal

resolution. Specially, due to the smaller size of the channels the precision of the measurements are fairly high.

In our setup MCP/phosphor detector was used in detecting ions (Figure 29). MCP detector is applied with -1550/+300 V for front and back plates respectively. The diameter of the MCP is 75 mm.

B. Delay Line Detector (DLD)

Delay line detector shares the concept of providing not only position information but also the temporal information about the photo-fragments. The exact arrival time of a particle can provide extra details about the collision process. Because of these 3D detection capabilities, DLD is widely used in the coincidence measurements.

Generally, the traditional imaging detectors consist of MCP and a phosphor screen. Retrieving either temporal (time of flight) or spatial information (imaging) separately using such detection system is fairly straightforward. But correlation of the time and position is quite challenging, especially with the phosphor screen and cameras. On the other hand, combining MCP with an anode which is capable to recode the position information together with the time information will be useful. The ability of recording more than one particle at a time (multi-hit) also becomes important. Delay line technique is one of those techniques with the capabilities of extracting both imaging and timing information from MCP device simultaneously. The combination of the delay-line readout with advanced timing electronics has achieved 3D detection.

The delay line anode is made of a layer of wires. The signal expressed on this layer will propagate to the end of the wires and then be processed. Based on the picked up

position and the propagation delay of the signal, the position measurements can be calculated. The difference between the arriving times at the adjacent ends will proportional to the position of the particle on MCP detector. The wires are either bent or helical shaped to increase the propagation time in order to be measurable (Figure 30). As it is possible to establish two dimensional position of a particle using two layers, for 2D position measurements (x,y) another delay line layer has to be implemented perpendicular to the first one. The charge cloud distribution among these layers can be adjusted using proper biasing of between layers. The other component, the timing

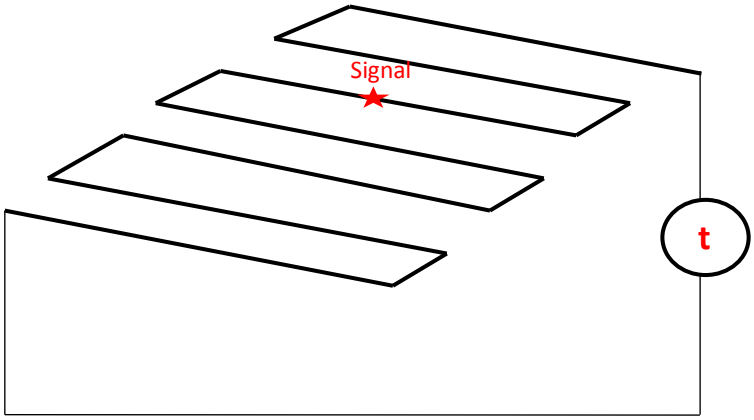

Figure 30: The principle of DLD extraction of particle-hit location.

measurements, should be processed with a device which is compatible with the detection rate and multi hit analysis. A time to digital converter (TDC) provides these requirements and is used in delay line technique.

A shortcoming of the two layered DLD is the loss of signal due to the electronic dead time: if the arrival time of two particles falls within the electronic pulse duration, the second particle information will be lost. In order to overcome this limitation a third layer

is implemented in DLD systems (Figure 31). These types of detectors are ideal for multiple hit events.

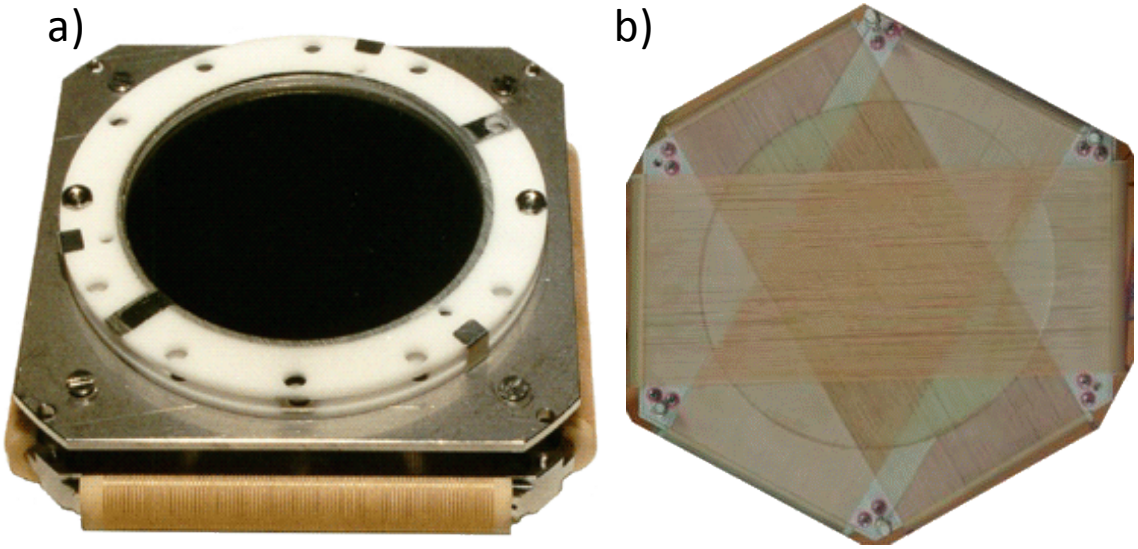

Figure 31: An image of 3-layered DLD (Hex75). a) Top view of MCP with the delay line anode. b) The three layers of the DLD.

For our experiments we have used a three layered Hexanode DLD (HEX75, Roentdek) together with TDC (Roentdek). This system provides ~25 ps time resolution and <0.1 mm position resolution. The multi hit dead time is 5 ns.

C. Reflection Mirror

In order to enhance the intensity of the XUV beam at the ionization point the XUV beam was reflected on to the molecular beam using a focusing mirror with a short focal length (Figure 32). The critical step is to find a suitable coating which has a higher reflectivity at the XUV wavelength (~60-200 nm). Since the reflectance in this wavelength is lower for any material multi layered mirrors are used.

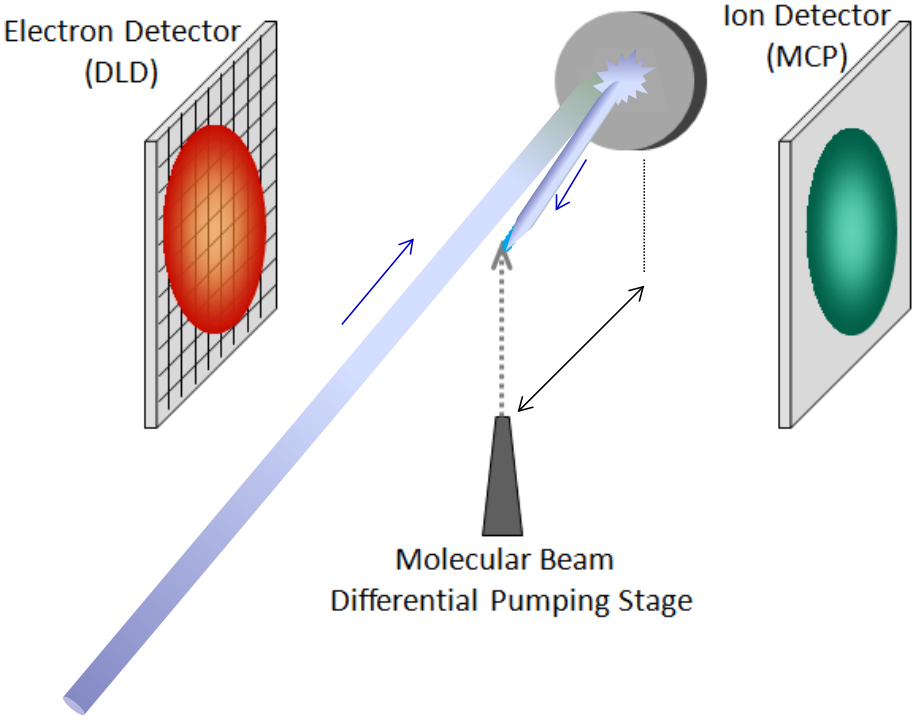

Figure 32: Schematic representation of the orientation of BC_4 reflective focusing mirror.

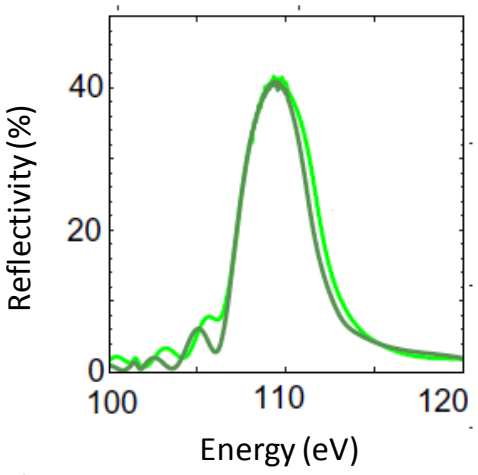

Figure 33: Adopted data for XUV reflectivity of a lanthanum–molybdenum multilayer mirror with 1 nm B_4C layer (green curve) which is used as a barrier layer[117]. The black curve represents the same mirror with no coating.

Specially the reflectivity in those mirrors can be based on the number of layers used [118]. These multi layered mirrors are known in enhancing characteristic of attosecond pulses[119, 120]. In our setup a mirror coated with boron carbide (B_4C) was used. The focal length of our mirror was 12.5 cm.

In our coincidence measurement setup (Figure 34) ions were detected using a conventional imaging detector which collects the momentum information. The produced electrons or ions are directed to the appropriate detector by the electric field generated by the ion optics from L1 to L6. The optimized voltages were L_1=0, L_2=(-200)V, L_3=(-383)V, L_4= (-427)V, L_5=(-625)V, L_6=(-710)V, respectively. Per each laser shot, the time of flight signal is collected by micro channel plate (MCP) and registered to a time-digital-converter (TDC).

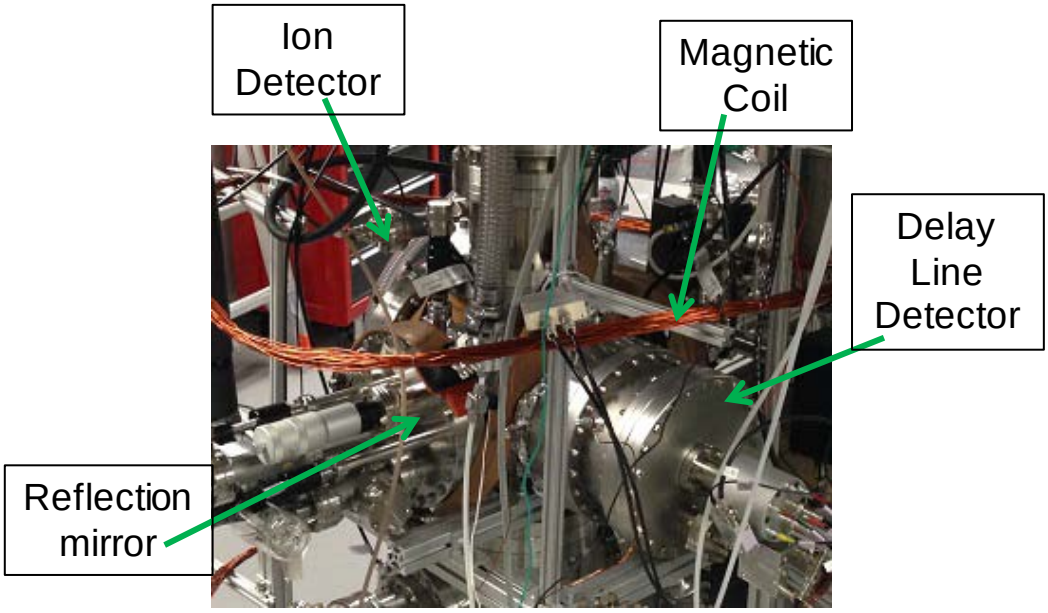

Figure 34: A snapshot of the coincidence measurement chamber in our lab.

Electrons are collected by a delay line detector (DLD) (Roentdek, HEX75) which registered both the position and the arrival time of the electrons. The electron signal also processed through the same TDC so that the coincidence among those can be ascertained. In addition the effect of the earth magnetic field was cancelled out using an opposite magnetic field generated by a copper coil installed around the chamber with a current of ~1 A.

4.5 Background Optimization

Another critical problem is achieving minimized background conditions to obtain more realistic coincidence measurements. In other words one should try to minimize the false coincidence measurements as much as possible.

False Coincidence: False coincidence can be taken place when the event counts related to the background is relatively larger than the ionization event of interest. These random events can be detected in a mutually overlapped time window with the signal, which causes the wrong assignments of the real event counts. The Poisson distribution will be used to statistically verify the best count rates to prevent the false coincidence. The goal of avoiding false coincidence can be accomplished by taking steps to reduce both ions and electrons as the event counts become less than one per laser shot. This task becomes even harder in our setup due to high flux XUV beam. Scattered XUV beam can produced high photoelectron background conditions which make it difficult to differentiate from the real electrons coming from the ionization event.

Unlike strong field experiments, due to the high energy in XUV beam it does not even have to be focused to produce ionization in residue gas and chamber surfaces. As a result, we had seen relatively high noise from the ionization of background gas particles in the interaction region as well. Additionally, for pulsed light sources the chances of false coincidence are even higher. When the light source is pulsed there is a better probability of detecting those unrelated events with the same masses arrives at the same time of flight. The best solution is to use a laser system with a higher repetition rate with still maintaining the probability of the ionization events less than one per laser shot. There are also researches on finding mathematical and statistical approaches to remove the false coincidence counts during the data analysis process [121,122]. However, the ideal situation is to reduce the possible background counts in the experimental setup and we have taken considerable effort on that.

In order to reduce electron background in our experiment a few steps were followed. First we have taken action to collimate the XUV beam. Towards this process, we have installed two apertures, 4 mm followed by 3 mm, in the beam line to collimate the beam before it enters to the reaction chamber (Figure35(a)). These two apertures are mounted on two translational stages to make the laser alignment process easier. This provides the flexibility for selecting the best part of the XUV beam directed at the reaction chamber. Then the beam was further collimated using another 4 mm aperture at the entrance of the reaction chamber (Figure 35(b)). All of these apertures are made from a stray light absorbing material (Edmund Optics). We also tried to replace our original stainless steel ion optics with a different material with a higher work function.

However, XUV photons are highly energetic; it will produce electrons from any material. We have done a trial and error approach on this issue and started with aluminum (Al). However, Al provided even higher photoelectron background than stainless steel. Next with a careful investigation magnesium (Mg) turns out to be the best candidate for this purpose. Some studies show that the photo electron yield of magnesium decreases with the increased photon energy[123]. Therefore, we have rebuilt the ion optics in Mg. Having Mg ion optics indeed reduced the photoelectron background considerably. The next step was to install a shielding plate in front of the electron detector in order to block stray electrons from reaching the detector. For that purpose we have mounted a stainless steel plate with a 10 mm hole in front of the detector. For further reductions, only the center part of the produced electron cloud was selected and sent to the detector before it expands. This condition was accomplished by using two small holes, 4 mm and 3 mm, in electron driven ion-optics (L3 and L2) (Figure 35(b)). With these modifications the scattered electron background was considerably lowered and the electron count rate become as low as <1 count /laser shot at the price of sacrificing a full 4π collection efficiency. Then attention was paid to minimize the possible background gas as much as possible. We have built a liquid nitrogen cooling system for both the reaction chamber and the beam line. Liquid nitrogen cooling helped to reduce water background to about 40% from the original value by improving the vacuum in the reaction chamber to around 10^{-10} torr. The possible background gas contribution from the beam line was further reduced by the differential pumping set up implemented in the beam line. We also used the advantage of the velocity focusing capabilities of imaging detector and exclusively filtered only the molecular beam spot

using a 5 mm shielding aperture in front of the MCP detector.

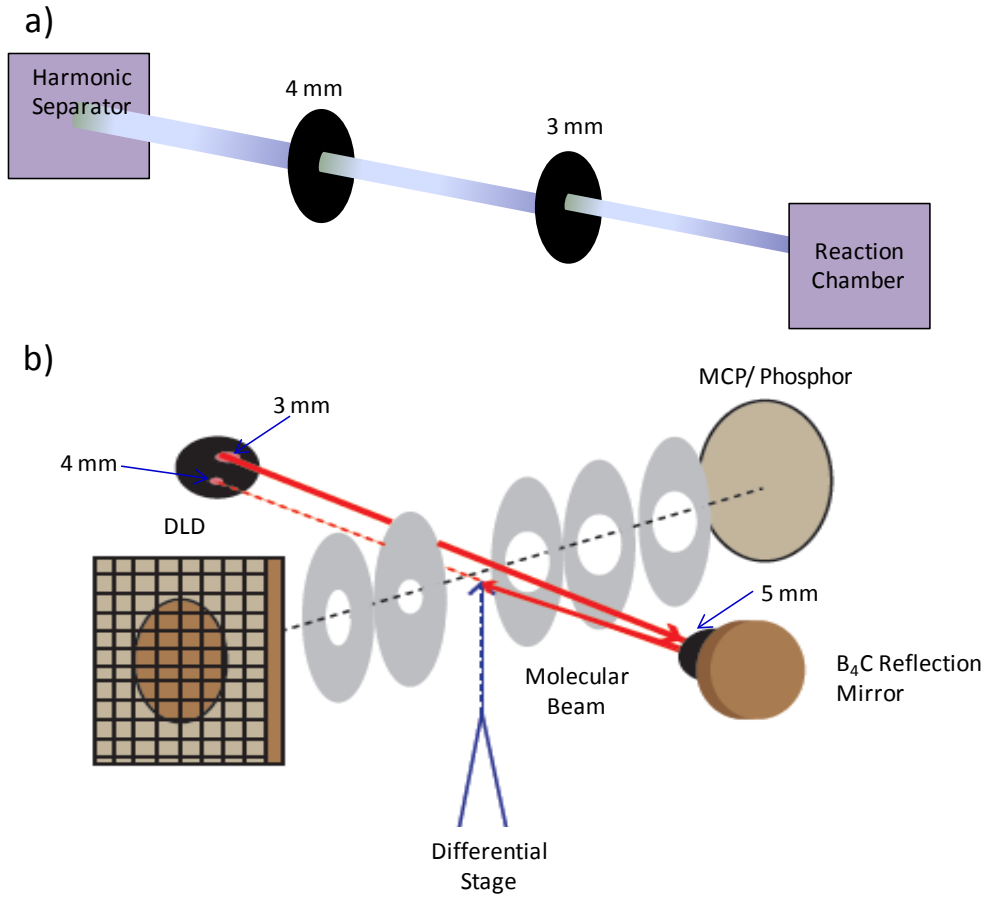

Figure 35: The aperture setup of the beam path to achieve well collimated XUV beam. a) First two apertures before the beam enter the chamber. b) Apertures inside the reaction chamber, at the entrance and in front of the reflection mirror.

This reduced the ion background significantly. To reduce the background that could arise from the molecular beam itself from the ionization by the incident XUV beam a special alignment orientation was implemented. The incident beam was aligned in such a way that it avoids hitting the molecular beam but directly sent to the reflective focusing mirror and focused on to the molecular beam.

All together these efforts utilize the background counts as low enough to detect both electrons and ions simultaneously with the counts rates about 0.4/laser shot and 0.3/laser shot, respectively. These conditions have permitted in performing ion-electron coincidence measurement in two photon double ionization using a XUV beam.

4.6 Preliminary Results

Our newly optimized experimental setup of APT generation with coincidence measurement capabilities have successfully been tested with atomic systems.

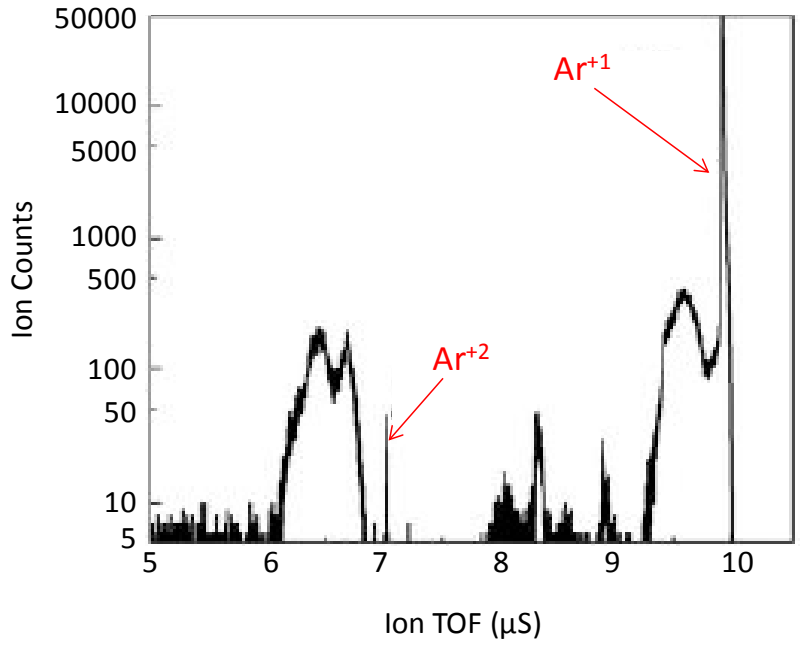

Figure 36: Ion time-of-flight spectrum of argon showing both single and double ionization using focused attosecond pulse trains produced in our setup.

The intensity profile achieved has the calculated ratios of 0.58:1:0.95 for 11^{th}:13^{th}:15^{th}. The focused APTs were able to provide the sufficient intensity to produced double

ionization of argon, krypton and xenon (Figure 36). The harmonics energy range is about 14 to 27 eV. The setup has also showed the capabilities in ion-electron coincidence measurements. The figure 37 shows the electron momentum spectrum in coincidence with single ionization of argon.

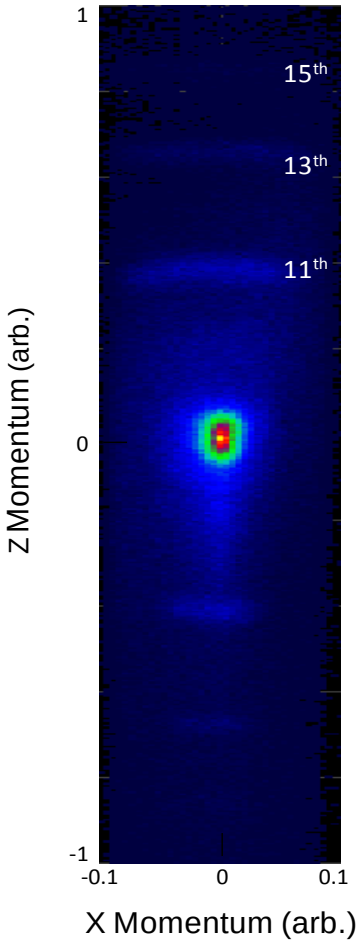

Figure 37: 2-D momentum distribution of electrons in coincidence with argon single cation (Z represents the TOF direction and X is along the laser propagation direction).

The preliminary data obtained for the double ionization of xenon and corresponding ion-electron coincidence measurements using XUV-pump XUV-probe setup will be described in the next chapter.

4.7 Summary

In this work, we have successfully implemented an experimental setup which is capable of producing intense APTs to perform attosecond spectroscopy using coincidence measurements. The higher (1 kHz) repetition rate and minimized background count rates would enhance the capabilities of our experimental system on more efficient coincidence measurements with higher accuracy. Our experimental system was tested using atomic systems first as the preliminary studies. The two photon double ionization of noble gases were investigated. We achieved an attosecond pulse flux to produce double ionization of atoms even as argon which has relatively higher double ionization potential. A detailed study of two photon double ionization of xenon using electron-ion coincidence measurements were performed and will be discussed in next chapter.

CHAPTER 5

XUV-pump-XUV-probe Two Photon Double ionization

5.1 Introduction

The correlations among electrons are the main feature which keeps the molecule together. As a result, the electron dynamics controls both structural and reactivity properties of chemical systems. Thereby, studies related to the electron correlation and reorganization in the attosecond time domain is a new frontier of science. Because electron correlation plays a fundamental role in many natural systems, these types of studies reveal the insight of those important processes in the most detailed way. A few good examples of such systems are chemical reactions and phase transitions. Accordingly, observing these basic level dynamics in real time will ultimately make it feasible to control related processes in real time.

A rational approach to understand these correlations among electrons is to start from simpler systems such as atomic systems[124]. A strong laser field can readily induce doubly or multiply charged ionization[81, 125] and thus the role of electron correlation has been studied extensively in strong field ionization[126, 127]. However, electron correlations in strong field are mainly induced by the interaction between the electron and the laser system. Therefore, these artificial correlations might be different from the natural correlations between electrons in reality. Accordingly, a weak probe as attosecond spectroscopy would be more useful to investigate these natural electron correlation dynamics. The attosecond time scale will facilitate the real time visualization of correlation between the electrons in reactions. As a result, recent

attention of the ultrafast research is directed to implement suitable experiments to perform attosecond XUV spectroscopy[56]. Even though many researches are working on this matter, the progress has been slow. Techniques like attosecond streaking experiments also were only able to capture the dynamics of one electron in attosecond time scale[1].

When it comes to observing electron-electron correlation dynamics, two photon double ionization becomes essential. Two photon double ionization can be defined as the ejection of two electrons by two photons. This process can be either sequential or direct/nonsequential. There are two factors contributing for sequential or direct two photon double ionization. One is the availability of bound-free absorption cross sections which is a parameter of the gas atoms. The other factor is pulse duration, the interaction time of the light and the atom, which can be adjusted according to the experimental needs. If the final ionization population is linearly related to the pulse duration the mechanism is direct two photon double ionization. If the final ionization population has a quadratic relation to the pulse duration the process has to be sequential. Theoretical studies have predicted that the shorter pulse durations will provide higher probabilities on direct two photon double ionization over the sequential two photon ionization[128]. Two photon double ionization processes in general will provide information about the electron correlations. But direct two photon double ionization is more affected by the electron-electron correlations. Evidently, XUV pulses should ideally provide dominant direct two photon double ionization which is favorable for studying electron correlation dynamics.

During the sequential regime one electron is ionized from the ground state and the second electron is ionized from the single ion itself. This pathway is only possible if the system has photons with higher energy than I_2 (photon energy (E_{ph}) > I_2). The other possible mechanism is nonsequential regime if the combination of two photons providing the energy higher than (I_1+ I_2), and the simultaneous absorption of two photons can lead to direct two photon double ionization. During this process two electrons in the ionization event will share the total energy. In other words, the temporary intermediate state was formed does not has to be at the (E_{ph} - I_1), but at this intermediate electrons can interact and exchange the energies for ejection.

In our experiment the two photon double ionization of xenon was studied using XUV-pump-XUV-probe setup. The produced APTs are intense enough to produce xenon double ionization. The first ion-electron coincidence measurements were obtained for xenon double ionization, using XUV pulses. The ultimate goal of this experiment is to perform triple coincidence measurements where you can obtain the electron-electron correlations. Even though we have achieved the ion-electron coincidence capabilities, the setup has to be further modified for ion-electron-electron coincidence measurements and will be further discussed under future directions. The remainder of this chapter will focuses on the preliminary ion-electron coincidence measurements, current difficulties associate with the setup and proposed improvements.

5.2 Experimental Approach

The two photon double ionization of xenon was studied using our newly built intense HHG beamline together with the coincidence measurement apparatus (a detailed description about experimental setup is given in chapter 4). Xenon beam was introduced to the reaction chamber through a differential pumping stage installed in the source chamber. The molecular beam was skimmed twice using two 500 µm apertures installed in between the reaction chamber and the source chamber. Relatively higher backing pressure, 40 psi, was used for xenon gas to increase the signal to noise ratio. The laser system (Ti:Sapphire, 800 nm, 25 fs, 1 kHz) operates at 10.0 mJ was used for HHG. The HHG gas cell pressure was optimized and the best results were obtained around 2 Torr. Argon gas was used to characterize the intensity profile of the produced high order harmonics. Then the focused XUV beam interacts with the xenon beam with a 90^0 orientation as described in chapter 4. The produced ions and electrons were then directed toward the appropriate detector. Both ion and electron signal was picked up and processed simultaneously through a time to digital converter (TDC) device. The count rates of ions and electrons were maintained about 0.4 counts/laser shot and 0.5 counts/laser shot, respectively. The signal was accumulated using CoboldPC software. During the data analysis process a time of flight (TOF) filter was set in such a way to filter out only the electrons corresponding to the ions of interest. In that way, the electron coincide with the particular ion can be isolated and the related dynamics can be studied exclusively.

5.3 Results and discussion

In this experiment we have obtained xenon double ionization using XUV photons. The ion-TOF spectrum shows corresponding peaks at the TOF of xenon single ionization and double ionization (Figure 38).

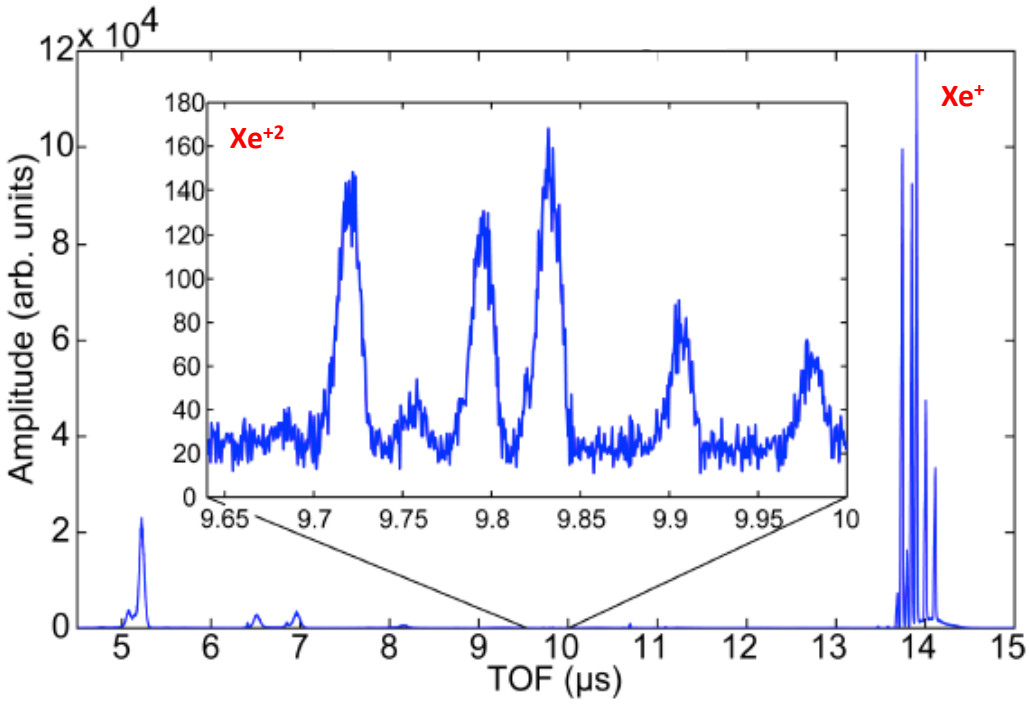

Figure 38: The ion-TOF spectrum of xenon. Inset represents the zoomed-in TOF for xenon dications (Xe^{+2}). Six peaks correspond to the six isotopes of xenon.

In our setup z-direction lies along the TOF axis and x-direction is perpendicular to the laser propagation direction and y is in parallel direction with the molecular beam (Figure 39). Figure 40 represents the extracted electron momentum distributions in coincidence with both single and double ions. The given momentum spectra (Figure 40) are showing the electron momentum of z-direction versus x-

direction. The corresponding electron momentum was extracted by setting up the TOF filters for corresponding mass to charge values.

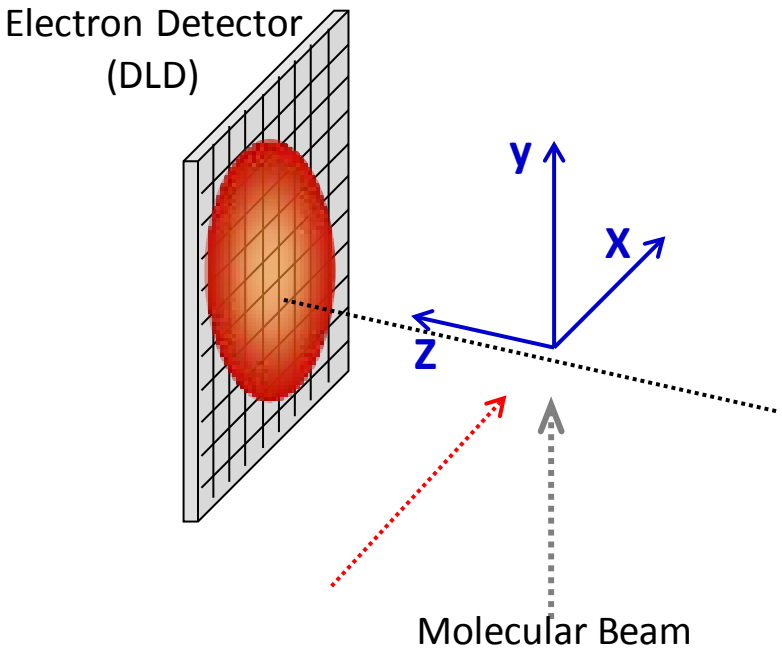

Figure 39: A demonstration of the momentum directions with respect to the electron detector.

The electron momentum distribution of single ionization verifies we have clearly seen high order harmonics from 9th to 13th. The first and second ionization potential of xenon is 12.12 eV (I_1) and 20.98 eV (I_2) respectively. The fundamental photon energy is calculated to be 1.57 eV from equation 5.1, where $\hbar$ is the reduced plank constant and ω is the fundamental laser frequency or (speed of light (c)/wavelength (λ)). For our laser λ= ~790 nm.

$$E_f = \hbar\omega = \hbar C/\lambda \qquad (5.1)$$

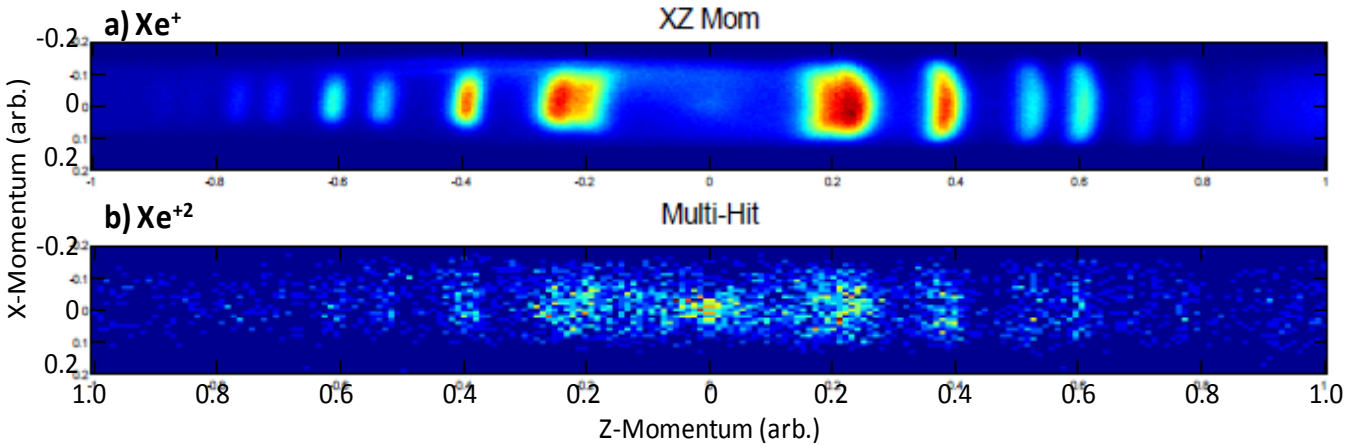

Figure 40: The z-momentum verses x-momentum plots of electron-ion coincidence measurements for a) Xe^{+} and b) Xe^{+2}.

Accordingly, the energy of each order harmonics can be given as nE_f, if n is the harmonic order. Therefore, the highest energy photon possible in our system is when n=15 and the energy is 24.1 eV (i.e. 15 X 1.61 eV). Hence the double ionization of xenon, 33.1 eV (I_1+ I_2) > 24.1 eV, even one highest energetic photon will not be enough to produce double ionization. Therefore we can conclude that the double ionization happens through a combination of two or more photons. For example, 11^{th} plus 11^{th} or 9^{th} plus 13^{th} and few other different combinations.

After constructing the momentum plots for the electrons in coincidence with xenon single (Xe^{+}) ionization and double ionization (Xe^{+2}), the corresponding electron energy information was extracted (Figure 41). The electron energy spectra should consists of peaks corresponding to the energy difference between the photon involved in the ionization and related ionization potential (E_{ph} - I).

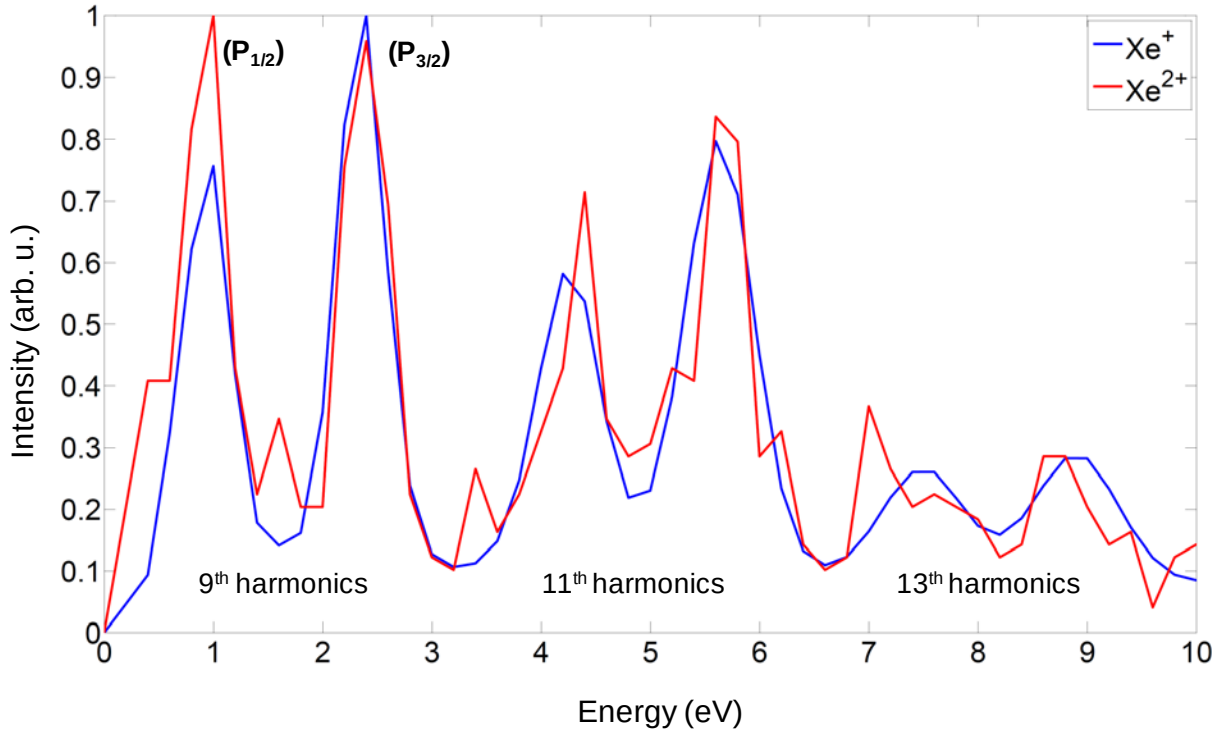

Figure 41: The kinetic energy spectra for electrons in coincidence with xenon single ionization (blue curve) and xenon double ionization (red curve).

In figure 41 the blue curve represents the transition from neutral xenon (Xe) to the Xe^{+} and black curve represents the energy spectrum related to the total Xe^{+2}. The obtained electron energy spectrum for Xe^{+} consists of peaks corresponding to the two states of Xe^{+}, $5P^5\ ^2P_{3/2}$ ($J_{3/2}$= 0.00 eV) and $^2P_{1/2}$ ($J_{1/2}$= 1.306 eV) for each order harmonic from 9th to 13th harmonics. According to the NIST atomic database the energy difference between these two states are known to be 1.306 eV. Our results are in good agreement with this. The experimental peak energies are in close agreement with the calculated values (Table 5.1) for the single ionization (Xe to Xe^{+}) (Figure 41 (blue)). On the other hand, the energy spectrum obtained for the double ionization event (Xe^{+2} (J_0 = 1.008 eV, J_1= 1.214 eV, J_2 = 0.000 eV)) showing different features compared to the energy

spectrum of the single ionization event. For example, extra peaks were observed around 0.5 eV, 1.5 eV and 3.5 eV for the double ionization than the single ionization spectrum. Evidently, these observations reflect the fact that we have successfully achieved the coincidence measurements of double ionization using two XUV photons. Then this experimental kinetic energy spectrum of the electrons from double ionization was compared with the theoretically predicted sequential double ionization spectrum of Xe^{2+} (Figure 42).

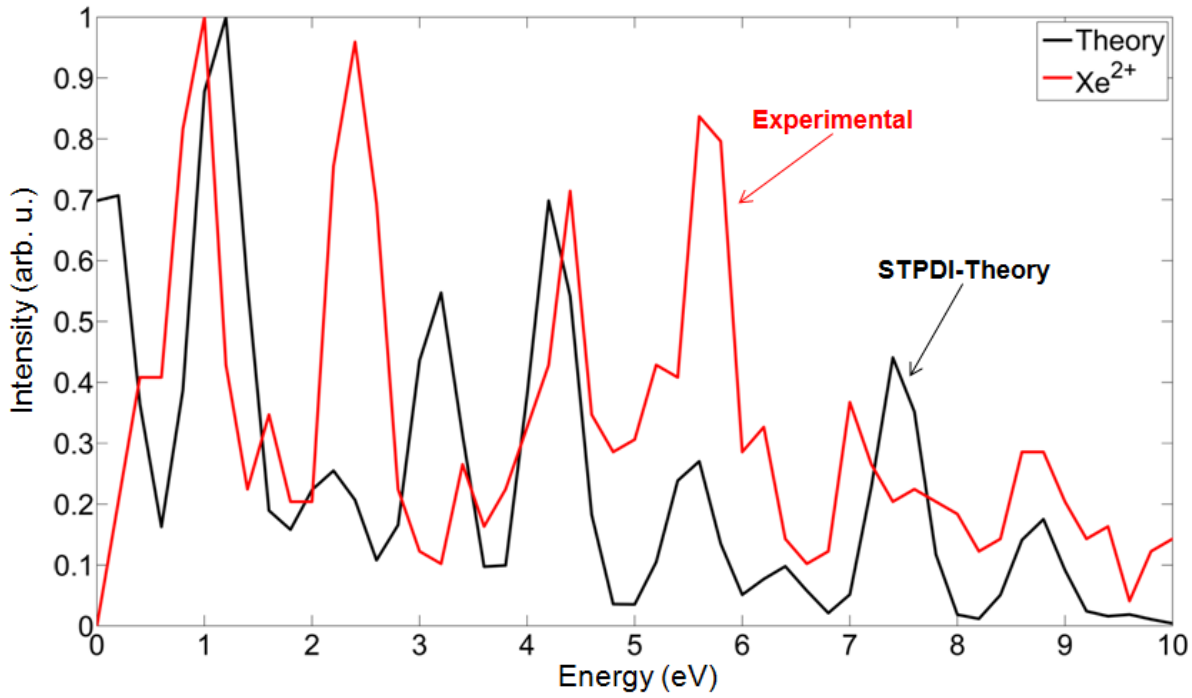

Figure 42: A comparison of the kinetic energy spectra for electrons in coincidence with xenon double ionization; experimental (red curve) to the theoretical sequential double ionization (black curve).

As shown by figure 42 the experimental kinetic energy spectrum for double ionization shows different features than the theoretically predicted kinetic energy spectrum for sequential two photon double ionization. This comparison indicates that the resulted double ionization is not purely a sequential process. If the double ionization is only a sequential process we would have seen only a similar spectrum to the theoretical curve. Therefore, the observed double ionization might also have a higher influence from the direct double ionization process. The energies of the additional peaks seen in double ionization spectrum respect to the single ionization spectrum are in close agreement with the calculated energies for the nonsequential process (Table 5.2). In general, a clear difference was observed in the kinetic energy spectrum of electrons in coincidence with the double ionization to the single ionization as well as to the theoretical curve for sequential two photon double ionization.

Description	Energy (eV)
$9\hbar\omega$ - I_1- $J_{1/2}$	1.02
$9\hbar\omega$ - I_1	2.33
$11\hbar\omega$ - I_1- $J_{1/2}$	4.23
$11\hbar\omega$ - I_1	5.54
$13\hbar\omega$ - I_1- $J_{1/2}$	7.45

Table 5.1: The calculated energy values corresponding to the kinetic energy spectrum of Xe^+.

Nonsequential	Energy (eV)
$(22\hbar\omega - I_1 - I_2 - J_1)/2$	0.47
$(22\hbar\omega - I_1 - I_2 - J_0)/2$	0.58
$(22\hbar\omega - I_1 - I_2)/2$	1.12
Sequential	**Energy (eV)**
$13\hbar\omega - I_2 + J_{1/2}$	1.21
$15\hbar\omega - I_2$	3.12
$15\hbar\omega - I_2 + J_{1/2} - J_1$	3.21
$15\hbar\omega - I_2 + J_{1/2} - J_0$	3.42
$15\hbar\omega - I_2 + J_{1/2}$	4.43

Table 5.2: The calculated energy values corresponding to the kinetic energy spectrum of Xe^{+2} from two possible mechanisms; nonsequential and sequential.

The next possibility we should rule out is whether these features are coming purely from XUV or there is any infrared contribution to these effects. Experimentally, before each data acquisition we have verified there was no infrared contribution. In a presence of infrared we can clearly observe the sidebands related to (13^{th}+1) harmonics in argon, so-called side band. As a precaution we have verified no such sideband present with argon before we accumulate the data for xenon. In addition, to produce second ionization with the infrared photons alone or XUV+IR requires many IR photons which the residue IR intensity cannot allow. Therefore the probability of nonsequential double ionization produced by infrared contribution is negligible in the

current setup. Take these facts in to consideration we can conclude that we have accomplished the measurements of electron in coincidence with the double ionization produced by two XUV photons for the first time. However, there are ongoing further investigations on the IR contribution in the current setup, which has not been finalized yet. For example we are trying to obtain the electron energy spectrum in coincidence with Xe^{+2} in the presence of IR, in order to compare it with our original experimental data. This approach will clearly verify the current uncertainties of the current experiment.

However, in our setup so far only one electron in coincidence with the double ionization event was detected. This is due to the fact that the dead time of the DLD being as large as 5 ns, which prevents the detection of both electrons coming from the same pulse. Therefore an extended investigations will be needed to improve the current setup with a new time and position detector with lower dead time as low as 1 ns. A detailed description of the current obstacle and the possible solutions are provided in the next section as future directions.

5. 4 Future Directions

5.4.1 Triple coincidence measurements

The dynamical studies of correlation among two or many electrons become interesting phenomena, which happens in the attosecond time domain. These correlation studies are extremely important, since any quantum or classical correlations among electrons will affect the dynamics in an enormous way. Specially, when it comes to observe fast changing processes as chemical reactions, phase changes etc., a real time observation would help to pin-down the stepwise process. However still there is only a limited knowledge found on this particular area of correlation electron dynamics. Even the theoretical modeling on these correlations becomes quite challenging these. More realistic approach would be measuring the momentum spectra for two electrons in same ionization event and look for the correlations among those. Figure 43 represents a simple illustration of how to picture the correlation information. The momentum spectrum of first electron verses second electron was considered. Base on how the relative momentum is distributed one can predict the correlation between those two electrons. If an isotropic momentum distribution was observed (Figure 43 (a)), there is no strong correlation present. On the other hand a diagonal momentum distribution tells information about the present correlations. According to the momentum directions (negative or positive) the plot consists of four regions. If the momentum events are appeared in first and third quarters (Figure 43 (b)), the corresponding two electrons are emitted in the same direction. But if the events appeared in second and fourth quarters (Figure 43 (c)), two electron emissions happens in opposite directions.

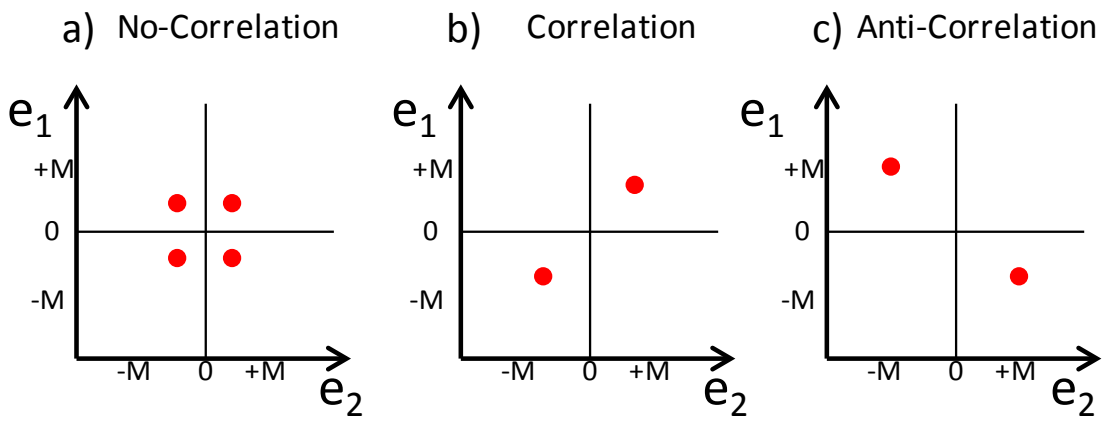

Figure 43: The schematic illustration of the momentum spectra showing possible electron correlations: a) the symmetric momentum distribution showing no correlation. The Diagonal momentum distribution showing, b) a correlation or c) an anti-correlation.

Non-sequential double ionization (NSDI) is a common example to evident the electron-electron correlations. Therefore many strong filed ionization experiments of electron correlation dynamics were carried out to study correlation between the two electron emission process in NSDI[126, 127]. Still the issue being the measurements of near single cycle laser pulse will not be able to provide the direct correlation dynamics of the NSDI process[129]. According to those facts the attosecond pulse duration would be essential in extracting direct correlation dynamics. The ideal experimental condition of extracting this kinematical information is the momentum measurements in coincidence with the two electron emission in a two photon process using XUV pump and XUV probe.

In our lab we are driving our investigation towards that goal. We have obtained preliminary results for the ion-electron coincidence measurements. According

to our ongoing research, the main obstacle for achieving triple coincidence is still being a lack of detection capabilities of low energy electrons due to relatively longer dead time of DLD detector.

Dead Time: A Dead time of a detector can be defined as the time interval corresponding to the detection of the next event after the previous event was detected. Dead time is also a factor in determining the multi hit capability. A long dead time will limit the multi hit capability.

The dead time of the current DLD detector used in our set up is 5 ns. However the range of the TOF of our total electron signal is generally less than 5 ns. This leads to a higher probability of the second electron of double ionization event to be missed. Consequently, to overcome this issue a detection system with a shorter dead time will be needed. Recently our group successfully implemented a three dimensional (3D) detector, capable of measuring both time and two-dimensional position, with a much shorter dead time (< 1 ns)[130, 131].

Time and position sensitive detection with fast frame camera: The newly developed 3D detector consists of a conventional microchannel plate (MCP)/phosphor screen, a fast frame CMOS (complementary metal oxide semiconductor) camera, and a high-speed digitizer. The concept is to locate the position information using a conventional imaging detector, MCP/phosphor plus CMOS camera setup while the temporal information (the corresponding arrival time of the detector) is processed through a high speed digitizer with a 5 gigasamples per second (GS/s) sampling rate. Previously, a detection system using MCP/phosphor together with CCD camera in 3D

detection was introduced[132]. In that studies they have used a multi-anode photomultiplier tube (PMT), to roughly measure the temporal information. The application of this system on fast ion beam coincidence experiments shows a limitation of the frame rate of the camera (< 100 Hz)[133]. For our experiments the desired frame rate is 1 kHz, and by implementing CMOS camera which is known to work at high frame rates [134] with the MCP/Phosphor, should be compatible in performing coincidence ion imaging at 1 kHz. In this case, the temporal information was measured using single anode photomultiplier tube (PMT) and was successfully used recently in coincidence ion imaging measurements by our group[130]. However, adopting this system towards the electron detection seems even challenging. Specially to achieve the high resolution to differentiate two electrons coming from the same event needed to be implemented. Furthermore, to perform successful triple coincidence measurements a shorter dead time even less than DLD has to be accomplished. In this newly developed detector [131] for electron imaging the temporal information was extracted from the MCP through a signal decoupler. This has narrow down the rise time and the pulsed width to 3 ns which enhance the multi-hit capabilities. Then the temporal resolution was improved up to 32 ps using an interpolation method permitting better resolving power for electrons. As the TOF separation of two electrons going opposite directions being small as 1 ns, such temporal resolution is ideal for the ion-electron-electron coincidence studies. Further improvements of the temporal resolution can be achieved using digitizer with a higher speed as 10 GS/s. The only drawback would be the high cost of such digitizers. Obviously, as any other coincidence experiments, minimizing the false coincidence is another important step. According to the studies presented by Lee *et al.* for this new

detection system, significantly lower false coincidence conditions were achieved by maintaining a low count rates as low as less than one event count per laser shot.

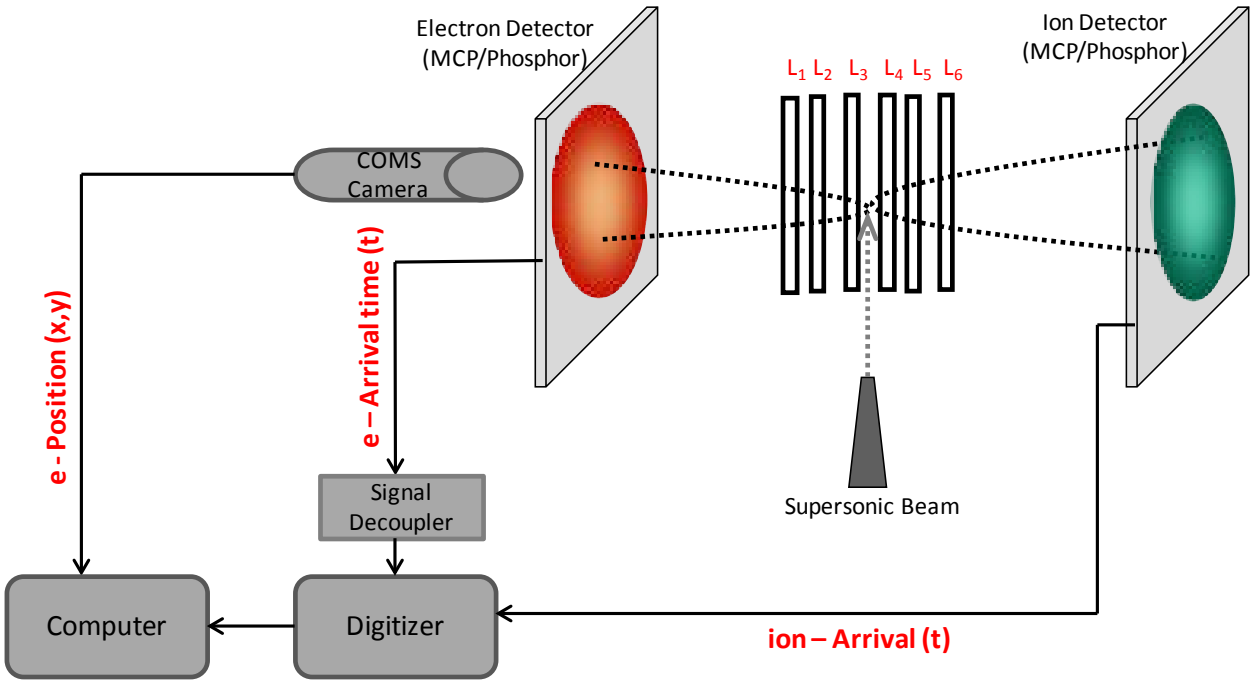

Figure 44: The proposed modification of the coincidence measurement chamber. The system is triggered by the laser at 1 kHz repetition rate and recorded position and time information for both ions and electrons are processed through the digitizer and then be established according to their coincidence.

Consequently, if the electron detector (DLD detector) in our current setup for coincident measurement was replaced with this newly developed detector, we would be able to do ion-electron-electron coincidence measurements. Figure 44 shows the schematic representation of the modifications on our current coincidence measurement chamber towards the triple coincidence measurements. The improved dead time (~1 ns) will facilitate the detection of both electrons from the same ionization event. Therefore,

this system is a better setup for studying triple coincidence of two photon double ionization event. Ideally, combination of this modified detection system together with attosecond pulse duration would make it feasible to achieve the real time electron correlation studies. Evidently, the non-linear attosecond spectroscopic studies of chemical systems would be possible in the near future.

5. 5 Summary

In conclusion, our newly developed experimental setup of HHG is capable of producing APTs with sufficient flux and energy to perform two photon double ionization using a XUV-pump-XUV-probe setup. Our setup also achieaved the ion-electron coincidence measurements of xenon double ionization using an intense APT source for the first time. The extracted kinetic energy spectrum of electron in coincidence with xenon dications shows nonsequential signature, suggesting the capability of our apparatus in studying electron correlations with attosecond time resolution. A new 3D imaging detector (dead time < 1 ns) will furthur enhance the ability to detect both electrons arising from two photon double ionization events. The mommentum correlation information between those two electrons will reveal the electron correlation dynamics in real time, which has been calculated but never experimentaly studied before.

APPENDIX A

Focal Volume and Related Equations

In this section the details related to the laser beam which is considered as a Gaussian beam and the dimensions such as focal spot and focal length will be discussed in terms of the extra information related to the material presented in chapter 4 (Describes the loose focusing geometry).

Gaussian Beam: Usually a laser beam can be represented as a wave given by the Gaussian function since its transverse electric field and the intensity fits well with the Gaussian function as follows:

$$E(r) = E_0 . exp\left(-r^2/\omega^2\right)$$

Where, $E(r)$ is the electric field amplitude at r distance while r is the radial distance along the propagation direction. E_0 is the amplitude of the electric field at $r=0$ and ω is the radius of the laser beam.

The focused Gaussian beam is given by figure A.1. The focal point is the place where the beam radius ω reached to its minimum value, ω_0. This minimum value is known as the beam waist and given by equation (A .1) for the case of $f >>> \omega_b$.

$$\omega_0 = \frac{2\lambda f}{\pi \omega_b} \qquad \text{(A .1)}$$

Where λ is the wavelength of the beam, f is the focal length and ω_b is the incident beam radius.

After the focal point, beam starts diverging again with the divergence angle of $\vartheta_{div} = \frac{\lambda}{\pi\omega_0}$. As given by the inset of figure A.1, the beam waist will remain approximately similar over a certain length around the focal length. This length is so-called Rayleigh range (Z_R) and given by equation (A.2).

$$Z_R = \frac{\pi{\omega_0}^2}{\lambda} \tag{A.2}$$

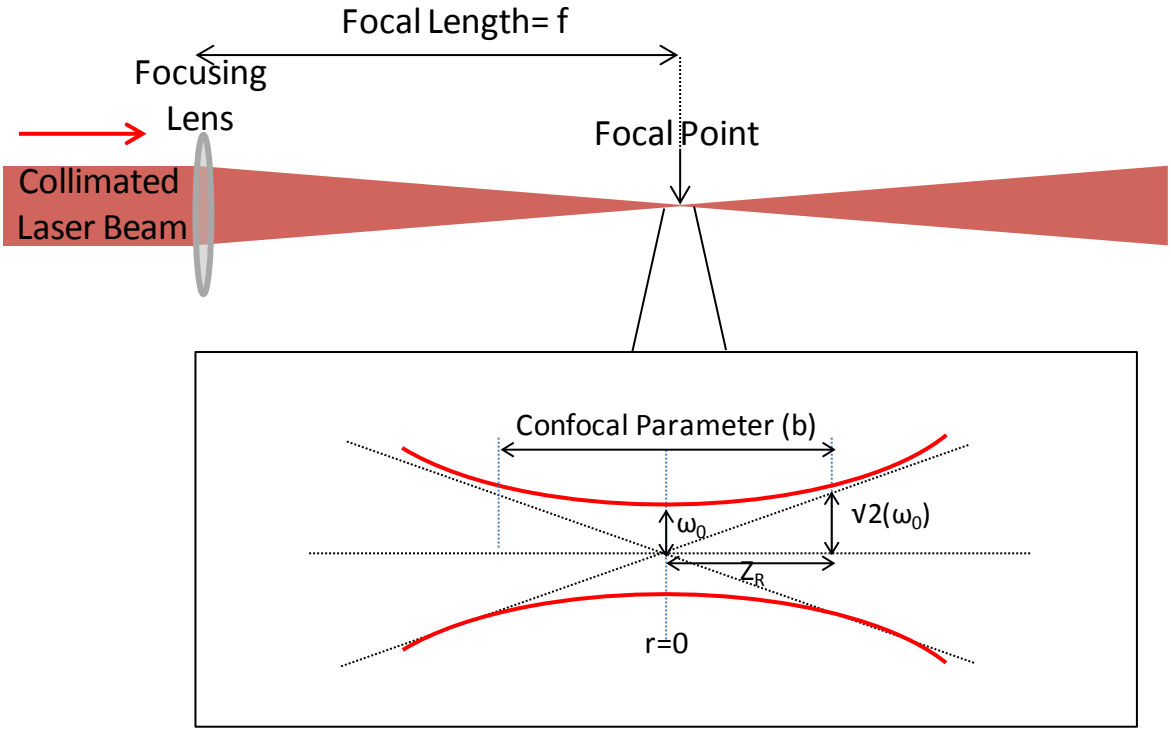

Figure A.1: The parameters of a focusing condition of a Gaussian beam. The inset represents a closer look on focal spot and related terms.

The Z_R can be defined as the distance that it takes to increase the beam radius square root to two times of that of the beam waist ($\sqrt{2}\,\omega_0$). The other interesting term related to the focal region is the confocal parameter (b), which is twice as the Z_R (Figure A.2 (inset)).

$$b = 2Z_R = \frac{2\pi {\omega_0}^2}{\lambda} \tag{A.3}$$

These equations are providing details corresponding to the concept behind the loose focusing geometry, where the focal volume has increased using a long focal length lens to increase the flux of the HHG.

APPENDIX B

American Physical Society
License Details

Feb 17, 2015

This is an Agreement between Thushani N Herath ("You") and American Physical Society ("Publisher"). It consists of your order details, the terms and conditions provided by American Physical Society, and the payment instructions.

License Number	3571420144496
License date	Feb 17, 2015
Licensed content publisher	American Physical Society
Licensed content publication	Reviews of Modern Physics
Licensed content title	Attosecond physics
Licensed copyright line	Copyright © 2009, American Physical Society
Licensed content author	Ferenc Krausz and Misha Ivanov
Licensed content date	Feb 2, 2009
Volume number	81
Type of Use	Thesis/Dissertation
Requestor type	Student
Format	Print, Electronic
Portion	chart/graph/table/figure
Number of charts/graphs/tables/figures	3
Portion description	Figure 5: Evolution of ultrafast science, Figure 15: Optical field ionization of an atom....etc, Figure 17: Trajectories of electrons returning....etc
Rights for	Main product
Duration of use	Life of current edition
Creation of copies for the disabled	no
With minor editing privileges	no
For distribution to	United States
In the following language(s)	Original language of publication
With incidental promotional use	no
The lifetime unit quantity of new product	0 to 499
The requesting person/organization is:	Thushani Herath
Order reference number	None
Title of your thesis / dissertation	Developing a toolbox to probe reaction dynamics with strong field ionization and non-linear attosecond spectroscopy
Expected completion date	May 2015

AIP PUBLISHING LLC LICENSE TERMS AND CONDITIONS

Feb 17, 2015

All payments must be made in full to CCC. For payment instructions, please see information listed at the bottom of this form.

License Number	3571430246296
Order Date	Feb 17, 2015
Publisher	AIP Publishing LLC
Publication	Journal of Chemical Physics
Article Title	Orbital alignment in photodissociation probed using strong field ionization
Author	Yun Fei Lin,Lu Yan,Suk Kyoung Lee, et al.
Online Publication Date	Dec 20, 2011
Volume number	135
Issue number	23
Type of Use	Thesis/Dissertation
Requestor type	Author (original article)
Format	Print and electronic
Portion	Figure/Table
Number of figures/tables	4
Title of your thesis / dissertation	Developing a toolbox to probe reaction dynamics with strong field ionization and non-linear attosecond spectroscopy
Expected completion date	May 2015
Estimated size (number of pages)	120
Total	0.00 USD

Terms and Conditions

AIP Publishing LLC -- Terms and Conditions: Permissions Uses

AIP Publishing LLC ("AIPP"") hereby grants to you the non-exclusive right and license to use and/or distribute the Material according to the use specified in your order, on a one-time basis, for the specified term, with a maximum distribution equal to the number that you have ordered. Any links or other content accompanying the Material are not the subject of this license.

1. You agree to include the following copyright and permission notice with the reproduction of the Material:"Reprinted with permission from [FULL CITATION]. Copyright [PUBLICATION YEAR], AIP Publishing LLC." For an article, the copyright and permission notice must be printed on the first page of the article or book chapter. For photographs, covers, or tables, the copyright and permission notice may appear with the Material, in a footnote, or in the reference list.
2. If you have licensed reuse of a figure, photograph, cover, or table, it is your responsibility to ensure that the material is original to AIPP and does not contain the copyright of another entity, and that the copyright notice of the figure, photograph, cover, or table does not indicate that it was reprinted by AIPP, with permission, from another source. Under no circumstances does AIPP, purport or intend to grant permission to reuse material to which it does not hold copyright.
3. You may not alter or modify the Material in any manner. You may translate the Material into another language only if you have licensed translation rights. You may not use the Material

American Physical Society
License Details

Feb 17, 2015

This is an Agreement between Thushani N Herath ("You") and American Physical Society ("Publisher"). It consists of your order details, the terms and conditions provided by American Physical Society, and the payment instructions.

License Number	3571420722675
License date	Feb 17, 2015
Licensed content publisher	American Physical Society
Licensed content publication	Physical Review Letters
Licensed content title	Strong-Field Ionization Rate Depends on the Sign of the Magnetic Quantum Number
Licensed copyright line	© 2012 American Physical Society
Licensed content author	Thushani Herath et al.
Licensed content date	Jul 25, 2012
Volume number	109
Type of Use	Thesis/Dissertation
Requestor type	Student
Format	Print, Electronic
Portion	chapter/article
Rights for	Main product
Duration of use	Life of current edition
Creation of copies for the disabled	no
With minor editing privileges	no
For distribution to	United States
In the following language(s)	Original language of publication
With incidental promotional use	no
The lifetime unit quantity of new product	0 to 499
The requesting person/organization is:	Thushani Herath
Order reference number	None
Title of your thesis / dissertation	Developing a toolbox to probe reaction dynamics with strong field ionization and non-linear attosecond spectroscopy
Expected completion date	May 2015
Expected size (number of pages)	120
Total	0.00 USD

Terms and Conditions

Date: Thu, 19 Feb 2015 09:11:26 +0000 [04:11:26 AM EST]

From: Permissions <permissions@iop.org>

To: thushani@chem.wayne.edu

Subject: Re: IOP Publishing ? Permissions request form: Response Received

Dear Thushani Herath,
Thank you for your request to reproduce IOP Publishing material.

Figure 4 - New Journal of Physics 13 (2011) 063038 to be reused in your thesis - "Developing a toolbox to probe reaction dynamics with strong field ionization and non-linear attosecond spectroscopy".

We are happy to grant permission for the use you request on the terms set out below.

Conditions
Non-exclusive, non-transferrable, revocable, worldwide, permission to use the material in print and electronic form will be granted subject to the following conditions:
· Permission will be cancelled without notice if you fail to fulfil any of the conditions of this letter.
· You will make reasonable efforts to contact the author(s) to seek consent for your intended use. Contacting one author acting expressly as authorised agent for their co-authors is acceptable.
· You will reproduce the following prominently alongside the material:
o the source of the material, including author, article title, title of journal, volume number, issue number (if relevant), page range (or first page if this is the only information available) and date of first publication. This information can be contained in a footnote or reference note; or
o a link back to the article (via DOI); and
o the words ?© IOP Publishing & Deutsche Physikalische Gesellschaft. CC BY-NC-SA?
· The material will not, without the express permission of the author(s), be used in any way which, in the opinion of IOP Publishing, could distort or alter the author(s)? original intention(s) and meaning, be prejudicial to the honour or reputation of the author(s) and/or imply endorsement by the author(s) and/or IOP Publishing.
· Payment of £0 is received in full by IOP Publishing prior to use.
If you have any questions, please feel free to contact our Permissions team at permissions@iop.org.
I should be grateful if you would acknowledge receipt of this email.
Kind regards,
Lucy Evans
Publishing Assistant
IOP Publishing

Please note: We do not usually provide signed permission forms as a separate attachment. Please print this email and provide it to your publisher as proof of permission.

From: "FormsCentral Notifications" <formscentral-notifications@acrobat.com>
To: permissions@iop.org,
Date: 17/02/2015 21:23
Subject: IOP Publishing ? Permissions request form: Response Received

REFERENCES

1. Krausz, F. and M. Ivanov, *Attosecond physics.* Reviews of Modern Physics, 2009. **81**(1): p. 163-234.
2. Pedersen, S., J.L. Herek, and A.H. Zewail, *The Validity of the "Diradical" Hypothesis: Direct Femtoscond Studies of the Transition-State Structures.* Science, 1994. **266**(5189): p. 1359-1364.
3. Okabe, H., *Photochemistry of Small Molecules*. 1978, New York: Wiley.
4. Corkum, P.B., *Plasma Perspective on Strong-Field Multiphoton Ionization.* Physical Review Letters, 1993. **71**(13): p. 1994-1997.
5. Kulander, K.C., K.J. Schafer, and J.L. Krause, *Dynamics of Short-Pulse Excitation, Ionization and Harmonic Conversion*, in *Super-intense laser-atom physics*, B. Piraux, A. L'Huillier, and K. Rzazewski, Editors. 1993, Plenum Press: New York. p. 95-110.
6. Yudin, G.L. and M.Y. Ivanov, *Nonadiabatic tunnel ionization: Looking inside a laser cycle.* Physical Review A, 2001. **64**(1): p. 013409.
7. Ammosov, M.V., N.B. Delone, and V.P. Krainov, *Tunnel Ionization of Complex Atoms and Atomic Ions in a Varying Electromagnetic-Field.* Zhurnal Eksperimentalnoi I Teoreticheskoi Fiziki, 1986. **91**(6): p. 2008-2013.
8. Ilkov, F.A., J.E. Decker, and S.L. Chin, *Ionization of Atoms in the Tunneling Regime with Experimental-Evidence Using Hg Atoms.* Journal of Physics B-Atomic Molecular and Optical Physics, 1992. **25**(19): p. 4005-4020.

9. Yudin, G.L. and M.Y. Ivanov, *Physics of correlated double ionization of atoms in intense laser fields: Quasistatic tunneling limit* Physical Review A, 2001. **64**(1): p. 033404.

10. Gubbini, E., et al., *Core relaxation in atomic ultrastrong laser field ionization.* Physical Review Letters, 2005. **94**(5): p. 053602.

11. Bracker, A.S., et al., *Imaging the alignment angular distribution: State symmetries, coherence effects, and nonadiabatic interactions in photodissociation.* Journal of Chemical Physics, 1999. **110**(14): p. 6749-6765.

12. Bracker, A.S., et al., *Observation of Coherent and Incoherent Dissociation Mechanisms in the Angular Distribution of Atomic Photofragment Alignment.* Physical Review Letters, 1998. **80**(8): p. 1626-1629.

13. Clark, A.P., et al., *Atomic polarization in the photodissociation of diatomic molecules.* Physical Chemistry Chemical Physics, 2006. **8**(48): p. 5591-5610.

14. Suits, A.G. and O.S. Vasyutinskii, *Imaging atomic orbital polarization in photodissociation.* Chem Rev, 2008. **108**(9): p. 3706-46.

15. Brouard, M., et al., *O(^3P_J) Alignment from the Photodissociation of SO_2 at 193 nm.* The Journal of Physical Chemistry A, 2004. **108**(39): p. 7965-7976.

16. Brouard, M., et al., *The photodissociation dynamics of ozone at 193 nm: An O(D-1(2)) angular momentum polarization study.* Journal of Chemical Physics, 2006. **125**(13): p. 133308.

17. Brouard, M., et al., *The Photodissociation Dynamics of Ozone at 226 and 248 nm: O(^3P_J) Atomic Angular Momentum Polarization.* Journal of Chemical Physics, 2007. **127**(14): p. 144304.

18. Brouard, M., et al., *Photodissociation Dynamics of OCS at 248 nm: The S(^{1}D) Atomic Angular Momentum Polarization.* Journal of Chemical Physics, 2007. **127**(8): p. 084304.

19. Lee, S.K., et al., *S(1D2) atomic orbital polarization in the photodissociation of OCS at 193 nm: Construction of the complete density matrix.* J Chem Phys, 2006. **125**(14): p. 144318.

20. Lee, S.K., et al., *O(D-1(2)) orbital orientation in the ultraviolet photodissociation of ozone.* Physical Chemistry Chemical Physics, 2005. **7**(8): p. 1650-1656.

21. Townsend, D., S.K. Lee, and A.G. Suits, *Orbital polarization from DC slice imaging: S(D-1(2)) alignment in the photodissociation of ethylene sulfide.* Chemical Physics, 2004. **301**(2-3): p. 197-208.

22. Rakitzis, T.P., et al., *Photofragment helicity caused by matter-wave interference from multiple dissociative states.* Science, 1998. **281**(5381): p. 1346-1349.

23. Rakitzis, T.P., S.A. Kandel, and R.N. Zare, *Photolysis of ICl causes mass-dependent interference in the Cl(P-2(3/2)) photofragment angular momentum distributions.* Journal of Chemical Physics, 1998. **108**(20): p. 8291-8294.

24. Costen, M.L. and G.E. Hall, *Coherent and incoherent orientation and alignment of ICN photoproducts.* Physical Chemistry Chemical Physics, 2007. **9**(2): p. 272-287.

25. Gordon, R.J. and G.E. Hall, *Applications of Doppler spectroscopy to photofragmentation.* Advances in Chemical Physics, Vol 96, 1996. **96**: p. 1-50.

26. Rothe, E.W., R. Duren, and U. Krause, *Laser-Induced Dissociation of Na2 - Polarization of Atomic Fluorescence.* Bulletin of the American Physical Society, 1980. **25**(4): p. 493-493.

27. Loh, Z.H., et al., *Quantum state-resolved probing of strong-field-ionized xenon atoms using femtosecond high-order harmonic transient absorption spectroscopy.* Physical Review Letters, 2007. **98**(14): p. 143601.

28. Young, L., et al., *X-ray microprobe of orbital alignment in strong-field ionized atoms.* Physical Review Letters, 2006. **97**(8): p. 083601.

29. Lin, C.D. and X.M. Tong, *Dependence of tunneling ionization and harmonic generation on the structure of molecules by short intense laser pulses.* Journal of Photochemistry and Photobiology A: Chemistry, 2006. **182**(3): p. 213-219.

30. Li, W., et al., *Visualizing electron rearrangement in space and time during the transition from a molecule to atoms.* Proc Natl Acad Sci U S A, 2010. **107**(47): p. 20219-22.

31. Assion, A., et al., *Control of chemical reactions by feedback-optimized phase-shaped femtosecond laser pulses.* Science, 1998. **282**(5390): p. 919-922.

32. Levis, R.J., G.M. Menkir, and H. Rabitz, *Selective bond dissociation and rearrangement with optimally tailored, strong-field laser pulses.* Science, 2001. **292**(5517): p. 709-713.

33. Sussman, B.J., et al., *Dynamic stark control of photochemical processes.* Science, 2006. **314**(5797): p. 278-281.

34. Agostini, P. and L.F. DiMauro, *The physics of attosecond light pulses (vol 67, pg 813, 2004).* Reports on Progress in Physics, 2004. **67**(8): p. 1563-1563.

35. Zhao, K., et al., *Tailoring a 67 attosecond pulse through advantageous phase-mismatch.* Optics Letters, 2012. **37**(18): p. 3891-3893.

36. Born, M. and R. Oppenheimer, *Quantum theory of molecules.* Annalen Der Physik, 1927. **84**(20): p. 0457-0484.

37. Butler, L.J., *Chemical reaction dynamics beyond the Born-Oppenheimer approximation.* Annual Review of Physical Chemistry, 1998. **49**: p. 125-171.

38. Hartree, D.R., *The wave mechanics of an atom with a non-Coulomb central field Part II some results and discussion.* Proceedings of the Cambridge Philosophical Society, 1928. **24**: p. 111-132.

39. Remacle, F., et al., *Electronic control of site selective reactivity: A model combining charge migration and dissociation.* Journal of Physical Chemistry A, 1999. **103**(49): p. 10149-10158.

40. Corkum, P.B., *Plasma perspective on strong field multiphoton ionization.* Phys Rev Lett, 1993. **71**(13): p. 1994-1997.

41. Agostini, P., et al., *Free-Free Transitions Following 6-Photon Ionization of Xenon Atoms.* Physical Review Letters, 1979. **42**(17): p. 1127-1130.

42. McPherson, A., et al., *Studies of multiphoton production of vacuum-ultraviolet radiation in the rare gases.* Journal of the Optical Society of America B, 1987. **4**(4): p. 595-601.

43. Ferray, M., et al., *Multiple-harmonic conversion of 1064 nm radiation in rare gases.* Journal of Physics B: Atomic, Molecular and Optical Physics, 1988. **21**(3): p. L31.

44. Liang, Y., et al., *High harmonic generation in atomic and diatomic molecular gases using intense picosecond laser pulses-a comparison.* Journal of Physics B: Atomic, Molecular and Optical Physics, 1994. **27**(20): p. 5119.

45. Macklin, J., J. Kmetec, and C. Gordon, *High-order harmonic generation using intense femtosecond pulses.* Physical Review Letters, 1993. **70**(6): p. 766-769.

46. Salieres, P., et al., *Study of the spatial and temporal coherence of high order harmonics.* arXiv preprint quant-ph/9710060, 1997.

47. Popmintchev, T., *Bright coherent ultrahigh harmonics in the keV x-ray regime from mid-infrared femtosecond lasers.* Science (New York, N.Y.), 2012. **336**(6086): p. 1287-1291.

48. Yakovlev, V.S., M. Ivanov, and F. Krausz, *Enhanced phase-matching for generation of soft X-ray harmonics and attosecond pulses in atomic gases.* Optics Express, 2007. **15**(23): p. 15351-15364.

49. Bahabad, A., M.M. Murnane, and H.C. Kapteyn, *Quasi-phase-matching of momentum and energy in nonlinear optical processes.* Nat Photon, 2010. **4**(8): p. 570-575.

50. Gibson, E.A., *Coherent soft x-ray generation in the water window with quasi-phase matching.* Science (New York, N.Y.), 2003. **302**(5642): p. 95-98.

51. Viktor, T.P. and V.V. Strelkov, *Generation of high-order harmonics in a high-intensity laser radiation field.* Quantum Electronics, 1998. **28**(7): p. 564.

52. Larsson, J.r., et al., *Two-colour time-resolved spectroscopy of helium using high-order harmonics.* Journal of Physics B: Atomic, Molecular and Optical Physics, 1995. **28**(3): p. L53.

53. Descamps, D., et al., *Extreme ultraviolet interferometry measurements with high-order harmonics.* Optics letters, 2000. **25**(2): p. 135-137.

54. Harris, S.E., J.J. Macklin, and T.W. Hänsch, *Atomic scale temporal structure inherent to high-order harmonic generation.* Optics Communications, 1993. **100**(5–6): p. 487-490.

55. Schafer, K. and K. Kulander, *High Harmonic Generation from Ultrafast Pump Lasers.* Physical Review Letters, 1997. **78**(4): p. 638-641.

56. Lepine, F., M.Y. Ivanov, and M.J.J. Vrakking, *Attosecond molecular dynamics: fact or fiction?* Nat Photon, 2014. **8**(3): p. 195-204.

57. Costello, J.T. *Photoionization experiments with the ultrafast EUV laser'FLASH'–free electron laser in Hamburg*. in *Journal of Physics: Conference Series*. 2007. IOP Publishing.

58. Kelkensberg, F., et al., *Molecular Dissociative Ionization and Wave-Packet Dynamics Studied Using Two-Color XUV and IR Pump-Probe Spectroscopy.* Physical Review Letters, 2009. **103**(12): p. 123005.

59. Kienberger, R., et al., *Atomic transient recorder.* Nature, 2004. **427**(6977): p. 817-821.

60. Baltuška, A., et al., *Attosecond control of electronic processes by intense light fields.* Nature, 2003. **421**(6923): p. 611-615.

61. Lin, Y.F., et al., *Orbital alignment in photodissociation probed using strong field ionization.* Journal of Chemical Physics, 2011. **135**(23): p. 234311.

62. Herath, T., et al., *Strong-Field Ionization Rate Depends on the Sign of the Magnetic Quantum Number.* Physical Review Letters, 2012. **109**(4): p. 043004.

63. Brouard, M., et al., *The photodissociation dynamics of ozone at 226 and 248 nm: O(P-3(J)) atomic angular momentum polarization.* Journal of Chemical Physics, 2007. **127**(14).

64. Siebbeles, L., et al., *Vector Properties in Photodissociation: Quantum Treatment of the Correlation between the Spatial Anisotropy and the Angular Momentum Polarization of the Fragments.* Journal of Chemical Physics, 1994. **100**(5): p. 3610.

65. Townsend, D., M. Minitti, and A. Suits, *Direct Current Slice Imaging.* Review of Scientific Instruments, 2003. **74**(4): p. 2530.

66. Li, W., et al., *Megapixel ion imaging with standard video.* Review of Scientific Instruments, 2005. **76**(6): p. 063106.

67. Brouard, M., *O(P) Alignment from the Photodissociation of SO at 193 nm.* The journal of physical chemistry. A, Molecules, spectroscopy, kinetics, environment, & general theory, 2004. **108**(39): p. 7965-7976.

68. Smeenk, C., et al., *Precise in-situ measurement of laser pulse intensity using strong field ionization.* Optics Express, 2011. **19**(10): p. 9336-9344.

69. Rzazewski, K. and B. Piraux, *Circular Rydberg Orbits in Circularly Polarized Microwave-Radiation.* Physical Review A, 1993. **47**(3): p. R1612-R1615.

70. Zakrzewski, J., et al., *Ionization of Highly Excited Hydrogen-Atoms by a Circularly Polarized Microwave Field.* Physical Review A, 1993. **47**(4): p. R2468-R2471.

71. Tulenko, E.B. and B.A. Zon, *On the tunneling ionization of atoms in the presence of a circularly polarized laser field.* Laser Physics, 2003. **13**(4): p. 450-451.

72. Barth, I. and O. Smirnova, *Nonadiabatic tunneling in circularly polarized laser fields: Physical picture and calculations.* Physical Review A, 2011. **84**(6): p. 063415.

73. Corkum, P.B., N.H. Burnett, and M.Y. Ivanov, *Subfemtosecond Pulses.* Optics Letters, 1994. **19**(22): p. 1870-1872.

74. Sansone, G., et al., *Isolated single-cycle attosecond pulses.* Science, 2006. **314**(5798): p. 443-446.

75. Eckle, P., et al., *Attosecond Angular Streaking.* Nature Physics, 2008. **4**(7): p. 565-570.

76. Pfeiffer, A.N., et al., *Timing the release in sequential double ionization.* Nat Phys, 2011. **7**(5): p. 428-433.

77. Barth, I. and O. Smirnova, *Comparison of theory and experiment for nonadiabatic tunneling in circularly polarized fields.* Physical Review A, 2013. **87**(6): p. 065401.

78. Corkum, P.B., N.H. Burnett, and M.Y. Ivanov, *Subfemtosecond Pulses.* Opt Lett, 1994. **19**(22): p. 1870-1872.

79. Pfeiffer, A.N., et al., *Timing the release in sequential double ionization.* Nature Physics, 2011. **7**(5): p. 428-433.

80. Bethe, H., *Intermediate Quantum Mechanics*. 1964, New York: W.A. Benjamin. Inc.

81. Walker, B., et al., *Precision Measurement of Strong Field Double Ionization of Helium.* Physical Review Letters, 1994. **73**(9): p. 1227-1230.

82. Augst, S., et al., *Nonsequential triple ionization of argon atoms in a high-intensity laser field.* Physical Review A, 1995. **52**(2): p. R917-R919.

83. Fittinghoff, D., et al., *Observation of nonsequential double ionization of helium with optical tunneling.* Physical Review Letters, 1992. **69**(18): p. 2642-2645.

84. Bryan, W.A., et al., *Atomic excitation during recollision-free ultrafast multi-electron tunnel ionization.* Nat Phys, 2006. **2**(6): p. 379-383.

85. Weber, T., et al., *Correlated electron emission in multiphoton double ionization.* Nature, 2000. **405**(6787): p. 658-661.

86. Rudati, J., et al., *Multiphoton double ionization via field-independent resonant excitation.* Phys Rev Lett, 2004. **92**(20): p. 203001.

87. Walker, T.E.H. and J.T. Waber, *Spin-orbit coupling photoionization.* Journal of Physics B: Atomic and Molecular Physics, 1974. **7**(6): p. 674.

88. Becker, A., R. Dorner, and R. Moshammer, *Multiple fragmentation of atoms in femtosecond laser pulses.* Journal of Physics B-Atomic Molecular and Optical Physics, 2005. **38**(9): p. S753-S772.

89. Fittinghoff, D., et al., *Polarization dependence of tunneling ionization of helium and neon by 120-fs pulses at 614 nm.* Physical Review A, 1994. **49**(3): p. 2174-2177.

90. Dietrich, P., et al., *High-harmonic generation and correlated two-electron multiphoton ionization with elliptically polarized light.* Physical Review A, 1994. **50**(5): p. R3585-R3588.

91. Walker, B., et al., *Double ionization in the perturbative and tunneling regimes.* Physical Review A, 1993. **48**(2): p. R894-R897.

92. Wang, X. and J.H. Eberly, *Effects of Elliptical Polarization on Strong-Field Short-Pulse Double Ionization.* Physical Review Letters, 2009. **103**(10): p. 103007

93. Pfeiffer, A.N., et al., *Breakdown of the Independent Electron Approximation in Sequential Double Ionization.* 2011 Conference on Lasers and Electro-Optics (Cleo), 2011.

94. Guo, C., et al., *Single and double ionization of diatomic molecules in strong laser fields.* Physical Review A, 1998. **58**(6): p. R4271-R4274.

95. Cohen, O., et al., *Grating-Assisted Phase Matching in Extreme Nonlinear Optics.* Physical Review Letters, 2007. **99**(5): p. 053902.

96. Cohen, O., et al., *Optimizing quasi-phase matching of high harmonic generation using counterpropagating pulse trains.* Optics Letters, 2007. **32**(20): p. 2975-2977.

97. Brabec, T. and F. Krausz, *Intense few-cycle laser fields: Frontiers of nonlinear optics.* Reviews of Modern Physics, 2000. **72**(2): p. 545.

98. Strickland, D. and G. Mourou, *Compression of amplified chirped optical pulses.* Optics communications, 1985. **55**(6): p. 447-449.

99. Photonics, D.M., *Basic concept of laser, Power point Presentation*.

100. Paul, P.M., et al., *Observation of a Train of Attosecond Pulses from High Harmonic Generation.* Science, 2001. **292**(5522): p. 1689-1692.

101. Drescher, M., et al., *X-ray Pulses Approaching the Attosecond Frontier.* Science, 2001. **291**(5510): p. 1923-1927.

102. Wheeler, J., et al. *Attosecond lighthouses from plasma mirrors*. in *Conference on Lasers and Electro-Optics 2012*. 2012. San Jose, California: Optical Society of America.

103. Schnürer, M., et al., *Guiding and high-harmonic generation of sub-10-fs pulses in hollow-core fibers at 1015 W/cm2.* Applied Physics B, 1998. **67**(2): p. 263-266.

104. Kim, I.J., et al., *Highly Efficient High-Harmonic Generation in an Orthogonally Polarized Two-Color Laser Field.* Physical Review Letters, 2005. **94**(24): p. 243901.

105. Mairesse, Y., et al., *Attosecond synchronization of high-harmonic soft x-rays.* Science, 2003. **302**(5650): p. 1540-1543.

106. Kim, K.T., et al., *Single sub-50-attosecond pulse generation from chirp-compensated harmonic radiation using material dispersion.* Physical Review A, 2004. **69**(5): p. 051805.

107. Davies, J.A., et al., *Femtosecond time-resolved photoelectron–photoion coincidence imaging studies of dissociation dynamics.* The Journal of Chemical Physics, 1999. **111**(1): p. 1-4.

108. Davies, J.A., et al., *Femtosecond Time-Resolved Photoelectron Angular Distributions Probed during Photodissociation of NO_2.* Physical Review Letters, 2000. **84**(26): p. 5983-5986.

109. Keller, H., G. Klingelhöfer, and E. Kankeleit, *A position sensitive microchannelplate detector using a delay line readout anode.* Nuclear Instruments and Methods in Physics Research Section A: Accelerators, Spectrometers, Detectors and Associated Equipment, 1987. **258**(2): p. 221-224.

110. Becker, J., et al., *A system for correlated fragment detection in dissociation experiments.* Nuclear Instruments and Methods in Physics Research Section A: Accelerators, Spectrometers, Detectors and Associated Equipment, 1994. **337**(2–3): p. 409-415.

111. Strasser, D., et al., *An innovative approach to multiparticle three-dimensional imaging.* Review of Scientific Instruments, 2000. **71**(8): p. 3092-3098.

112. Jagutzki, O., et al., *Position sensitive anodes for MCP read-out using induced charge measurement.* Nuclear Instruments and Methods in Physics Research Section A: Accelerators, Spectrometers, Detectors and Associated Equipment, 2002. **477**(1–3): p. 256-261.

113. Martin, C., et al., *Wedge-and-strip anodes for centroid-finding position-sensitive photon and particle detectors.* Review of Scientific Instruments, 1981. **52**(7): p. 1067-1074.

114. Ullrich, J., et al., *Recoil-ion and Electron Momentum Spectroscopy: Reaction Microscopes.* Reports on Progress in Physics, 2003. **66**(9): p. 1463-1545.

115. Vredenborg, A., W.G. Roeterdink, and M.H. Janssen, *A photoelectron-photoion coincidence imaging apparatus for femtosecond time-resolved molecular dynamics with electron time-of-flight resolution of σ= 18ps and energy resolution ΔE/E= 3.5%.* Review of Scientific Instruments, 2008. **79**(6): p. 063108.

116. Eppink, A. and D. Parker, *Velocity Map Imaging of Ions and Electrons Using Electrostatic Lenses: Application in Photoelectron and Photofragment Ion Imaging of Molecular Oxygen.* Review of Scientific Instruments, 1997. **68**(9): p. 3477.

117. Hofstetter, M., et al., *Lanthanum–molybdenum multilayer mirrors for attosecond pulses between 80 and 130 eV.* New Journal of Physics, 2011. **13**(6): p. 063038.

118. Eriksson, F., et al., *Atomic scale interface engineering by modulated ion-assisted deposition applied to soft x-ray multilayer optics.* Applied Optics, 2008. **47**(23): p. 4196-4204.

119. Wonisch, A., et al., *Aperiodic nanometer multilayer systems as optical key components for attosecond electron spectroscopy.* Thin Solid Films, 2004. **464–465**(0): p. 473-477.

120. Wonisch, A., et al., *Design, fabrication, and analysis of chirped multilayer mirrors for reflection of extreme-ultraviolet attosecond pulses.* Applied Optics, 2006. **45**(17): p. 4147-4156.

121. Codling, K., et al., *The double photoionization/fragmentation of CF4 in the threshold region (35-80 eV).* Journal of Physics B: Atomic, Molecular and Optical Physics, 1991. **24**(5): p. 951.

122. Lahmam-Bennani, A., *Thirty years of experimental electron–electron (e,2e) coincidence studies: achievements and perspectives.* Journal of Electron Spectroscopy and Related Phenomena, 2002. **123**(2–3): p. 365-376.

123. Flodstrom, S. and J. Endriz, *Investigation of the vectorial photoelectric effect in magnesium.* Physical Review B, 1975. **12**(4): p. 1252.

124. Lambropoulos, P., P. Maragakis, and J. Zhang, *Two-electron atoms in strong fields.* Physics Reports, 1998. **305**(5): p. 203-293.

125. Fittinghoff, D.N., et al., *Observation of nonsequential double ionization of helium with optical tunneling.* Phys Rev Lett, 1992. **69**(18): p. 2642-2645.

126. Weber, T., et al., *Correlated electron emission in multiphoton double ionization.* Nature, 2000. **405**(6787): p. 658-661.

127. Bergues, B., et al., *Attosecond tracing of correlated electron-emission in non-sequential double ionization.* Nat Commun, 2012. **3**: p. 813.

128. Tzallas, P., E. Skantzakis, and D. Charalambidis, *Direct two-XUV-photon double ionization in xenon.* Journal of Physics B: Atomic, Molecular and Optical Physics, 2012. **45**(7): p. 074007.

129. Liu, X., et al., *Nonsequential double ionization at the single-optical-cycle limit.* Phys Rev Lett, 2004. **93**(26 Pt 1): p. 263001.

130. Lee, S.K., et al., *Coincidence ion imaging with a fast frame camera.* Review of Scientific Instruments, 2014. **85**(12): p. 123303.

131. Lee, S.K., et al., *Communication: Time- and space-sliced velocity map electron imaging.* The Journal of Chemical Physics, 2014. **141**(22): p. 221101.

132. Amitay, Z. and D. Zajfman, *A new type of multiparticle three-dimensional imaging detector with subnanosecond time resolution.* Review of Scientific Instruments, 1997. **68**(3): p. 1387-1392.

133. Hoops, A.A., et al., *Fast beam studies of I_2 and $I_2^- \cdot Ar$ photodissociation.* Chemical Physics Letters, 2003. **374**(3–4): p. 235-242.

134. Horio, T. and T. Suzuki, *Multihit two-dimensional charged-particle imaging system with real-time image processing at 1000 frames/s.* Review of Scientific Instruments, 2009. **80**(1): p. 013706.

ABSTRACT

DEVELOPING A TOOLBOX TO PROBE REACTION DYNAMICS WITH STRONG FIELD IONIZATION AND NON-LINEAR ATTOSECOND SPECTROSCOPY

by

THUSHANI N. HERATH

May 2015

Advisor: Dr. Wen Li

Major: Analytical Chemistry

Degree: Doctor of Philosopy

Electronic motions which happen in 10 to 100 of attoseconds are the heart of many processes in nature. Therefore monitoring and extracting details in this fundamental level will provide new prospect to the areas as information technology, basic energy science, medicine and life sciences. The challenge being, develop a tool to reach such a fast time scale for real time observation in atomic level. In this thesis we have addressed this matter using two interesting approaches related to the laser matter interaction: strong field ionization and nonlinear attosecond spectroscopy. The first part is based on the studies related to the strong field ionization probe. Strong field ionization probe was verified to be sensitive not only to the orbital alignment but also to the atomic orientation, which evident the capability of SFI in probing atomic polarization effect in photodissociation processes. The second part is based on non-linear attosecond spectroscopy. With the use 1 kHz laser and the loose focusing geometry we were able to produce attosecond pulse trains with a sufficient flux to perform two photon double ionization. Further, we were also able to extract ion-electron coincidence measurements

of the double ionization event of XUV-pump-XUV-probe system for the first time. The extended studies will be carried out with the combination of our newly developed 3D detector with improved dead time, to the current setup which will facilitate the triple coincidence capabilities. The proposed studies will facilitate the probing real time electron-electron correlation, which promises the probing and eventually controlling the fundamental processes in their natural time domain.

AUTOBIOGRAPHIC STATEMENT

THUSHANI NIKESHALA HERATH

I was born and raised in Sri Lanka. After finishing my high school education from St. Anthony's convent, Kandy, I started my Bachelor of Science degree at University of Peradeniya, Sri Lanka. In 2008, I joined Wayne State University as an undergraduate researcher under the supervision of Dr. Sarah Trimpin. Then I have started my doctoral degree at Wayne State University in 2009.

Publications

- **Herath T.** et al; "XUV-pump, XUV-probe attosecond spectroscopy, in preparation
- **Herath T.**; Yan L.; Lee S.K.; Li W.; Strong Field Ionization Rate Depends on the Sign of the Magnetic Quantum Number., *Phys. Rev. Lett*., **2012,** 109, 043004
- Lin Y.F.; Yan L.; Lee S.K.; **Herath. T.N**.; Li W. Orbital Alignment in Photodissocitaion Probed Using Strong Field Ionization., *J. Chem. Phys.*, **2011**, 135, 23311
- Trimpin. S.; **Herath T.N**.; Inutan E.D., Wager-Miller J.; Kowalski P.; Claude E.; Walker C. J.; Mackie K., Automated Solvent-Free Matrix Deposition for Tissue Imaging by Mass Spectrometry., *Anal. Chem*. **2010**, 82, 359-367
- Trimpin. S.; Inutan E.D.; **Herath T.N**.; McEwen C.N.; Matrix-Assisted Laser Desorption/Ionization Mass Spcetrometry Method for Selectively Producing Either Singly or Multiply charged Molecular Ions, *Anal. Chem*., **2010**, 82, 11-15
- Trimpin. S.; Inutan E.D.; **Herath T.N**.; McEwen C.N.; Laserspray Ionization, A New Atmospheric Pressure MALDI Method for Producing Highly Charged Gas-phase Ions of Peptides and Proteins Directly from Solid Solutions, *Mol. Cell Proteomics*., **2010**, 9, 362-367
- Trimpin. S.; **Herath T.N.**; Inutan E.D.; Cernat S.A.; Miller J.B.; Mackie K.; Walker J.M., Field-free Transmission Geometry Atmospheric Pressure Matrix-assisted Laser Desorption/ionization for rapid analysis of unadulterated tissue samples.,*Rapid Commun. Mass Spectro,.* **2009**, 23, 3023-3027